CONTRACT REPORT ARBRL-CR-00381

THEORETICAL STUDY OF TWO-PHASE FLOW ASSOCIATED WITH GRANULAR BAG CHARGES

Prepared by

Paul Gough Associates
P. O. Box 1614
Portsmouth, NH 03801

September 1978

US ARMY ARMAMENT RESEARCH AND DEVELOPMENT COMMAND
BALLISTIC RESEARCH LABORATORY
ABERDEEN PROVING GROUND, MARYLAND

Destroy this report when it is no longer needed.
Do not return it to the originator.

Secondary distribution of this report by originating or sponsoring activity is prohibited.

Additional copies of this report may be obtained from the National Technical Information Service, U.S. Department of Commerce, Springfield, Virginia 22161.

The findings in this report are not to be construed as an official Department of the Army position, unless so designated by other authorized documents.

The use of trade names or manufacturers' names in this report does not constitute indorsement of any commercial product.

REPORT DOCUMENTATION PAGE

READ INSTRUCTIONS BEFORE COMPLETING FORM

1. REPORT NUMBER: CONTRACT REPORT ARBRL-CR-00381
2. GOVT ACCESSION NO.:
3. RECIPIENT'S CATALOG NUMBER:

4. TITLE (and Subtitle): Theoretical Study of Two-Phase Flow Associated With Granular Bag Charges

5. TYPE OF REPORT & PERIOD COVERED:

6. PERFORMING ORG. REPORT NUMBER:

7. AUTHOR(s): Paul S. Gough

8. CONTRACT OR GRANT NUMBER(s):

9. PERFORMING ORGANIZATION NAME AND ADDRESS:
Paul Gough Associates
P.O. Box 1614
Portsmouth, NH 03801

10. PROGRAM ELEMENT, PROJECT, TASK AREA & WORK UNIT NUMBERS:
RDT&E 1L161102AH43

11. CONTROLLING OFFICE NAME AND ADDRESS:
USA Armament Research and Development Command
USA Ballistic Research Laboratory
ATTN: DRDAR-BL
Aberdeen Proving Ground, MD 21005

12. REPORT DATE: SEPTEMBER 1978

13. NUMBER OF PAGES:

14. MONITORING AGENCY NAME & ADDRESS (if different from Controlling Office):

15. SECURITY CLASS. (of this report): Unclassified

15a. DECLASSIFICATION/DOWNGRADING SCHEDULE:

16. DISTRIBUTION STATEMENT (of this Report)

Approved for public release; distribution unlimited.

17. DISTRIBUTION STATEMENT (of the abstract entered in Block 20, if different from Report)

18. SUPPLEMENTARY NOTES

19. KEY WORDS (Continue on reverse side if necessary and identify by block number)
Solid Propellant Gun
Pressure Wave
Computer Code
Interior Ballistics
Two Phase Flow
Numerical Integration

20. ABSTRACT (Continue on reverse side if necessary and identify by block number) (meg)

The two phase flow code NOVA is used to study the effect of neglect of the geometric details of the charge configuration by making psuedo-1D approximations of radial ullage. An axially uniform radial 1D flow assumption calculation showed all flow variables except porosity to be radially uniform. A calculation permitting mass transfer around and through the bag predicts ignition in front as well as in the rear of the charge, thereby, reducing the pressure wave amplitudes. A third calculation simulated a break in the center core (Cont'd)

20. Abstract (Cont'd)

igniter and subsequent burn through of the bag material separating zone increments. The obstruction little affected computed ballistics. Annular ullage was found to persist contrary to 1D models which assume radial uniformity.

Summary

The NOVA code is based on a quasi-one-dimensional model of the axial two-phase flow in a gun. The present study examines the extent to which the neglect of the initial details of the charge configuration is appropriate for the simulation of bag charges. Specifically, we appraise the probable influence of the bag material and of the circumferential ullage due to the fact that the bag does not fill the cross section of the tube.

In order to assess the radial structure of the flow, we first study the cylindrical flow induced in a long axially uniform propelling charge subjected to a uniform ignition stimulus at either the inside or the outside surface. The problem parameters are loosely based on the 155mm Howitzer with M30A1 propellant. The results show that a quasi-one-dimensional axial flow model may correctly assume all the flow variables to be uniform over the cross section of the tube except for the porosity. Circumferential ullage is persistent. Because it establishes a flow channel for the gas whose impedance is much less than that of the bed, the presence of circumferential ullage cannot be ignored.

Secondly, we examine the extent to which the circumferential ullage may affect the ballistic processes in the 155mm Howitzer. A baseline solution is generated by means of the present level NOVA code for a charge consisting of 10.9 kgm of seven perforation, M30A1 propellant ignited by a CBI base pad. The code is subsequently modified to recognize the presence of circumferential ullage. A second solution is generated which accounts for mass transfer around the bag, bag rupture and mass exchange between the bag and the ullage.

A comparison of the two solutions shows that the neglect of multi-dimensional features can result in a completely erroneous prediction of the manner of flamespreading. As expected, the presence of the circumferential ullage serves to reduce considerably the amplitude of ignition related axial pressure waves. However, the influence of a quasi-one-dimensional treatment of flamespreading is not found to be large in so far as the overall ballistic behaviour is concerned. The predictions of breech pressure history and muzzle velocity are found to be quite close for the two calculations.

Finally, we study the influence of an obstruction to the one-dimensional spreading of a convective flame in the same charge. Such an obstruction could occur, in general, due to the failure of a center core igniter to function properly since the flame would have to penetrate the cloth material separating zoned charge increments. We take the forward portion of the charge, 17% by weight, to be insulated for a predetermined length of time. Three values of the ignition delay due to obstruction are considered, based on available data.

Numerical solutions for these three cases, compared with the nominal or unobstructed case, reveal little influence of the flow obstruction on the ballistic behaviour. Although the amplitude of the first reverse gradient is increased as a consequence of the obstruction, damping quickly occurs and no significant increase in the subsequent pressure wave amplitudes is seen.

Accordingly, it is concluded that flow obstruction per se has an effect analogous to the inhibition of part of the charge and is not a probable direct cause of strong pressure waves. However, it is noted that strong compaction of the obstructed region can occur; therefore it is speculated that obstruction could lead to strong pressure waves if it produced fractures of the propellant grains.

Foreword

Contract DAAK11-77-C-0028 consisted of several Tasks all of which related to a quasi-one-dimensional two-phase flow model of the interior ballistics of guns known as the NOVA code. In accordance with the contractual requirements, the findings of Tasks I, II, and III were documented in three interim reports. The present report incorporates the contents of these interim reports and they should now be treated as obsolete.

Technical cognizance for the subject contract has been provided by Mr. C. W. Nelson, U.S. Army Ballistic Research Laboratories, DRXDR-PR

TABLE OF CONTENTS

LIST OF ILLUSTRATIONS

LIST OF TABLES

1.0 INTRODUCTION

The study which we describe in the present report is based on a computer code for the digital simulation of the interior ballistics of guns. The code, referred to herein as the NOVA code, incorporates an unsteady quasi-one-dimensional model of reacting two-phase flow. Its development, from the initial formulation of the theory to the most recent code level, can be traced in references 1 through 5.

The purpose of the present study is to assess the implications of certain assumptions which have been incorporated into the model. As such, the present study is part of a more comprehensive program of validation and critical evaluation of the NOVA code. The overall program has as its objective to determine which aspects of the code are most limiting in respect to its predictive capacity. The importance of such an investigation may be understood by reference to a recent paper by Horst et al[6]. The paper shows that the NOVA code is capable of matching the experimentally observed details of the pressure history in several guns using an uncompromized data base. However, in certain other cases of equal practical interest agreement may be obtained between theory and experiment only after manipulating the data base in an essentially ad hoc fashion.

---

1. *Gough, P.S. and Zwarts, F.J.*
   "Theoretical Model for Ignition of Gun Propellant"
   Final Report, Part II, Contract N00174-72-C-0223 *December 1972*

2. *Gough, P.S.*
   "Fundamental Investigation of the Interior Ballistics of Guns"
   Final Report, Contract N00174-73-C-0501 *1974*

3. *Gough, P.S.*
   "The Flow of a Compressible Gas Through an Aggregate of Mobile, Reacting Particles"
   Ph.D Thesis McGill University *1974*

4. *Gough, P.S.*
   "Computer Modelling of Interior Ballistics"
   Final Report Contract N00174-75-C-0131 *1975*

5. *Gough, P.S.*
   "Numerical Analysis of a Two-Phase Flow with Explicit Internal Boundaries"
   Final Report Contract N00174-75-C-0259 *1977*

6. *Horst, A.; Nelson, C. and May, I.*
   "Flame Spreading in Granular Propellant Beds: A Diagnostic Comparison of Theory to Experiment"
   Proc. AIAA/SAE 13th Joint Propulsion Conference
   Orlando, Florida *July 1977*

Accordingly, the predictive capacity of the NOVA code may be described as very good in certain cases, principally involving cased charges, and very poor in other cases, principally involving bagged charges.

In subsequent subsections of this introduction we provide a more detailed statement of the objectives of the present enquiry, some additional background discussion concerning the NOVA code and, finally, a description of the technical approach taken to satisfy the objectives.

In chapter 2.0 we present a statement of the governing equations for the code, without derivation. We comment briefly on the method of solution and we note those corrections and revisions which have been found necessary on the basis of computational experience with the version of the code described in reference 5. Chapters 3.0, 4.0 and 5.0 each present a discussion of a particular investigation of one aspect of the code. Chapter 6.0 contains an overall discussion of these findings and leads to the conclusions and recommendations which are summarized in chapters 7.0 and 8.0 respectively.

1.1 Objectives of Study

In general we may state the overall objective of the present study as an attempt to assess the implications, in the context of a particular bag propelling charge, of certain assumptions inherent to the NOVA code. The particular area of interest here relates to the representation of the flow within the gun as quasi-one-dimensional and the absence of a representation of the influence of bag material.

We may enumerate our specific objectives as follows.

[1] We assess the radial structure of the flow in a gun by examining the cylindrical flow induced in a propelling charge having axially uniform properties. The scope of this study, described in chapter 3.0, is such as to provide information concerning:

(a) The influence of the divergence term on flamespreading.
(b) The effect of annular ullage on flamespreading due to a center core igniter and on the radial velocity acquired by the bed prior to impact against the tube.
(c) The extent to which it is correct to assume uniformity of the flow properties over the cross section of the tube as is done in a quasi-one-dimensional model of axial flow.
(d) The nature of the flamespreading induced by an external ignition stimulus.

[2] We assess the extent to which the quasi-one-dimensional approximation embedded in the NOVA code limits its predictive capacity in respect to a particular bag charge. This is done by extending the model to recognize, in an approximate manner, that the propellant is initially contained within a bag, that the bag may serve as a flow impediment and that there exists, initially, a region of ullage between the cylindrical surfaces of the bag and the tube in addition to that in the breech and mouth of the chamber. This study is presented in chapter 4.0.

[3] Finally, we assess the ballistic consequences of an obstruction to quasi-one-dimensional flamespreading. Such an obstruction may be visualized as arising in a charge consisting of two or more zoned bags and for which the center core igniter fails to function. The axially propagating convective deflagration wave will be impeded by the bag material as it attempts to pass from one zone increment to the other.

1.2 Background Information

In order to understand the choice of topics considered in the present study, we summarize briefly the content of the NOVA code and then comment on the limitations imposed by the scope of phenomenological modeling. We also note some of the other topics which have either been evaluated or are in the process of being evaluated.

The NOVA code is based on a quasi-one-dimensional formulation of the two-phase flow defined by the solid propellant and its products of combustion. The balance equations which describe the evolution of the macroscopic averages of the state variables incorporate the exchanges of mass, momentum and energy that stem from combustion, heat transfer and interphase drag. These latter processes are modeled by means of empirical correlations which relate the complex boundary layer phenomena to the bulk or average properties of the flow. For example, the steady state combustion process is assumed to have the usual exponential dependence on pressure. In general, it is assumed that the steady state formulation is adequate; however, the code contains a theoretical extension from the steady state domain by means of the transient analysis of Zel'dovitch[7]. Similarly, the interphase drag is ordinarily represented by the steady state correlations of Ergun[8] and of Anderssen[9] although the code does contain a representation of the virtual mass effect[10]. However, the interphase heat

---

7. *Summerfield, M.; Caveny, L.H.; Battista, R.A.; Kubota, N.; Gostintsev, Yu, A. and Isoda, H.*
"*Theory of Dynamic Extinguishment of Solid Propellants with Special Reference to Non Steady Heat Feedback Law*"
J. Spacecraft & Rockets v.8, N.3 1971

8. *Ergun, S.*
"*Fluid Flow Through Packed Columns*"
Chem. Eng. Progr. vol.48 p89 1952

9. *Anderssen, K.E.B.*
"*Pressure Drop in Ideal Fluidization*"
Chem. Eng. Sci. vol.15 pp276-297 1961

10. *Batchelor, G.K.*
"*An Introduction to Fluid Mechanics*"
Cambridge University Press 1970

transfer is represented only in terms of the steady state correlations of Denton[11] and Gelperin and Einstein[12].

Granular stresses in excess of the ambient gas pressure are assumed to arise in the solid phase when sufficiently packed. These are represented according to steady state compactibility measurements. The compactions are taken to be irreversible so that bed expansion does not occur as a consequence of elastic rebound.

The action of the primer is represented by a predetermined rate of injection of energetic gas. However, the flamespreading which is driven by the concomitant axial convection is deduced from the two-phase flow by reference to the interphase heat transfer, the surface temperature of the solid phase as deduced from the unsteady heat conduction equation and a criterion for ignition based on the surface temperature.

Internal boundaries defined by discontinuities in porosity which occur at the interface between the mixture and a region of ullage or between bags are represented explicitly within the code. A shock may be recognized and represented in the forward region between the propellant and the projectile base. The forward external boundary is characterized by the complex motion of an aggregate of filler and/or spacer materials. Both external boundaries may be gas permeable.

Since the governing equations for the code comprise a system of non linear partial differential equations, the method of solution is based upon an explicit finite difference scheme supplemented by the method of characteristics at both the external and the internal boundaries.

As part of the overall enquiry into the code we have assessed the influence of the method of solution. These results have been reported elsewhere[13,14] and will not be repeated here. Some preliminary results

---

11. *Denton, W.H.*
"General Discussion on Heat Transfer"
Inst. Mech Eng. and Am. Soc. Mech. Eng. *London* *1951*

12. *Gelperin, N.I. and Einstein, V.G.*
"Heat Transfer in Fluidized Beds"
Fluidization, edited by J.F.Davidson and D. Harrison
Academic Press *1971*

13. *Gough, P.S.*
"The Influence of an Implicit Representation of Internal Boundaries on the Ballistic Predictions of the NOVA Code"
Proc. 14th Jannaf Combustion Meeting *1977*

14. *Gough, P.S.*
"The Influence of the Representation of Internal Boundaries on the Ballistic Predictions of the NOVA Code"
Final Report Task I Contract N00174-77-C-0103 *1977*

of an assessment of the importance of transient burning have also been reported[15]. Finally, the influence of grain fracture, a phenomenon not represented in the code, has been studied[16]. As expected, grain fractures were found to be very influential in respect to the formation of pressure waves.

When we consider the limitations of the code we see that an obvious omission is the neglect of multi-dimensional flow. Whereas the axial distribution of the propellant is sharply resolved, the details of the radial distribution are lost. Moreover, the influence of a bag is completely absent from the model. No assessment may be made of its confining influence, its rupture or of its interference with flamespreading.

The assumption that the flow is uniform on each cross section of the tube seems reasonable for many applications of interest including base ignited small arms propelling charges and case charges in which the primer is short and good radial confinement of the charge is provided. However, in the case of bag charges, the assumption of one-dimensional behaviour is hard to justify.

The typical bag charge rests on the bottom of the chamber, is surrounded by ullage both circumferentially and axially and is ignited by a stimulus due to a center core charge of black powder contained in a nitrocellulose tube. The circumferential or annular ullage may be extremely influential during the early stages of the interior ballistic cycle since gas may flow around the charge and the path of flamespreading is thereby modified. In order to apply a one-dimensional model to a bag charge one has to suppose that fluidization occurs very early and that the radial ullage is quickly eliminated.

Present understanding of the causes of pressure waves in guns is essentially based on the idea of inhomogeneity. That is to say, the causes of ignition transients are associated with the localization of the propellant distribution, so that axial ullage is present, or to the localization of the ignition stimulus or to the interplay between these effects. But the importance of these mechanisms is inherently associated with the low permeability of the granular bed since it is this attribute which prevents rapid equilibration of the pressure throughout the chamber. The presence of radial ullage will therefore be most influential since it provides a mechanism whereby axial pressure gradients can be minimized through mass transfer.

---

15. *Nelson, C.W., Robbins, F.W. and Gough, P.S.*
"Predicted Effects of Transient Burning in Gun Flamespreading"
Proc. 14th Jannaf Combustion Meeting 1977

16. *Horst, A.W., May, I.W. and Clarke, E.V. Jr.*
"The Missing Link Between Pressure Waves and Breechblows"
Proc. 14th Jannaf Combustion Meeting 1977

On the other hand, the inhibition of flamespreading by the bag material may contribute to inhomogeneity; it may well act to decrease the axial permeability of the charge.

We mention in this context the case of the Navy 76mm malfunction. Although bag material was not present in this charge, it was believed[17] that the cause of the malfunction was the flow obstruction associated with the rupture of the bag of flash suppressant and the dispersal of the grains of salt within the forward part of the charge. It was established that the deliberate introduction of the salt in the manner believed to have occurred during the malfunction produced greatly increased pressure wave phenomena by comparison with the nominal case.

The presence of flow inhibition leads to two closely related effects. Since the gas cannot penetrate into the obstructed region, the isolated portion of the charge is subjected to high pressure over the interface with the external gas. This will result in large granular stresses due to compaction of the isolated region and, if the loads are imbalanced as in the case of a one-dimensional flow, the isolated region may be strongly accelerated. Accordingly, the grains in the isolated region may be propelled to a significant velocity prior to impacting against one of the external boundaries of the chamber. The impact itself is associated with two processes which can introduce a strong reversed gradient. The sudden stagnation of the isolated region as it impacts will produce a compression wave in the gas. If the impact occurs at the forward end of the chamber, the amplitude of the compression wave may be sufficient to reverse the pressure gradient. Secondly, if the stresses experienced by the solid phase are sufficiently high, fracture may occur resulting in a locally increased burning surface which will favor a reversed pressure gradient.

In the present report we confine our attention to the influence of flow obstruction on the motion and compaction of the isolated region. The influence of grain fracture is not taken into account.

---

17. Olenick, P.J. Jr.
"Investigation of the 76mm/62 Caliber Mark 75 Gun Mount Malfunction"
NSWC/DL TR-3144 October 1975

We conclude this discussion of background information by noting that several other two-phase models of interior ballistics have been advanced[18-22]. With the exception of the works by Fisher et al, all of these other models have also been based on a one-dimensional formulation of the flow and have neglected the possible influence of bag material. The works of Fisher et al pay considerable attention to the presence of annular ullage and, in certain cases, to the influence of the bag material. We comment further on the relationship between Fisher's work and the studies presented here when we describe our technical approach, in the next section.

1.3 Approach and Findings

The technical approach taken to investigate the radial structure of the flow is extremely straightforward, involving only minor modifications to the NOVA code. We pose the problem as one of obtaining solutions to the governing equations for one-dimensional flow with cylindrical symmetry. Accordingly, the balance equations are dependent on time and the radial coordinate alone. There appears in the continuity and energy equations a term reflecting the divergence of the cylindrical flow. In fact, this term is formally equivalent to the existing area dependence term which is incorporated in the present code. Thus it is possible to generate a cylindrical flow in the present level of the NOVA code by manipulation of the input alone. However, some coding changes would still be required to treat properly the singularity which arises at the center-

---

18. *Fisher, E.B. and Graves, K.W.*
"Mathematical Model of Double Base Propellant Ignition and Combustion in the 81mm Mortar"
CAL Report DG-3029-D-1 1972

19. *Fisher, E.B. and Trippe, A.P.*
"Development of a Basis for Acceptance of Continuously Produced Propellant"
CALSPAN Report VQ-5163-D-1 1973

20. *East, J.L. and McClure, D.R.*
"Projectile Motion Predicted by a Solid/Gas Flow Interior Ballistic Model"
Proc. 10th Jannaf Combustion Meeting 1973

21. *Krier, H.; van Tassel, W.F.; Rajan, S. and VerShaw, J.*
"Model of Flame Spreading and Combustion Through Packed Beds of Propellant Grains"
Technical Report AAE74-1, University of Illinois at Urbana - Champaign 1974

22. *Kuo, K.K.; Koo, J.H.; Davis, T.R. and Coates, G.R.*
"Transient Combustion in Mobile Gas-Permeable Propellants"
ACTA ASTRONAUTICA Vol.3 No.7-8 pp574-591 1976

line. This being the case, we simply added the cylindrical divergence term in the appropriate places.

In order to assess the importance of the cylindrical divergence term we perform an analysis of a planar and a cylindrical two-phase flow having the same nominal characteristics. We find that qualitatively the two flows are very similar. As would be expected, however, the rate of flame-spreading in the cylindrical flow is less than in the planar flow, the ignition stimulus being located at the center of the charge.

This baseline comparison is performed for a charge having interior ullage corresponding to the dimensions of a typical 155mm Howitzer center core igniter. No external ullage is considered, the charge being in contact with the external boundary. Subsequently, we consider the influence of having an external gap of 1.27 cm and 2.54 cm surrounding the charge. These figures bracket the observed values of radial ullage in a typical 155mm Howitzer at the 12 o'clock position. The influence of the bag is ignored. Particular attention is given, in these calculations, to the radial pressure gradient as a function of time and to the radial expansion velocity of the bed. Large grain velocities are not observed, the maximum being approximately 10 m/sec. This value may be compared with the axial velocities of typically 250 m/sec which have been observed in Navy 5-inch guns[23].

Because it is easy to envisage cases when the ignition stimulus will occur at the outside of the charge, we present two calculations involving a 2.54 cm external gap and no internal ullage with primer venting in the exterior. This situation would represent the response of a charge in a gas permeable bag with no center core igniter and an ignition stimulus due to a base bad whose products of combustion flow around the bag.

By analogy with the linear wave propagation problem, one might expect a significant reflected wave due to the convergence of the convective flame on the centerline. Such is not the case. The solutions have even less radial structure in the pressure distributions than those determined on the basis of an internal ignition stimulus. Naturally, the grain velocities are very small.

Perhaps the most important finding of chapter 3.0 relates to the persistence of the annular ullage. We find that all the flow variables become essentially uniform over the cross section with the exception of the porosity. The importance of this point becomes clearer when we turn to chapter 4.0 in which the influence of annular ullage is assessed.

In order to discuss the technical approach taken in chapter 4.0 we refer to figure 1.3.1 in which we depict schematically the actual configuration of a typical Army bag propelling charge together with one-dimensional and two-dimensional axisymmetric representations. In actuality the charge rests on the bottom of the chamber, its distance

---

23. *Culbertson, D.W. and DeVost, V.F.*
"Instrumentation Techniques and the Application of Spectral Analysis and Laboratory Simulation to Gun Shock Problems"
Shock and Vibration Bulletin, 42, part 5, pp47-59 January 1972

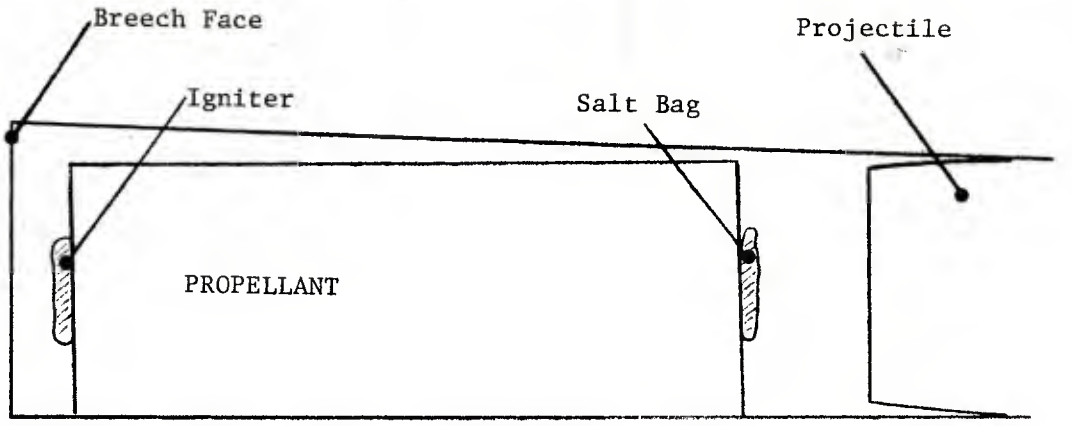

(a) Actual Bag Configuration

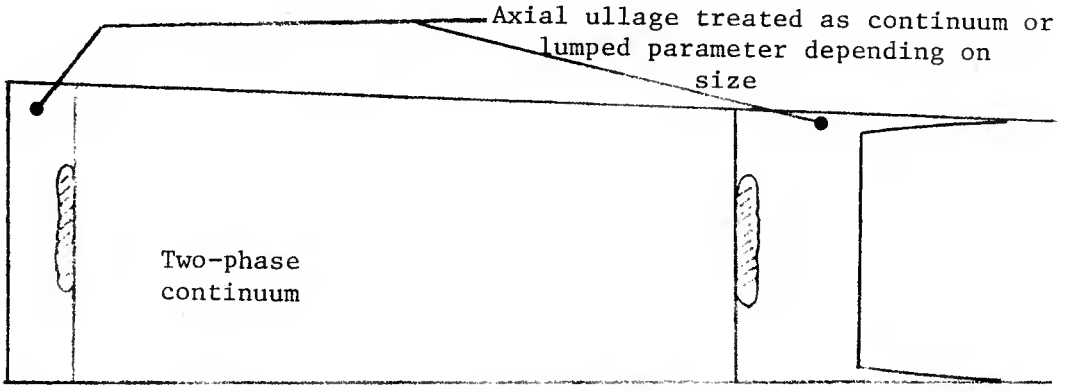

(b) Quasi-One-Dimensional Representation

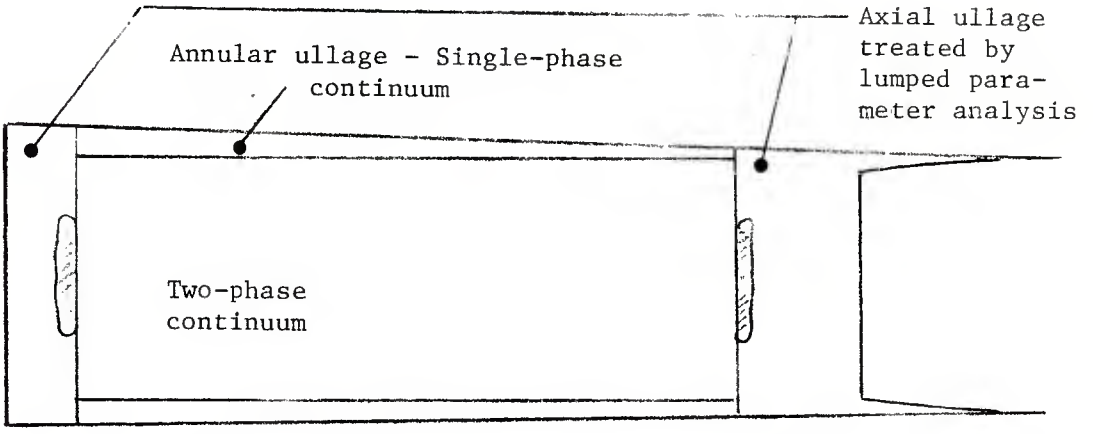

(c) Quasi-Two-Dimensional Representation

Figure 1.3.1 Schematic Representations of Bag Charge Configuration

from the mushroom being controlled by spacing pins. The distribution is therefore not axisymmetrical and the flow possesses three-dimensional characteristics. The base pad is ignited by a stimulus transmitted through the mushroom. The products of combustion flow partially into the bag and partially around the charge as a consequence of the radial ullage. The bag material may have a variable permeability since regions of the circumferential portion may be lined with lead. Accordingly, the igniter gas may enter the bag in more than one location and flamespreading may be very complex.

The quasi-one-dimensional analysis of this problem necessarily neglects the influence of radial ullage. The charge is depicted as uniformly distributed between its axial delimiters. Or, possibly, the variation in porosity associated with the varying cross section is taken into account. However, the topology of the flamespreading process is simplified considerably. Ignition must occur in the breech and spread monotonically towards the mouth of the chamber.

Finally we consider what we will call a quasi-two-dimensional representation of the propelling charge. The charge is represented by an axisymmetric distribution. However, the presence of the axial ullage is recognized so that the model may incorporate mass transfer around the charge.

The quasi-one-dimensional representation reflects the present status of the NOVA code. This version is used to generate a baseline solution for the 155mm Howitzer. Then the magnitude of the error associated with the neglect of multidimensional flow is assessed by means of the quasi-two-dimensional model, the analysis of which may be summarized as follows.

The chamber is divided into four regions. The end regions correspond to ullage and are treated according to a lumped parameter formulation. The two remaining regions are coaxial and consist of the two-phase core flow and the region of radial ullage which surrounds the bag. Each of these is treated according to a quasi-one-dimensional continuum analysis.

The behaviour of the bag is taken to correspond to that of a flexible, impermeable membrane until such a time as the pressure within the bag exceeds that outside by 0.035 Mpa. At that point, the bag is assumed to rupture and mass transfer between the bag and the ullage must be taken into account. These considerations apply only to the radial boundary. The axial boundaries are treated as though the end closures were always permeable. The assumptions on which the present calculation rests therefore correspond to a charge wrapped in a permeable bag which has a lead foil liner around the circumference.

The analysis is quasi-two-dimensional in the sense that an explicit representation is made of an internal radial boundary. In essence the present approach is very close to that pioneered by Fisher[19]. However, we do not find it necessary to introduce the concept of "pseudoholes".

The radial mass transfer follows from the conditions of adiabatic flow. Moreover, we consider the compaction of the charge due to excess pressure outside the unruptured bag and, once the bag is ruptured, the motion of the radial boundary is deduced from the mass transfer relationship.

The predictions of flamespreading differ considerably in the two calculations. The quasi-two-dimensional calculation predicts ignition to occur first in the breech as does the one-dimensional calculation. But whereas the one-dimensional calculation predicts a monotonic spreading of the flame from the breech to the mouth of the chamber, the quasi-two-dimensional calculation predicts ignition at the front due to convection around the charge and two flame fronts are seen, moving to the center of the charge. The pressure gradient in the chamber is much alleviated by the presence of the annular ullage; however, the influence of the ullage on the breech pressure history is not found to be large.

It is emphasized, however, that particular aspects of the foregoing are strongly influenced by the choice of the constitutive laws for the bag. Thus, had we taken the bag to be permeable and included the convective heating due to radial heat transfer, yet another flamespreading path would have been opened. The importance of the bag material as an element of the ignition system is therefore emphasized and we now turn to the discussion of the bag as an obstruction to flamespreading.

In order to study this topic it is necessary to solve three problems, namely: establish a numerical procedure for the determination of the solution during the period in which the flow obstruction is present; establish a likely range of values of the flamespreading delay associated with the obstruction; and finally, establish a procedure for the transformation of the internal boundary condition from one of obstruction to one of unimpeded gas flow. We discuss our approach to each of these problems successively. Complete details are given in chapter 5.0.

In order to establish a numerical procedure we decided to neglect changes in the state of the gas phase in the insulated region and to analyze the response of the propellant according to the lumped parameter formulation previously developed to simulate compactible filler materials[5]. The neglect of changes in the gas phase in the insulated region during this period is expected to be an excellent assumption.

No appreciable convection of the gas in the insulated region is expected since both phases are initially at rest, there is no combustion and the boundaries of the region are impermeable. Accordingly, changes in the state of the gas phase will be due solely to the compaction of the solid propellant and will therefore be small.

Concerning the range of ignition delays due to obstruction we proceed as follows. The study of Fisher and Graves[18] provides some independent data for the time required to burn through bag material in a mortar together with a relationship between the heat transfer rate and the pressure of the attacking jet. These are used to extrapolate to our own

problem assuming similar material characteristics. A probable nominal delay of 1 msec is deduced in this manner. Three values are selected corresponding approximately to nominal, one half nominal and twice nominal. These values are slightly modified to reflect available solution levels as previously saved on disc, coincidence with a physically interesting stage of the interior ballistic process and finally, to incorporate a delay for flamespreading through the insulated region following rupture of the bag.

By physically interesting stages of the interior ballistic process we mean the following. It is found that the insulated region is blown forward, separating from the remainder of the propelling charge. It acquires a significant velocity and eventually impacts against the base of the projectile becoming extremely compacted in the process. Subsequently, the remainder of the charge catches up to the forward region and impacts against it. The three values of ignition delay that we use are such as to allow bag rupture first as the forward region is being accelerated strongly, secondly just after impact against the projectile and thirdly, just after the two regions of propellant have again made contact.

The third problem relates to the analysis of the flow directly following rupture. Physically, we would expect rupture to be a rather gradual process so that the boundary conditions would change from impermeable to fully permeable over some small but finite period. The importance of such a finite period of relaxation is that it permits the flow within the previously insulated region to adjust, thereby alleviating the numerical difficulties. However, given the nature of the present enquiry, we did not consider it worthwhile to study this relaxation and the subsequent spreading of the flame into the insulated region. The region in question is found to be quite short, no more than 10 cms, at the time of rupture. Accordingly, flamespreading is expected to require no more than 0.2 msec and therefore represents a detail whose fineness is comparable to the uncertainty in rupture delay. Thus we assume that at the instant of rupture, the previously insulated material is uniformly ignited and pressurized throughout.

The nominal configuration selected for this study is the same as that considered in chapter 4.0. It is found that the interior ballistic cycle for this charge is remarkably tolerant of having a forward region, corresponding to 17% of the charge by weight, insulated for as much as 2 msec. A significant difference is seen in the first minimum of the history of pressure difference taken between the mouth and breech of the chamber. However, the subsequent events are changed only slightly. It is expected that our findings would have been different had we considered the possibility of grain fracture since the insulated region strikes the base of the projectile at a much higher velocity than is observed in the nominal case.

2.0 DISCUSSION OF THE NOVA CODE

The introduction has already provided some discussion of the NOVA code. We have summarized the theory as a system of partial differential equations which express, in a macroscopic sense, the balances of mass, momentum and energy together with empirical constitutive laws for the interphase transport phenomena. In the present chapter we have two objectives. First of all, we wish simply to state those governing equations which are relevant to the present enquiry. Secondly, we wish to note such corrections and modifications as have been found necessary since the code was last documented[5].

The governing equations are summarized in section 2.1. In section 2.2 we discuss the corrections and modifications. These consist principally of changes in the numerical procedures which have been found necessary in order to avoid breakdown of computation or to speed up the convergence of algorithms. However, we also provide some discussion of the influence of the covolume on the mass transfer relationships used to analyze the boundary conditions. As we have noted previously[14], the current formulation[5] neglects the influence of the covolume. This approximation is not believed to introduce any significant errors in the numerical results, particularly when uncertainties in other constitutive laws are taken into account. However, we have previously treated this approximation as though it were exact[4,5], stating that the covolume did not influence the mass transfer relationships at all. This is simply untrue; reference 4 contains an error of analysis, the results of which have been preserved in reference 5. Our purpose, in repeating the discussion of reference 14 in the present report is simply to ensure recognition of the error by Army as well as Navy users of the code.

2.1. Governing Equations and Method of Solution

We state the balance equations in section 2.1.1 and the relevant constitutive laws in 2.1.2. In 2.1.3 we comment on the boundary and initial conditions while describing the method of solution. A more complete statement of the mass transfer relationships is given in section 2.2 where we also address the influence of the covolume. It should also be noted that we incorporate a minor correction to the terms in the gas phase balance equations which relate to the density of the condensed phase of the primer gas, a source term.

2.1.1 Balance Equations

The model assumes only piecewise continuity of the state variables. The computational domain is divided into regions which are separated by boundaries internal to the flow and whose motion is part of the numerical solution. Each such region is occupied either by a two-phase flow or by a single-phase, gas flow. The regions of single-phase flow correspond to axially distributed ullage and are analyzed according to either a continuum or a lumped parameter formulation depending on their size relative to the computational domain as a whole. In addition, the right hand boundary of the flow is assumed to correspond with the first of any compactible filler materials which may be interposed between the propelling charge and the projectile in accordance with the demands of packaging.

Here we simply state the balance equations for the two-phase flow. Those for the continuum representation of ullage follow from the two-phase flow equations in the limit as the porosity tends to unity. Those for the lumped parameter representation follow in turn by an integration of the continuum laws, the state variables being viewed as spacewise uniform. Finally, we do not consider the presence of filler materials in any of the present calculations. However, the formulation previously developed for the filler elements is adopted, in chapter 5.0, for another purpose. Accordingly, in chapter 5.0 we present a discussion of the relevant equations. Likewise, chapter 4.0 contains some discussion of the lumped parameter formulation of regions of ullage. Both chapters 3.0 and 4.0 contain statements of the balance equations for two-phase flow in circumstances somewhat different from those in which the equations were originally formulated[5]. Hence the statement given here serves for comparative purposes.

The balance equations for the two-phase flow do not include a statement of balance of energy for the solid phase. The solid phase is presumed to consist of packed or dispersed grains which are individually incompressible, although they are susceptible to deformation. Accordingly, the bulk or average solid phase temperature is uncoupled from the flow. Only the surface temperature of the solid phase is of interest, as governing the event of ignition, and this follows from the interphase heat transfer and the rate of conduction according to Fourier's law.

We state the balance equations in terms of a convective coordinate scheme. If the mixture occupies the physical region $[z_L(t), z_R(t)]$ we introduce the quantity ζ which maps this region onto the unit line:

$$\zeta = (z - z_L(t))/z_B(t) \qquad 2.1.1.1$$

where $z_B = z_R - z_L$

We also put:

$$\eta = \dot{z}_I + \zeta \dot{z}_B \qquad 2.1.1.2$$

In this coordinate frame, the balance equations for quasi-one-dimensional flow through a duct of cross sectional area A(z) may be written as follows:

Balance of Mass of Gas Phase

$$\frac{\partial \varepsilon\rho}{\partial t} + \frac{u-\eta}{z_B}\frac{\partial \varepsilon\rho}{\partial \zeta} + \frac{\varepsilon\rho}{Az_B}\frac{\partial}{\partial \zeta} Au = (1-\varepsilon)\rho_p{}^2 \frac{S_p}{M_p}\dot{d} + \psi\left(1 - \frac{\varepsilon\rho}{\rho_{IG}}\right) \qquad 2.1.1.3$$

Balance of Momentum of Gas Phase

$$\varepsilon\rho\left[\frac{\partial u}{\partial t} + \frac{u-\eta}{z_B}\frac{\partial u}{\partial \zeta}\right] + \frac{\varepsilon g_o}{z_B}\frac{\partial p}{\partial \zeta} = -f_s + (1-\varepsilon)\rho_p{}^2\frac{S_p}{M_p}\dot{d}(u_p - u) - \psi u \qquad 2.1.1.4$$

Balance of Energy of Gas Phase

$$\varepsilon\rho\left[\frac{\partial e}{\partial t} + \frac{u-\eta}{z_B}\frac{\partial e}{\partial \zeta}\right] + p\left[\frac{\partial \varepsilon}{\partial t} + \frac{u-\eta}{z_B}\frac{\partial \varepsilon}{\partial \zeta}\right] + \frac{\varepsilon p}{Az_B}\frac{\partial Au}{\partial \zeta}$$

$$= \frac{f_s}{g_o}(u - u_p) - (1-\varepsilon)\rho_p\frac{S_p}{M_p}q_s$$

$$+ (1-\varepsilon)\rho_p^2\frac{S_p}{M_p}\dot{d}\left[e_p - e + \frac{p}{\rho_p} + \frac{(u-u_p)^2}{2g_o}\right]$$

$$+ \psi\left[e_{IG} + \frac{P}{\rho_{IG}}(1-\varepsilon) - e + \frac{u^2}{2g_o}\right] \qquad 2.1.1.5$$

Balance of Mass of Solid Phase

$$\frac{\partial \varepsilon}{\partial t} + \frac{u_p-\eta}{z_B}\frac{\partial \varepsilon}{\partial \zeta} - \frac{(1-\varepsilon)}{Az_B}\frac{\partial}{\partial \zeta}Au_p = (1-\varepsilon)\rho_p\frac{S_p}{M_p}\dot{d} + (1-\varepsilon)\frac{\psi}{\rho_{IG}} \qquad 2.1.1.6$$

Balance of Momentum of Solid Phase

$$\rho_p(1-\varepsilon)\left[\frac{\partial u_p}{\partial t} + \frac{u_p-\eta}{z_B}\frac{\partial u_p}{\partial \zeta}\right] + (1-\varepsilon)\frac{g_o}{z_B}\frac{\partial p}{\partial \zeta} + \frac{g_o}{z_B}\frac{\partial}{\partial \zeta}(1-\varepsilon)R = f_s \qquad 2.1.1.7$$

Here we have used ε, porosity, ρ, gas phase density, p, gas phase pressure, e, gas phase internal energy, u, gas phase velocity, u_p, solid phase velocity, R, granular stress due to contact of particles, $\dot{d}$, rate of surface regression, ρ_p, solid phase density (a constant), S_p and M_p, surface area and mass of a single particle, e_p, chemical energy released in combustion of solid phase, ψ, rate of venting of primer gas, ρ_{IG}, density of condensed primer propellant, f_s the steady state velocity dependent interphase drag and q_s, the steady state interphase heat transfer.

By comparison with earlier work[5], it should be noted that the virtual mass effect and heat loss to the tube have been neglected and that we have allowed for only one granular specie.

2.1.2 Constitutive Laws

Certain of the constitutive laws need not be stated here since they are either not used in the present study or are obvious. In the latter category we include the form functions for M_p and S_p and the composition dependence of the molecular weight and specific heats of the gas phase.

The laws of interest here are as follows:

Covolume Equation of State for Gas Phase

$$e = \frac{p(1-b\rho)}{(\gamma-1)\rho} \qquad 2.1.2.1$$

where b is the covolume and γ the ratio of specific heats.

Granular Stress Law

We put:

$$\frac{D}{Dt_p}(1-\varepsilon)R = -\frac{\rho_p a^2}{g_o}\frac{D\varepsilon}{Dt_p} \quad , \quad \text{if } \frac{D\varepsilon}{Dt_p} \leq 0 \qquad 2.1.2.2$$

where D/Dt_p is the convective derivative along the average particle streamline and a is the rate of propagation of intergranular disturbances, assumed to obey:

$$a(\varepsilon) = \begin{cases} a_1\varepsilon_o/\varepsilon & , \quad \varepsilon \leq \varepsilon_o \\ a_1 \exp[-\kappa(\varepsilon-\varepsilon_o)], & \varepsilon_o < \varepsilon < \varepsilon_* \\ 0 & , \quad \varepsilon > \varepsilon_* \end{cases} \qquad 2.1.2.3$$

Here, a_1 is the value of a when $\varepsilon = \varepsilon_o$, the settling porosity, κ is referred to as the stress attenuation factor and ε_* is the porosity above which $a(\varepsilon) = 0$. In all the results presented here we have taken $\kappa = 45$ and $\varepsilon_* = \varepsilon_o + 0.1535$.

However, during unloading of the bed we set R = 0 independently of the porosity.

Interphase Drag Law

The interphase drag is assumed to obey:

$$\frac{f_s}{\frac{1-\varepsilon}{D_p}\rho|u-u_p|(u-u_p)} = \begin{cases} 1.75 & \varepsilon \leq \varepsilon_o \\ 1.75\left[\frac{1-\varepsilon}{1-\varepsilon_o}\frac{\varepsilon_o}{\varepsilon}\right]^{0.45} & \varepsilon_o < \varepsilon \leq \varepsilon_1 \\ 0.3 & \varepsilon_1 < \varepsilon \leq 1 \end{cases} \qquad 2.1.2.4$$

where $\varepsilon_1 = \left[1 + 0.02\left(\frac{1-\varepsilon_o}{\varepsilon_o}\right)\right]^{-1}$. Equation 2.1.2.4 is based on the correlations of Ergun[8] and Anderssen[9]. The quantity D_p is the effective particle diameter given by:

$$D_p = \frac{6M_p}{\rho_p S_p} \qquad 2.1.2.5$$

Interphase Heat Transfer

We assume that:

$$Nu_p = \begin{cases} 0.4\ Pr^{1/3}\ Re_p^{0.7}, & \varepsilon < \varepsilon_o \\ 0.4\ Pr^{1/3}\ Re_p^{2/3}, & \varepsilon \geq \varepsilon_o \end{cases} \qquad 2.1.2.6$$

where $Nu_p = hD_p/k_f$, $h = q_s/(T-T_p)$, $Re_p = \rho|u-u_p|D_p/\mu_f$, $Pr = 4\gamma/(9\gamma - 5)$. The gas phase thermal conductivity, k_f, and viscosity, μ_f, are determined at the film temperature $(T + T_p)/2$ according to a Sutherland-type law. Here T is the gas phase average temperature and T_p is the surface temperature of the solid phase.

Solid Phase Surface Temperature

Based on a cubic profile solution to the unsteady, one-dimensional heat conduction equation for the solid phase[24], we have:

$$T_p = T_{p_o} - \frac{2}{3}\frac{hH}{k_p^2} + \left[\left(T_{p_o} - \frac{2}{3}\frac{hH}{k_p^2}\right)^2 + \frac{4}{3}\frac{hTH}{k_p^2} - T_{p_o}\right]^{1/2} \qquad 2.1.2.7$$

---

24. Eckert, E.R.G. and Drake, R.M.
"Analysis of Heat and Mass Transfer"
McGraw-Hill 1972

Here, T_{p_o} is the initial surface temperature and H satisfies:

$$\frac{DH}{Dt_p} = \alpha_p q_s \qquad 2.1.2.8$$

where α_p is the thermal diffusivity of the solid phase.

Rate of Surface Regression

The rate of surface regression is assumed to obey the usual exponential law:

$$\dot{d} = B_1 + B_2 p^n \qquad 2.1.2.9$$

2.1.3 Method of Solution: Initial and Boundary Values

In fact, the numerical technique used to solve the equations is complex, due to the provisions for handling the internal boundaries[5]. Here we will confine ourselves to the briefest possible summary.

The initial conditions are straightforward; both phases are assumed to be at rest although their temperatures may differ. The state variables are all uniform initially, with the exception of the porosity which is only piecewise continuous. The external boundaries are assumed to be at most gas permeable. The left hand boundary is taken to correspond to the breech and is assumed to be stationary. The right hand boundary is, of course, mobile. At the internal boundaries the state variables are assumed to satisfy macroscopic forms of the jump conditions at a discontinuity and the granular stress $(1-\varepsilon)R$ is taken to be continuous. The transfer of gas is taken to be adiabatic and either isentropic or choked, depending on the pressure ratio.

Internal points of the finite difference mesh are updated by means of the MacCormack scheme[25], modified to recognize the nonhomogeneous terms and to use upstream differencing for the convective terms in the solid phase balance equations. Boundary points are updated by the method of characteristics supplemented by the solid phase balance equations based on one sided spacewise differences whenever insufficiently many characteristics occur as a consequence of the lack of total hyperbolicity of the balance equations.

---

25. MacCormack, R.W.
"The Effects of Viscosity in Hypervelocity Impact Cratering"
AIAA 7th Aerospace Sciences Meeting, Paper 69-354 1969

2.2 Corrections and Modifications to Mass Transfer Analysis

Since we will require a statement of the mass transfer relationships in order to discuss modifications to the analysis of the boundary between the two-phase flow and a region of ullage represented according to a lumped parameter formulation, we first address the influence of the covolume. Subsequently, by setting the covolume to zero we will have the relations currently used in the code. We will conclude with a comment on the analysis of flow reversal through an internal boundary which separates two continuum regions.

2.2.1 Influence of Covolume on Mass Transfer

We assume that the transfer from state 1 to state 2 is quasi-steady and adiabatic:

$$e_1 + \frac{p_1}{\rho_1} + \frac{u_1^2}{2g_o} = e_2 + \frac{p_2}{\rho_2} + \frac{u_2^2}{2g_o} \qquad 2.2.1.1$$

For a gas satisfying the covolume equation of state this may be written as:

$$c_p(T_1-T_2) + b(p_1-p_2) = \frac{u_2^2-u_1^2}{2g_o} \qquad 2.2.1.2$$

where c_p is the specific heat at constant pressure and is related to c_v, the specific heat at constant volume, according to $c_p = c_v + R_g$, R_g being the gas constant. If the transfer is isentropic we also have:

$$\frac{p_1}{p_2} = \left(\frac{T_1}{T_2}\right)^{\frac{\gamma}{\gamma-1}} \qquad 2.2.1.3$$

By substituting 2.2.1.3 into 2.2.1.2 and using the equation of state to determine the density we may express the isentropic rate of mass transfer through area A_e, at which state 2 occurs, as:

$$\dot{m}_{isen} = \frac{A_e\left\{\frac{2g_o}{\gamma-1}(\gamma R_g T_o)\left[1-\left(\frac{p_2}{p_o}\right)^{\frac{\gamma-1}{\gamma}}\right] + 2g_o b p_o\left[1-\frac{p_2}{p_o}\right]\right\}^{\frac{1}{2}}}{\frac{R_g T_o}{p_o}\left(\frac{p_o}{p_2}\right)^{\frac{1}{\gamma}} + b} \qquad 2.2.1.4$$

where T_o is the stagnation temperature and p_o the corresponding isentropic pressure.

The mass flow rate given by 2.2.1.4 may not be physically realizable, particularly if a throat or section of minimum area occurs between 1 and 2. We may regard $\rho_2 u_2$ as a function of p_2/p_o and seek the pressure ratio at which the flow per unit area is maximized. We put:

$$x = p_2/p_o \qquad 2.2.1.5$$

$$y = bp_o/R_g T_o \qquad 2.2.1.6$$

and find that the value of x at which the flow per unit area is maximized is given by:

$$2\left(1+\frac{\gamma-1}{\gamma}y\right)x^{\frac{1-\gamma}{\gamma}} - 2\frac{(\gamma^2-1)}{\gamma}y\,x^{\frac{1}{\gamma}} - (\gamma-1)y^2 x^{\frac{2}{\gamma}} = \gamma+1 \qquad 2.2.1.7$$

While the transcendental nature of 2.2.1.7 defies a closed form solution, particular results are quoted by Corner[26] for the case $\gamma = 1.25$. We have:

$$(p_2/p_o)_{crit} = \left(\frac{2}{\gamma+1}\right)^{\frac{\gamma}{\gamma-1}}\left[1-0.248y+0.117y^2+0(y^3)\right] \qquad 2.2.1.8$$

$$(\rho_2 u_2)_{crit} = \left[\frac{\gamma g_o}{R_g}\left(\frac{2}{\gamma+1}\right)^{\frac{\gamma+1}{\gamma-1}}\right]^{\frac{1}{2}}\frac{p_o}{\sqrt{T_o}}\left[1-0.224y+0.104y^2\right] \qquad 2.2.1.9$$

Corner notes that even at a pressure of 350 Mpa, the covolume correction to the critical flow rate only amounts to about 6.5%

---

26. Corner, J.
"Theory of the Interior Ballistics of Guns"
New York, John Wiley and Sons, Inc. 1950

We neglect the influence of the covolume whereupon the mass transfer is given by:

$$\dot{m} = \min (\dot{m}_{isen}, \dot{m}_{crit})$$

where:

$$\dot{m}_{isen} = A_e \sqrt{\frac{\gamma g_o}{R_g}} \frac{P_2}{\sqrt{T_o}} \left(\frac{P_o}{P_2}\right)^{\frac{\gamma-1}{2\gamma}} \left\{\frac{2}{\gamma-1}\left(\left(\frac{P_o}{P_2}\right)^{\frac{\gamma-1}{\gamma}} - 1\right)\right\}^{\frac{1}{2}} \qquad 2.2.1.10$$

$$\dot{m}_{crit} = A_* \left[\frac{\gamma g_o}{R_g}\left(\frac{2}{\gamma+1}\right)^{\frac{\gamma+1}{\gamma-1}}\right]^{\frac{1}{2}} \frac{P_o}{\sqrt{T_o}} \qquad 2.2.1.11$$

and A_* is the throat area between 1 and 2. It should also be noted that 2.2.1.10 was stated incorrectly on page 69 of reference 5, although it was programmed correctly into the NOVA code.

2.2.2 Treatment of Ullage

As we have stated in the introduction, regions of ullage are described according to either a continuum or a lumped parameter formulation on the basis of their size relative to the computational domain as a whole. We found it necessary, however, in certain cases to revise this approach and to retain a lumped parameter formulation even when the region of ullage is quite large.

We have found that during flamespreading a sonic condition can arise at the internal boundary between the mixture and a large region of ullage. This is due to the rapid rise in pressure within the bed as the convective flame approaches the boundary and the inability of the pressure in the ullage to keep pace. This condition exists for only a short time but it represents a computational barrier if a continuum representation is made of the ullage since the code does not provide for a sonic condition in this case.

Accordingly, the mach number at the internal boundary is checked at each stage of the calculation. If it becomes large we effect a lumped parameter representation of the ullage independently of its size. Equations 2.2.1.10 and 2.2.1.11 form the basis for determining the rate of mass transfer.

2.2.3 Treatment of Internal Boundary Between Continua

The algorithm which we have previously developed[5] to analyze mass transfer through an internal boundary has been found to be very inefficient when the flow is undergoing reversal. However, in such a case the thermodynamic variables are very nearly continuous across the boundary. Therefore, if the mach number is sufficiently low, we treat the pressure and internal energy as continuous and deduce the jump in velocity of the gas phase from the jump in porosity.

3.0 CYLINDRICAL TWO-PHASE REACTING FLOW

In this chapter we study the cylindrical flow induced in a propelling charge having axially uniform properties. Such a condition may be envisaged as occurring in a chamber length charge subjected to the stimulus of a uniformly venting center core igniter, prior to the onset of significant motion of the projectile. The scope of the study is such as to permit answers to the following questions:

a) What is the influence of the divergence term? This question is answered by comparing the cylindrical flow with a related planar flow. Particular interest is given to the rate of flamespreading.

b) What is the effect of annular ullage, or the initial presence of a gap between the propelling charge and the tube? This question is answered by determining solutions for three values of the initial gap which effectively bracket the range observed in actual propelling charges. Particular interest is given to the radial velocity acquired by the edge of the bed prior to impact against the tube.

c) To what extent is it correct to assume uniformity of the flow over the cross section as is done in a quasi-one-dimensional formulation of the axial flow? This point is investigated principally by reference to the structure of the pressure and porosity distributions at various times.

d) How does an external ignition stimulus compare with an internal stimulus? We answer this question by comparing a solution for a simulated center-core igniter with two in which the igniter gas is dumped into a region of annular ullage surrounding the propelling charge.

The analysis and code modifications necessary to treat this topic are contained in section 3.1. In section 3.2 we discuss the data bases for the various problems which we presently solve. The solutions are given in section 3.2 through 3.5. A general discussion of the findings of this chapter in relation to the other studies considered in this investigation is contained in chapter 6.0.

3.1 Analysis

As we have stated in the introduction, the analysis required by this particular study is extremely straightforward. We have only to recast the balance equations slightly to reflect cylindrical rather than planar symmetry. Thus we consider, in the next two sections, the forms of the balance equations for the continuum and lumped parameter regions. The remainder of this section provides some discussion of programming considerations; these, too, are straightforward.

It is tacitly assumed, in the present investigation, that all the closure relations remain unchanged as we pass from planar to cylindrical flow. This is probably true of the equations of state for each of the phases and of the burning rate law. In view of the extreme shortness of the radial dimensions - amounting to only a few grain diameters - it is not clear that this assumption is correct in so far as the interphase heat transfer and drag are concerned.

3.1.1 Balance Equations for Two-Phase Cylindrical Flow

Since we have previously given the three-dimensional form of the balance equations[2,3] it is only necessary to express them in cylindrical coordinates and express the symmetry by dropping the azimuthal and axial derivatives. We recall that for the case of cylindrical symmetry, the divergence of a vector $\vec{\phi}$ has the form:

$$\nabla \cdot \vec{\phi} = \frac{1}{r} \frac{\partial}{\partial r} r\phi_r = \frac{\partial \phi_r}{\partial r} + \frac{\phi_r}{r} \qquad 3.1.1.1$$

Then in our usual terminology the balance equations for the two-phase flow become:

Balance of Mass of Gas Phase

$$\frac{\partial \varepsilon\rho}{\partial t} + \frac{\partial}{\partial r}\varepsilon\rho u = \dot{m} - \frac{\varepsilon\rho u}{r} + \psi\left(1 - \frac{\rho\varepsilon}{\rho_{IG}}\right) \qquad 3.1.1.2$$

Balance of Mass of Solid Phase

$$\frac{\partial \varepsilon}{\partial t} - \frac{\partial}{\partial r}(1-\varepsilon)u_p = \frac{\dot{m}}{\rho_p} + (1-\varepsilon)\frac{u_p}{r} + (1-\varepsilon)\frac{\psi}{\rho_{IG}} \qquad 3.1.1.3$$

Balance of Momentum of Gas Phase

$$\varepsilon\rho \frac{Du}{Dt} + \varepsilon \frac{\partial p}{\partial r} = -f_s + \dot{m}(u_p - u) - \psi u \qquad 3.1.1.4$$

Balance of Momentum of Solid Phase

$$(1-\varepsilon)\rho_p \frac{Du_p}{Dt_p} + (1-\varepsilon)\frac{\partial p}{\partial r} + \frac{\partial}{\partial r}(1-\varepsilon)R = f_s \qquad 3.1.1.5$$

Balance of Energy of Gas Phase

$$\begin{aligned} \varepsilon\rho \frac{De}{Dt} + p\frac{D\varepsilon}{Dt} + \varepsilon p \frac{\partial u}{\partial r} &= -\varepsilon \frac{pu}{r} + f_s(u-u_p) \\ &- (1-\varepsilon)\rho_p \frac{S_p}{m_p} q_s + \psi\left(e_{IG} + \frac{p}{\rho_{IG}}(1-\varepsilon) - e + \frac{u^2}{2}\right) \qquad 3.1.1.6 \\ &+ \dot{m}\left[e_{CHEM} - e + \frac{p}{\rho_p} + \frac{(u-u_p)^2}{2}\right] \end{aligned}$$

By comparing these equations for those which govern the quasi-one-dimensional model of the NOVA code, as summarized in chapter 2.0, it will be apparent that formal identity is obtained if we set A = r in the latter. Of course, we use r here to represent the radial coordinate.

3.1.2 Balance Equations for Cylindrical Lumped Parameter Region

As in the preceding section, the modification is slight and may be established by setting A = r in the quasi-one-dimensional axial flow equations.

Thus we have:

$$\dot{m}_s = \int_{r_i}^{r_o} \psi r dr \qquad 3.1.2.1$$

as the rate of mass generation per radian in a lumped parameter region bounded by r_i, within, and r_o, without. The rate of change of volume of the lumped parameter region is:

$$\dot{V}_o = \frac{\dot{m}_s}{\rho_{IG}} + r_o \dot{r}_o - r_i \dot{r}_i \qquad 3.1.2.2$$

The mass balance is:

$$\dot{\rho}_c = \frac{1}{V_c} \left[\dot{m}_s \left(1 - \frac{\rho_c}{\rho_{IG}}\right) + r_i \dot{m}_i - r_o \dot{m}_o + \rho_c (\dot{r}_i r_i - \dot{r}_o r_o)\right] \qquad 3.1.2.3$$

where we take the convention that a positive value of $\dot{m}_i$ corresponds to influx and a positive value of $\dot{m}_o$ corresponds to efflux.

The energy balance is:

$$\dot{e}_c = \frac{1}{\rho_c V_c} \left[\dot{m}_s (e_{IG} - e) + r_i \dot{m}_i \left(e_i + \frac{p_i}{\rho_i} + \frac{(u_i - u_c)^2}{2g_o} - e_c\right) - \frac{p_c}{\rho_c} \dot{m}_o r_o \right.$$

$$\left. - p_c (r_i \dot{r}_i - r_o \dot{r}_o)\right] \qquad 3.1.2.4$$

provided $\dot{m}_i$, $\dot{m}_o > o$. If either $\dot{m}_i$ or $\dot{m}_o$ is negative the coefficient must be appropriately modified.

3.1.3 Computational Considerations

The analysis of the cylindrical flow entailed only minimal code changes. Indeed, as we have observed, we could have effected the solutions simply by putting A = r in the input data file. However, it is necessary to provide a means of treating the divergence terms near the centerline where the presence of r in the denominator can produce computational difficulties. This

problem is simply solved since by L'Hospital's rule:

$$\lim_{r \to o} \frac{\phi}{r} = \frac{\partial \phi}{\partial r}$$

Hence if ϕ is any flow property, symmetry demands $\frac{\partial \phi}{\partial r} \to 0$ and we therefore have $\phi/r \to o$ at the centerline.

A more significant problem arose in treating the case with 2.54 cm exterior ullage and ignition on the centerline. As discussed in section 2.2.2, the venting became sonic at the external boundary of the bed and numerical instability occurred when we attempted to perform a continuum analysis of the ullage. Therefore, we represented the external ullage according to a lumped parameter formulation. Although we were able to perform a stable analysis of the 1.27 cm case using a continuum formulation, we repeated this case with a lumped parameter formulation to assure compatibility between the two cases.

Because the external ullage was large in the cases considered here, we did not feel that it was appropriate to impose the condition of isentropic stagnation which is customarily used by the NOVA code in the case of a small lumped parameter region. Thus the mass transfer was taken to be adiabatic and either choked or isentropic depending on the ratio of stagnation pressure at the exit plane to the static pressure in the region of ullage.

3.2 Discussion of Data Base

We present results from a total of six different problems. All the problems have been predicated on essentially the same data base for the code, as exhibited in Tables 3.2.1 - 3.2.5. The differences, which are summarized in Table 3.2.6, relate to the location of the charge, the presence or absence of internal and external ullage, the region of venting of the primer and the nature of the symmetry of the flow, planar or cylindrical.

The choice of the problem parameters is loosely based on the configuration of the 155mm Howitzer. Thus we set the external boundary at 7.62 cm in all cases. In problems 1-4 we consider internal ignition, or base ignition in case 1 which has planar symmetry. The rate of venting is predicated on the properties of a center core igniter having 0.11 kgm of black powder in a nitrocellulose tube whose internal and external diameters are 1.91 cm and 3.18 cm respectively and whose length is 47 cm. The geometry of the problems studied here is nominal in the sense that we have not attempted to reflect the precise structure of the primer. The internal radius of the charge is set at 1.27 cms for the cases of internal ignition. The primer is taken to vent uniformly over the region of ullage and, to avoid a sharp change in the source term, to vent over an additional 0.3 cm at a rate which drops linearly to zero with distance.

It will be noted that the code requires values of the tube cross sectional area, a quantity which is meaningless in the cases of cylindrical flow. However, the area is used to convert the input tabulation of primer venting data into a rate per unit volume. Since this involves a division by

Table 3.2.1 Thermophysical Data

(1) General Properties of Initial Ambient Gas:	
Initial Temperature (°K)	294.4
Initial Pressure (atm)	1.0
Molecular Weight (gm/gm-mol)	29.0
Ratio of Specific Heats (-)	1.4
(2) General Properties of Propellant Bed:	
Initial Temperature (°K)	294.4
Virtual Mass Constant (-)	0.
Rate of Propagation of Intergranular Stress in Settled Bed (m/sec)	442.
Settling Porosity of Bed (-)	0.4094
(3) Properties of Propellant:	
Internal Boundary (cms)*	1.27
External Boundary (cms)	7.62
Initial Porosity (-)	0.4094
Density (gm/cm^3)	1.583
Outside Diameter of Grain (cms)	1.0528
Perforation Diameter of Grain (cms)	0.0813
Length of Grain (cms)	2.413
Number of Perforations of Grain (-)	7
Solid Phase Thermochemical Data:	
Burning Rate Additive Constant	0.
Burning Rate Pre-exponential factor ($cm/sec/(Mpa)^n$)	0.3436
Burning Rate Exponent (-)	0.67
Ignition Temperature (°K)	450.
Thermal Conductivity (J/cm-sec-°K)	2.661×10^{-2}
Thermal Diffusivity (cm^2/sec)	8.677×10^{-4}
Emissivity Factor (-)	0.6
Gas Phase Thermochemistry:	
Chemical Energy Released in Burning (J/gm)	4426.
Molecular Weight (gm/gm-mol)	23.46
Ratio of Specific Heats (-)	1.24
Covolume (-)	26.15
(4) Properties of Primer:	
Chemical Energy Released in Burning (J/gm)	3465.
Ratio of Specific Heats (-)	1.24
Molecular Weight (gm/gm-mol)	22.40
Specific Volume (cm^3/gm)	0.634

* Set equal to zero in cases 5 and 6 for which an external ignition stimulus was considered.

Table 3.2.2 Tabular Values Used to Specify Geometry

Distance from Center (cms)	"Tube Radius"* (cms)
0	1.43
10.16	1.43

* Input quantity predicated on quasi-one-dimensional axial flow. Value produces cross sectional area of unity in code units. This is significant only in respect to computations of primer injection for which tabulated values of Tables 3.2.4 and 3.2.5 are divided by cross sectional area.

Table 3.2.3 Tabular Values Used to Specify Resistance to Motion of External Boundary

Distance from Center (cms)	Resistive Pressure Mpa
7.62	690.0
10.16	690.0

Table 3.2.4 Tabular Values Used to Specify Rate of Discharge of Internal Primer

	Rate of Discharge (kg/cm/sec)		
Position (cms)	0	1.270	1.297
Time (msec)			
0	0.273	0.273	0.
20	0.273	0.273	0.

Table 3.2.5 Tabular Values Used to Specify Rate of Discharge of External Primer

	Rate of Discharge (kg/cm/sec)		
Position (cms)	7.59	7.62	10.16
Time (msec)			
0	0.00	0.273*	0.273*
20	0.00	0.273*	0.273*

* *For problem 5 only. In problem 6 the rate of discharge was set equal to 0.0273 kg/cm/sec.*

Table 3.2.6 Summary of Cases Considered in Study of Cylindrical Flow

Problem	Geometry	Internal Radius of Charge -cms-	External Radius of Charge -cms-	External Radius of Container -cms-	Primer Location
1	Planar*	1.27	7.62	7.62	Base
2	Cylindrical	1.27	7.62	7.62	Inside
3	Cylindrical	1.27	7.62	8.89	Inside
4	Cylindrical	1.27	7.62	10.16	Inside
5	Cylindrical	0.0	7.62	10.16	Outside
6	Cylindrical	0.0	7.62	10.16	Outside**

* Dimensions here are axial figures

** Problem 6 differs from problem 5 in respect to the strength of the primer.

the area we simply used a value for the tube radius which would provide a unit value for the cross sectional area in the code system of measurement. The values of bore resistance were simply chosen to be sufficiently large as to preclude motion of the right hand or external boundary.

From an inspection of the tables we see that problems 1 and 2 have identical data bases. However, problem 1 is predicated on planar symmetry while problem 2 is predicated on cylindrical symmetry. The results of these two cases are presented and compared in section 3.3.

Problems 3 and 4 are similar to 2, all having cylindrical symmetry; however, they introduce external ullage by means of enlarging the external boundary of the container, the charge being fixed. These problems are discussed in section 3.4.

Finally, problems 5 and 6 are similar to 4. However, they contain no internal ullage and the primer is taken to vent in the exterior region. These results are given in section 3.5.

3.3 Comparison of Cylindrical and Planar Solutions

We now present and compare the solutions to problems 1 and 2 which are identical except for the nature of their respective symmetries. Problem 1 has planar symmetry and corresponds to the base ignition of a rather short propelling charge. This solution was generated with the unmodified version of the NOVA code. In problem 2 we simulate the center core ignition of a charge having the same dimensions but cylindrical geometry. In each case ignition occurs rapidly and is followed by smooth flamespreading throughout the bed. However, ignition at the forward end (problem one) or the outside (problem two) is delayed since the impermeable boundary condition results in a very low rate of convective heating.

Figures 3.3.1 through 3.3.7 present distributions of density, temperature, pressure, gas velocity, solid phase velocity, granular stress and porosity in the planar case. Figures 3.3.8 through 3.3.14 present the corresponding distributions in the cylindrical flow at essentially the same instants in time.

Figure 3.3.15 presents a comparison of the rate of flamespreading in each of the two cases and we begin with a discussion of this figure. As we might expect, ignition at the left side (planar case) or inside (cylindrical case) occurs at essentially the same time in the two problems. However, as flamespreading proceeds, the flow becomes increasingly sensitized to the divergence in the cylindrical case. Convective flamespreading depends on the presence of a large pressure gradient to force the hot combustion products into the unreacting material and ignite it. As the cylindrical flame progresses it envelopes volume at a faster rate than its planar counterpart. This has the result of impeding its progress since the rate of production of gas behind the flame does not keep pace. Figure 3.3.15 shows the planar flame to propagate roughly 50% faster than its cylindrical counterpart.

The figure also shows just how extended the delay becomes near the forward (planar case) or external boundary (cylindrical case). However, after 0.2 msec both cases show most of the bed to have been ignited.

There remains one feature of figure 3.3.15 which requires discussion. Ignition is seen to occur first just inside the bed rather than on the boundary. This is a consequence of the representation of the rate of primer discharge according to which there is some intrusion into the bed. The rate of discharge per unit volume is computed to be higher just inside the bed than it is outside. Therefore, the flow is initially to the left (planar case) or the inside (cylindrical case). Subsequently, as the interior ullage is pressurized, the flow begins to move uniformly to the right (planar case) or outwards (cylindrical case). Thus the convection at the boundary becomes quite small as the flow reverses. This loss in heat transfer is sufficient to delay ignition on the boundary relative to neighboring points within the bed for which the flow direction remains constant.

Turning now to the various distributions we first consider figures 3.3.1, 3.3.2 and 3.3.3. We see that the density distributions in the planar case are quite flat except for a wave like structure at the earliest time and a substantial excursion near the forward boundary. Reciprocal behaviour is shown by the temperature distributions in figure 3.3.2. The waviness at the earliest time is due to adiabatic compression of the gas near the region of primer venting. Likewise, the density and temperature excursions near the forward boundary reflect pressure equilibration through a region where the gas is cold due to the absence of combustion.

Figure 3.3.3 illustrates the extent to which the pressure distribution throughout the chamber becomes uniform once flamespreading is essentially complete. The pressure field has virtually no structure at all at the later times. Even during flamespreading, the pressure gradient is not extreme. By comparison with previous studies of axial flamespreading in a gun the distributions look very flat indeed. In fact, this is due in large measure to the scale of the present problem. The entire chamber is only 7.62 cms in length and this is not much larger than the thickness of the pressure profile through the flame.

Figures 3.3.8, 3.3.9 and 3.3.10 present the corresponding distributions for the cylindrical case. These are qualitatively similar to those for the planar problem and do not exhibit any new structural details. However, it is noteworthy that the pressure in the cylindrical case is less than in the planar case at the corresponding times. This observation correlates with the difference in the respective rates of flamespreading as discussed previously.

Figures 3.3.4 and 3.3.11 present distributions of gas velocity in the planar and cylindrical cases respectively. These are qualitatively similar although there are differences which we discuss presently. The two solutions have the following features in common. Very strong forward or outward convection is seen at the earliest time. The relatively sharp variation in the rate of primer venting is imprinted in the earliest distributions which reflect a certain amount of numerical noise in their detailed structure. A

period of moderate forward or outward blowing occurs in each case during and after flamespreading. Subsequently, after about 0.3 msec there is virtually no velocity profile in either case. The flow has damped almost completely as a consequence of the interphase drag and the near equilibration of the pressure field as seen in figures 3.3.3 and 3.3.10. At times later than those shown here the velocity in the cylindrical case reverses reaching a minimum value of about - 800 cm/sec before returning towards the quiescent state. Accordingly, it appears that for axially uniform center core ignition with no external ullage, the radial flow velocity does not exceed roughly 10m/sec in absolute value once flamespreading is complete. Further damping would probably occur but the influence of the motion of the projectile at later times makes such a statement speculative in nature since the present solution can no longer be applied.

The principal differences between the two solutions are as follows: Figure 3.3.11 shows considerably more feeding of the outside of the charge at any time than does figure 3.3.4 for the planar case. This, again, is a reflection of the more rapid increase in volume behind the convective flame in the cylindrical case. Moreover, figure 3.3.11 shows considerably more motion of the internal boundary than does 3.3.4 as may be deduced from the positions of the velocity jumps. This reflects the capacity of the cylindrical charge to accommodate dilation of its internal boundary with less overall compaction than the planar charge which is therefore stiffer. The relative motions of the internal boundaries may also be seen clearly by turning to figures 3.3.7 and 3.3.14 which present distributions of porosity.

Apart from making clear the extent of the motion of the internal boundaries, the porosity distributions reveal little interesting information. The distributions are rather flat in both cases. Also, both cases show a progressive decrease in porosity at all the times of interest here. This indicates that the compaction of the charge by the primer blast continues to overwhelm the influence of combustion for the first 0.5 msec.

As would be expected from the porosity distributions, the distributions of solid phase velocity show an essentially monotonic decrease from the primer interface to the opposite boundary. This statement is true with only minor qualification in the case of cylindrical flow, figure 3.3.12. This figure shows some inflections at the latest time when the charge is beginning to respond to the external boundary condition. Figure 3.3.5 does show a pronounced variation from purely monotonic behaviour in the planar case. Indeed, the distribution at 0.25 msec has considerable structure. This correlates directly with the behaviour of the granular stress distributions and we conclude our discussion of these solutions with some comments on this quantity.

The distributions of granular stress are shown in figures 3.3.6 and 3.3.13. These frankly show more structure than intuition is able to credit to the physical problem. The root of the difficulty lies in the irreversible granular stress law according to which the solid phase experiences an average stress different from the gas phase only when the bed is undergoing

progressive compaction. If the bed dilates, even infinitesimally, the granular stress is set equal to zero locally. The structure of the solid phase velocity distribution at 0.25 msec, shown in figure 3.3.5 is easily understood by reference to the corresponding distribution of granular stress, figure 3.3.6. An enormous gradient is produced by the relaxation of the material forward of the position 4.5 cm. This results in a local increase in solid phase velocity at the corresponding location. Figures 3.3.6 and 3.3.13 illustrate, in our opinion, the difficulty of working with a non-analytic constitutive law. It may be worthwhile, in later work, to incorporate an experimentally supported unloading curve. The purpose, in so doing, will not be so much to increase the accuracy of physical modeling as to alleviate the difficulty of obtaining a well behaved numerical solution. In any event, a better posed constitutive law should be used even if experimental data are unavailable. As presently posed, the granular stress law is appropriate only to problems in which a single load/unload cycle occurs.

3.4 Influence of Radial Ullage on Grain Velocity

The preceding section has shown that the transition from planar to cylindrical geometry introduces no unexpected features. Principally, the differences amount to a retardation of the convective flame and an increase in motion of the internal boundary due to primer blast. The preceding cases have taken the outside of the propellant bed to be in contact with the external boundary. In this section we displace the external boundary first by 1.27 cm and subsequently by 2.54 cm so as to introduce external ullage.

The choice of values for the gap between the charge and the external boundary is based on the characteristics of the 155mm Howitzer charge. At the breech the chamber has a diameter of 17.78 cms while the charge has a diameter of approximately 15.24 cms. Thus a gap of 1.27 cms produces external ullage whose cross sectional area is the same as that which occurs in the asymmetrical charge configuration. However, due to the asymmetry of the actual charge configuration, the gap between the bag and the chamber wall varies from zero at the six o'clock position to 2.54 cms at the 12 o'clock position. Previous studies of Navy propelling charges[3,4] have shown the importance of run up on the grain velocity as the bed approaches the base of the projectile. By analogy, it was felt that the radial run up length might play a similarly influential role in the present study.

Accordingly, the choice of a gap of 1.27 cm represents an attempt to capture the volume of the ullage. The value of 2.54 cms represents an attempt to capture the run up length at the 12 o'clock position. It is expected that the actual charge configuration would exhibit behaviour intermediate to the two examples considered here.

The results of these calculations are contained in figures 3.4.1 through 3.4.8. They are compared with each other and with the zero ullage case, problem 2, in figures 3.4.9 through 3.4.12. Figures 3.4.1 through 3.4.4 present

distributions of pressure, gas velocity, solid phase velocity and porosity at four times for the case of 1.27 cm ullage. These are chosen to exhibit the behaviour shortly after flamespreading ends, as the bed moves outwards and finally, after the bed has contacted the outside wall of the tube. Figures 3.4.5 through 3.4.8 present similar information for the case of 2.54 cm ullage, although the solution is not continued to the point of contact with the external boundary.

We begin by discussing the comparative data. Figures 3.4.9 and 3.4.10 show that there is a substantial difference in the pressure histories in each of the cases not only at the outside of the charge - as expected - but also at the center. By reference to figures 3.4.1 and 3.4.5 we see that this is due to an almost complete absence of any radial pressure gradient shortly after flamespreading is complete.

The nature of the radial pressure gradient in each of the three cases is seen quite clearly in figure 3.4.11. The figure presents the difference between the pressure at the center of the charge and that at the outside. Interestingly, the maximum is virtually independent of the external ullage and reflects pressurization of the interior prior to the arrival of the convective flame at the outside of the charge. The maximum value of approximately 2 Mpa is very modest by comparison with the levels experienced in the axial direction in even well behaved propelling charges. Only the most minute reverse gradient is seen.

Figure 3.4.12 presents the rates of flamespreading in the three calculations. The only noticeable difference occurs at the external boundary of the bed. As would be expected, the introduction of ullage enhances flamespreading since the convection is not restricted.

We now return to the detailed distributions for the case of 1.27 cm ullage, problem 3. Figure 3.4.1 presents the distributions of pressure. We see that shortly after flamespreading is complete the pressure is virtually uniform across the chamber. The impact of the bed against the external boundary is not associated with any sort of pressure wave phenomena.

Figure 3.4.2 presents the distributions of gas velocity. We see that once the flamespreading transient is complete, the flow develops an almost stationary character. The distributions at 1.13, 1.76 and 2.32 msec are almost identical. The magnitudes of the velocity at these times are not especially large. They range from - 60 m/sec to + 20 m/sec. These values are very small by comparison with the axial flow velocities which will be of the order of the projectile velocity, namely 1000 m/sec. We note, from the positions of the jump in the gas velocity, the substantial motion which the external ullage permits the internal boundary to develop.

This is seen more clearly in figure 3.4.3 which presents the distributions of solid phase velocity and in figure 3.4.4, distributions of porosity. The internal boundary which was initially at 1.27 cm is pushed out to just over 4.0 cm as a consequence of the primer blast. Only at the latest time considered here does the solid phase velocity reverse, becoming negative

after the impact against the external boundary. Even so, the velocities at this time are very small. Accordingly, one must conclude from this calculation that radial ullage may be very persistent. The assumption of uniformity of properties incorporated into a quasi-one-dimensional axial flow analysis may be very poor in respect to the porosity. We will return to this point in chapter 6.0.

The corresponding distributions for the 2.54 cm case, problem 4, are given in figures 3.4.5 through 3.4.8. We see that the pressure distributions, figure 3.4.5, exhibit somewhat greater structure than their counterparts in figure 3.4.1. However, following the completion of flamespreading it is again true that there is very little radial pressure gradient. Likewise, figure 3.4.6 shows the distributions of gas velocity to damp considerably. The magnitude of the radial gas velocity is similar to that in the 1.27 cm case.

Figures 3.4.7 and 3.4.8 exhibit clearly the radial expansion of the bed. The enlargement of the central ullage by the primer blast is even greater in this case, as expected. Since the previous case did not exhibit the formation of a pressure wave upon impact of the propellant against the external boundary, we did not continue problem 4 beyond the point shown.

We conclude this section with a discussion of the radial velocity experienced by the outside of the charge. From figures 3.4.3 and 3.4.7 we observe that in both cases the grains develop a certain velocity during flamespreading when the pressure gradients and interphase drag are at a maximum. Subsequently, the boundary velocity is virtually constant as the bed expands. There is a clear dependence on the magnitude of the external ullage. The boundary velocity is approximately 6 m/sec in the 1.27 cm case and approximately 12 m/sec in the 2.54 cm case. These results indicate a linear dependence of boundary velocity on external gap size. However, it is by no means clear that this relationship has a general validity beyond the cases examined here and it should be quoted with caution.

3.5 Comparison of Internal and External Ignition Stimuli

Thus far we have considered only those cylindrical flows for which ignition is first stimulated at the center of the charge. These problems have corresponded to the functioning of a long center core igniter with an axially uniform rate of venting. We may visualize cases, however, where the ignition is stimulated externally. This may happen in a region where there is no center core primer, or there is one but it fails to work. The ignition of the propellant in this region of the charge will either occur as a consequence of axial flamespreading or, if there is external ullage, as a consequence of local intrusion of the products of combustion of the base pad. In such a case the effect of the ignition sequence will be, initially, to compact the charge rather than to blow the grains out towards the wall of the tube.

In order to investigate the response of a propelling charge to an external ignition stimulus we take essentially the configuration of problem 4 with no internal ullage. Thus the charge is a solid cylinder of radius 7.62 cms enclosed in a container of radius 10.16 cms. We consider that the primer

vents uniformly in the region of ullage with a rapid ramp down to zero at the edge of the bed. We choose two values for the rate of venting, both speculative. In the case of problem 5, which we refer to as the strong external ignition case, we use the same value as was used for the previous internal ignition cases. In problem 6, the weak external ignition case, we use one tenth of this value. In each case flamespreading is found to occur in the presence of an external pressure of 1-4 Mpa, values which are comparable with those seen in the 155mm Howitzer prior to ignition[27]. It is believed that the rate of external pressurization is the correct parameter to consider here. The size of the ullage is believed to be of secondary importance. As we will see when we perform a continuum analysis of the flow in the ullage, its properties are quite uniform.

Figures 3.5.1 through 3.5.4 present distributions of pressure, gas velocity, solid velocity and porosity for the strong external ignition case and figures 3.5.5 through 3.5.8 present corresponding information for the weak external ignition case. In figures 3.5.9 and 3.5.10 we compare the history of radial pressure difference across the bed as deduced for each external ignition case with that deduced in problem 4 using internal ignition. Finally, in figure 3.5.11 we present the rates of flamespreading in each of the external ignition cases.

Figure 3.5.11 reveals an anomalous feature. Near the center of the charge the direction of flamespreading is reversed slightly in the case of the strong ignition stimulus. This is believed to reflect numerical noise rather than a physical event. As we will see, the solution for this case contains some numerical wiggles and it is to these that we attribute the flamespreading anomaly. In neither case does the flame reach the center. This is due to the absence of convection and is similar in nature to the condition at the outside of the charge in problem 2. In practice, of course, flamespreading will continue but by mechanisms which are not reflected in the phenomenology of the code.

Figures 3.5.9 and 3.5.10 show that there is little to choose between internal and external ignition from the standpoint of the radial pressure gradient. Naturally, the difference is initially reversed in sign. All converge to zero following flamespreading. The oscillations seen in the difference history for the case of strong external ignition are thought to represent numerical noise for reasons which will be clear when we inspect the pressure distributions.

Figure 3.5.1 shows the pressure distributions to become quite flat following flamespreading to the center, although the center is never ignited in this calculation. The oscillation near the center is thought to represent numerical noise. This sort of wiggle is not seen in the previous calculations. It is probably driven by the strong inwardly propagating pressure field. Study of the solution suggests that the problem is aggravated by the irreversible granular stress law and could be alleviated by suitable modifications. However, the specific modifications would require investigation of a scope inconsistent with the purpose of the present study and have not been pursued.

27. *Rocchio, J., White, K., Ruth, C. and May, I. "Propellant Grain Tailoring to Reduce Pressure Wave Generation in Guns" Proc. 12th Jannaf Combustion Meeting August 1975*

Figure 3.5.2 presents the distributions of gas velocity. It is noteworthy that once the flame has spread to the center, the velocity is damped almost completely. Wiggles are seen near the center. These correlate with those in the pressure distributions. Figure 3.5.3 presents the solid phase velocity distributions in the case of a strong external stimulus. These contain numerical noise at quite an early time. It is possible that the numerical error is first associated with this variable. Once flamespreading is complete the solid phase is virtually at rest, having a velocity of only - 2 m/sec.

The distributions of porosity, figure 3.5.4, reveal two interesting features. First, as we would expect, the external boundary is but little displaced by comparison with the internal boundary in the previous cases. Secondly, because of the convergence of sections as we approach the center, even a mild displacement of the external boundary can be associated with large changes in the porosity near the center. We see that there is, in effect, an implosion. The porosity is decreased by roughly 25% near the center, while the value at the outside is only slightly depressed.

The behaviour of the weak external ignition case is reflected by figures 3.5.5 through 3.5.8. We see that all the features are qualitatively similar although, as expected, the compaction of the bed is substantially less. The solution is carried further forward in time than the preceding case. Accordingly, we see, in figure 3.5.6, venting of the bed to the external ullage at a rate of about 40 m/sec. As may be seen, in figure 3.5.7, this causes a reversal of the initial compaction of the bed. The solid phase is beginning to move outwards although its radial velocity is a very modest 1 m/sec.

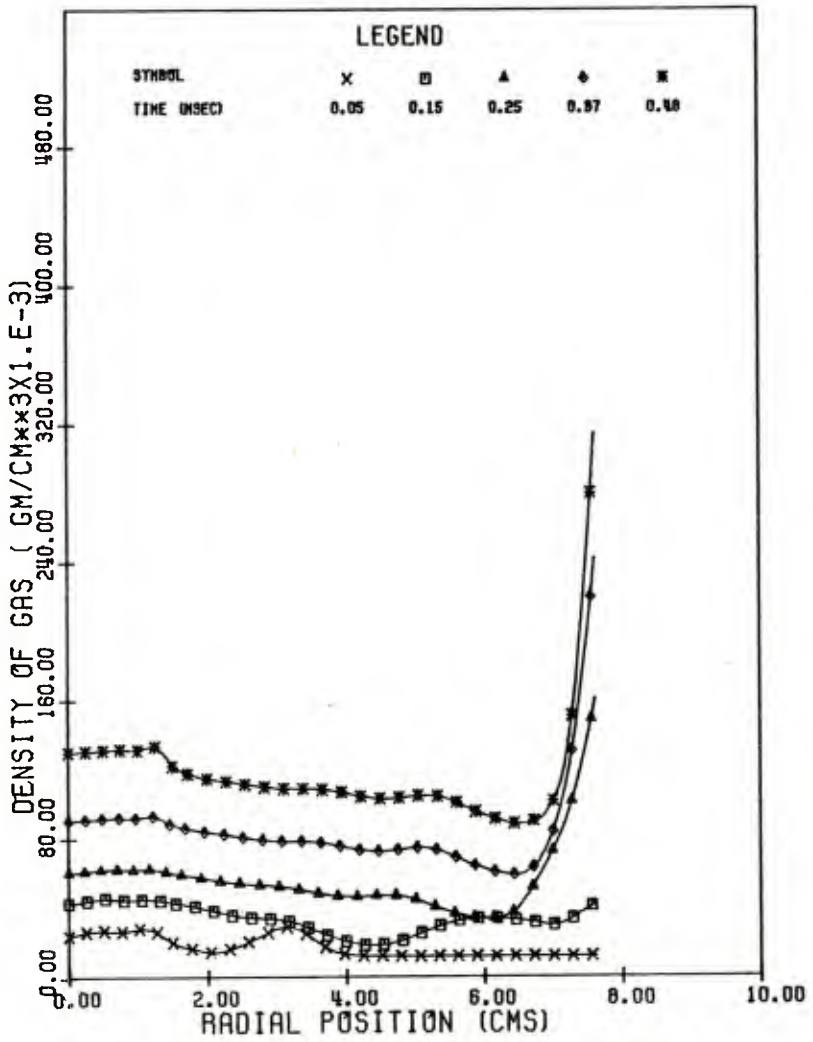

FIG.3.3.1 DISTRIBUTIONS OF DENSITY ACCORDING TO PLANAR SOLUTION

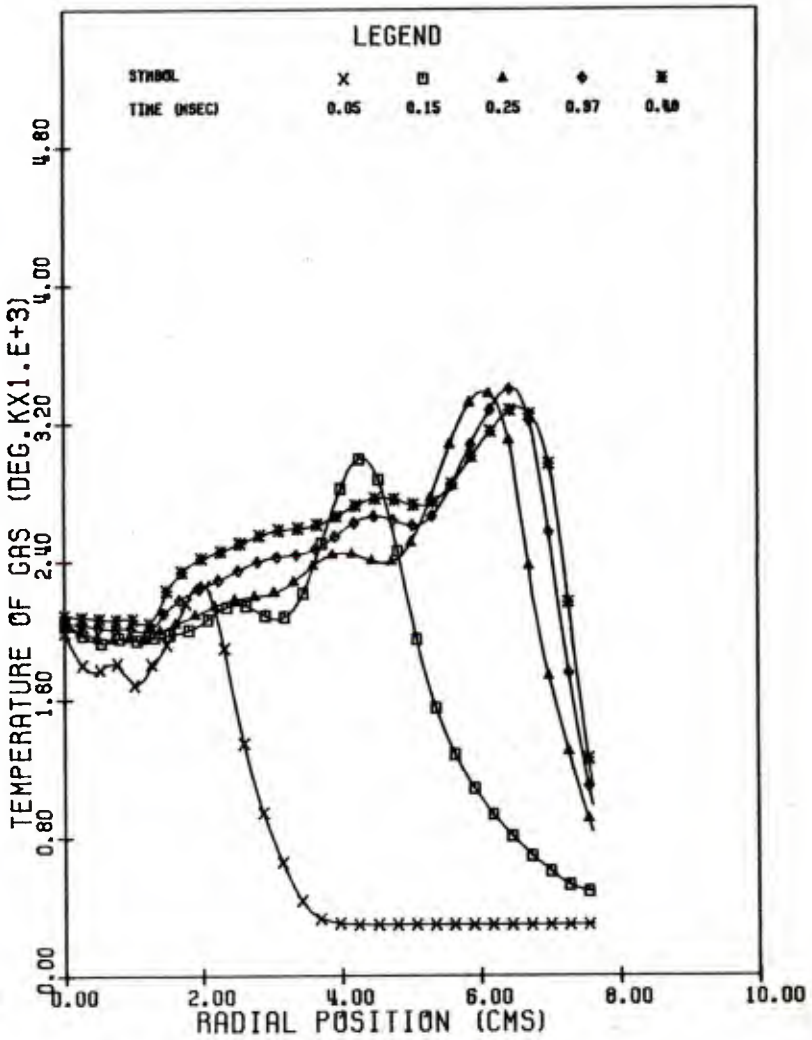

FIG.3.3.2 DISTRIBUTIONS OF TEMPERATURE ACCORDING TO PLANAR SOLUTION

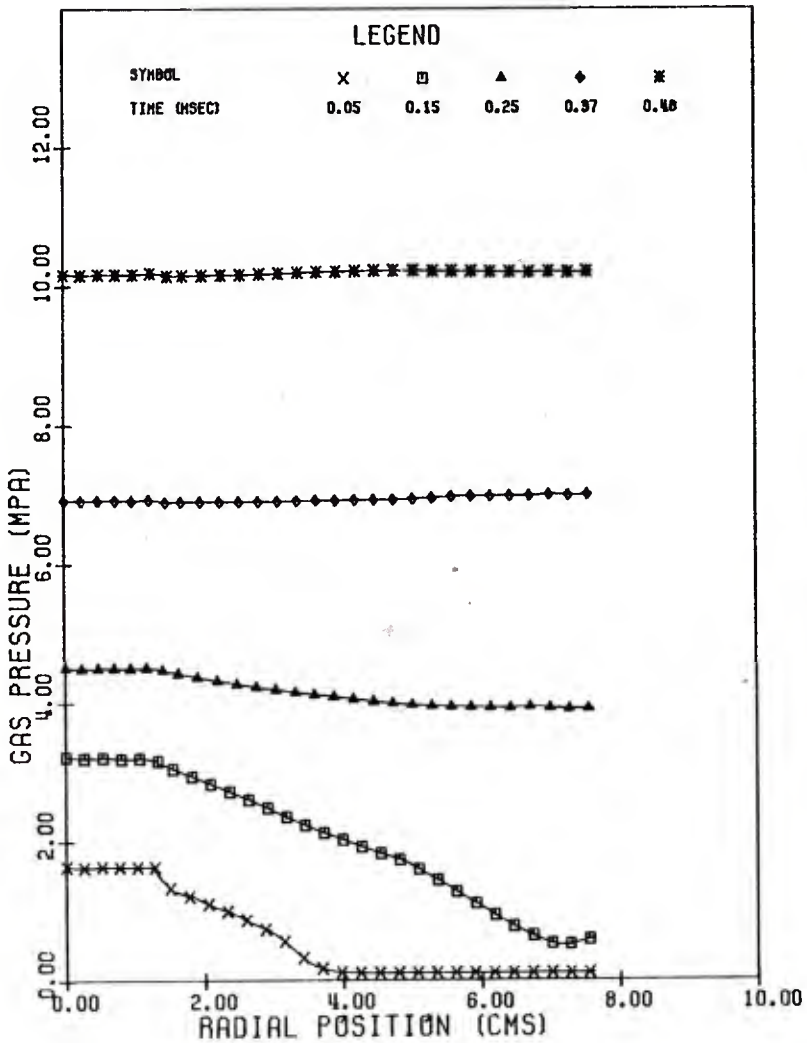

FIG.3.3.3 DISTRIBUTIONS OF PRESSURE ACCORDING TO PLANAR SOLUTION

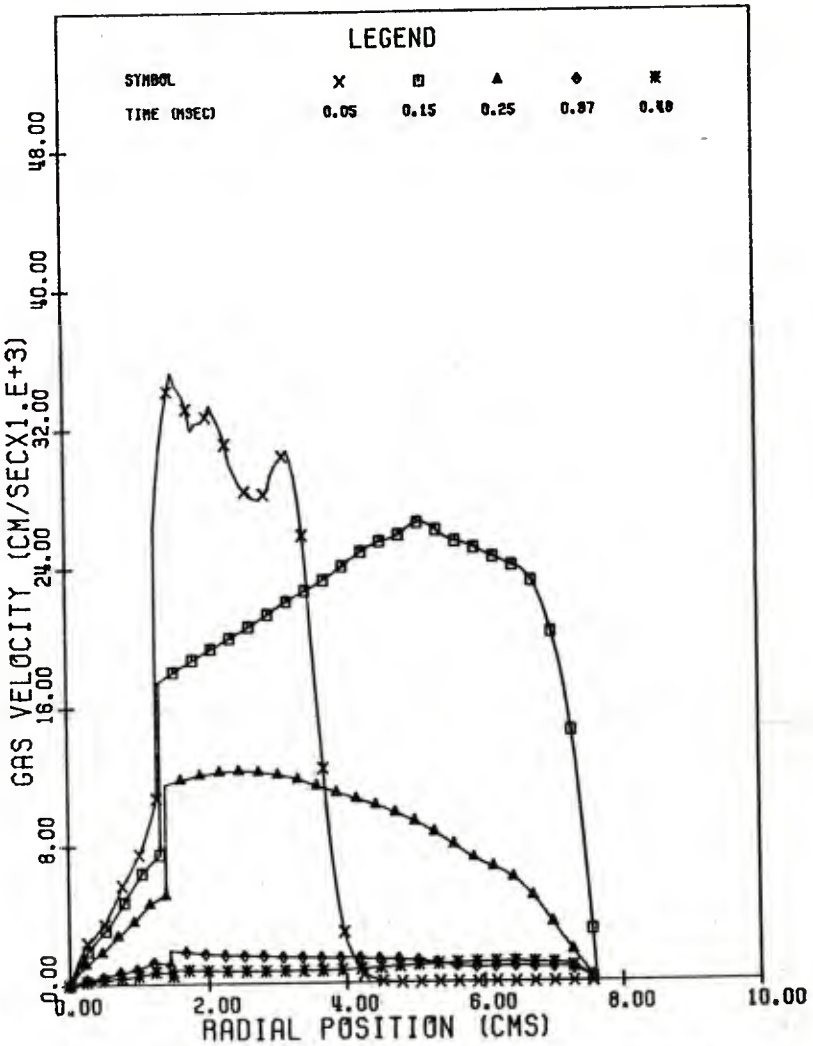

FIG.3.3.4 DISTRIBUTIONS OF GAS VELOCITY ACCORDING TO PLANAR SOLUTION

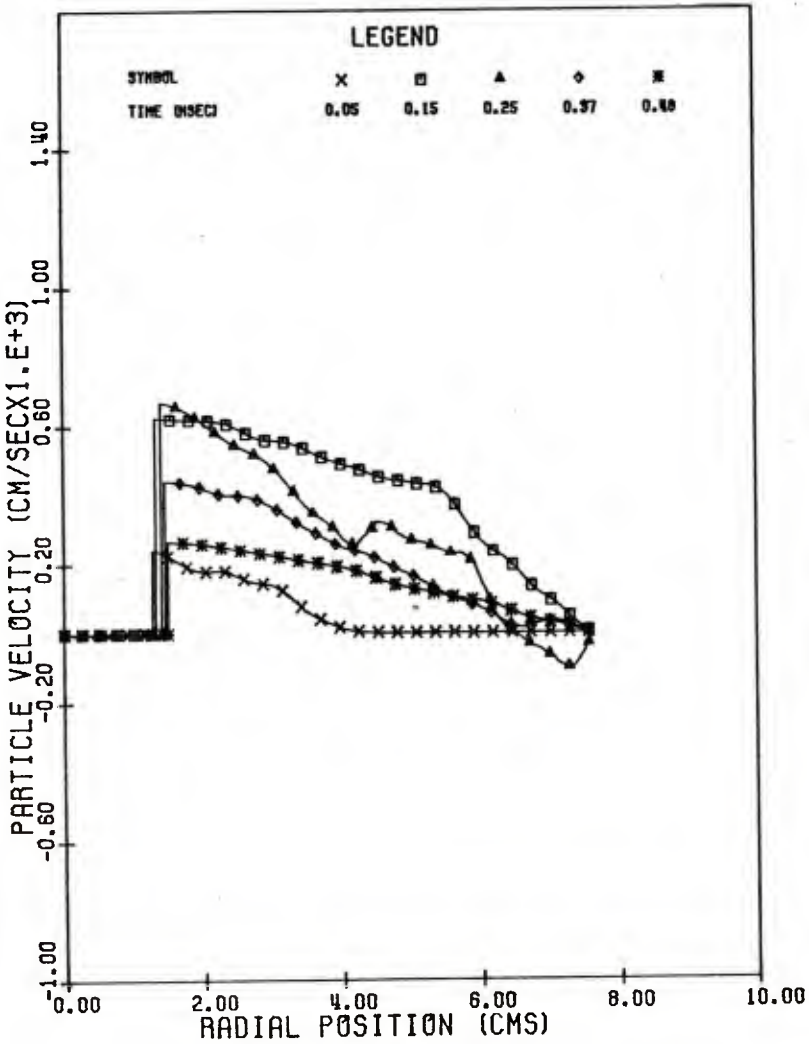

FIG.3.3.5 DISTRIBUTIONS OF SOLID VELOCITY ACCORDING TO PLANAR SOLUTION

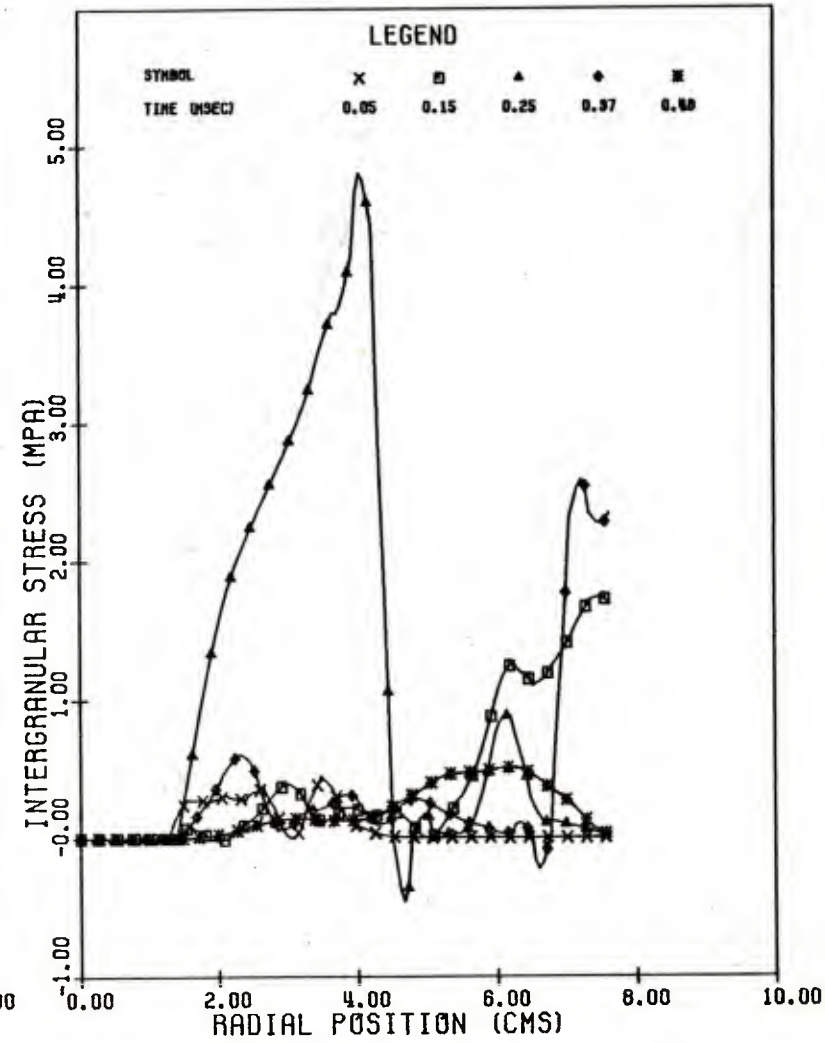

FIG.3.3.6 DISTRIBUTIONS OF GRANULAR STRESS ACCORDING TO PLANAR SOLUTION

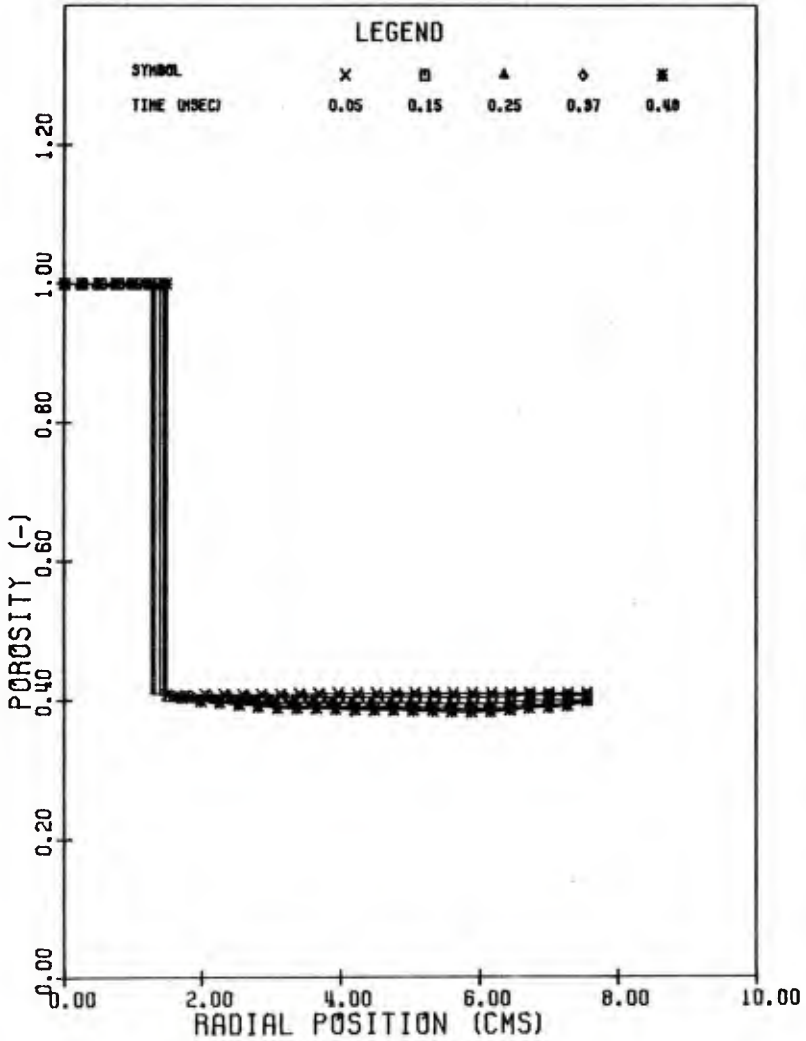

FIG.3.3.7 DISTRIBUTIONS OF POROSITY ACCORDING TO PLANAR SOLUTION

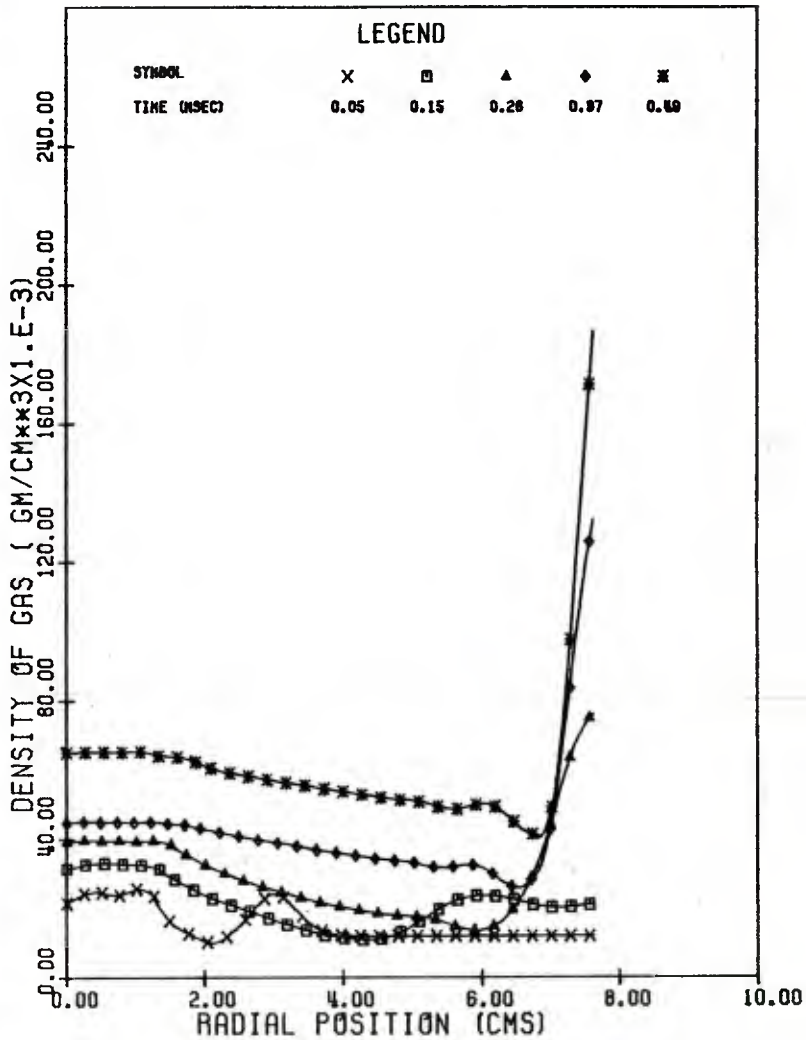

FIG.3.3.8 DISTRIBUTIONS OF DENSITY ACCORDING TO CYLINDRICAL SOLUTION

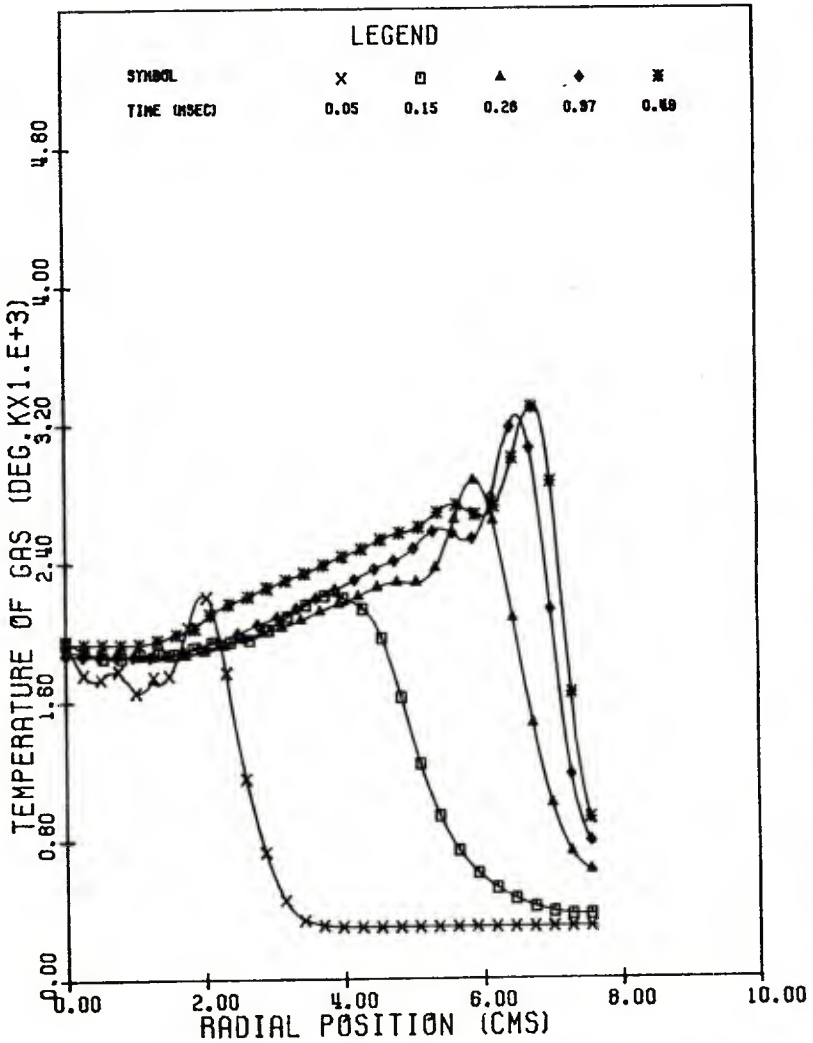

FIG.3.3.9 DISTRIBUTIONS OF TEMPERATURE ACCORDING TO CYLINDRICAL SOLUTION

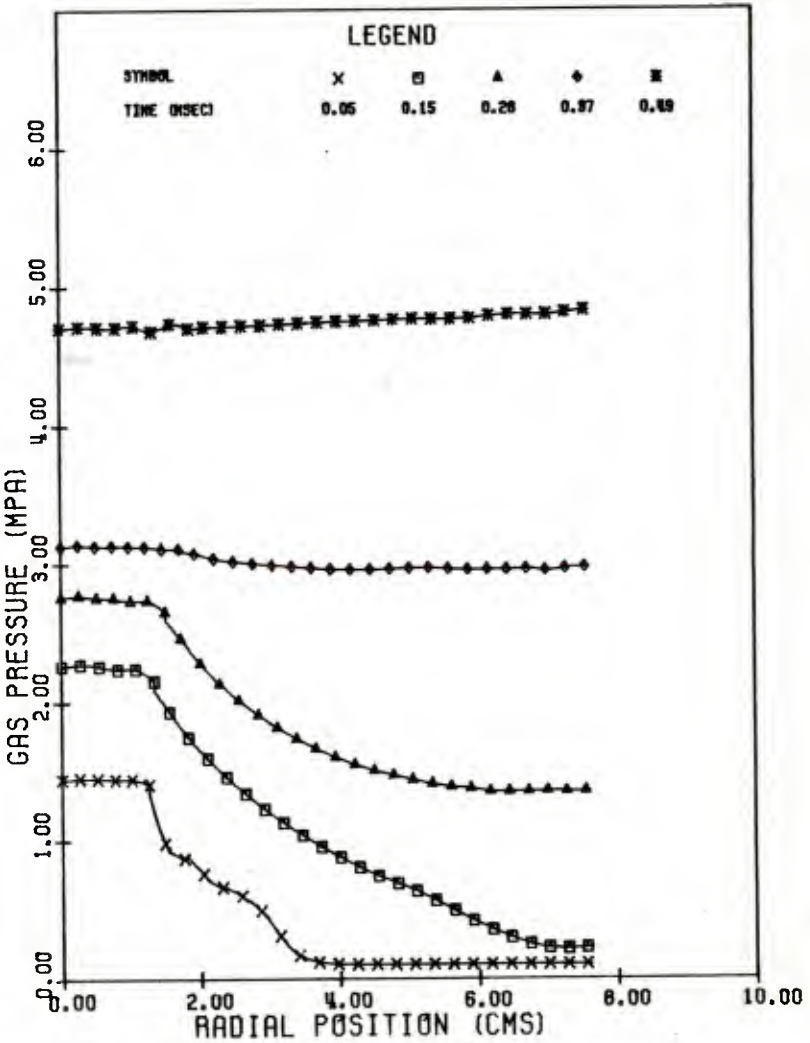

FIG.3.3.10 DISTRIBUTIONS OF PRESSURE ACCORDING TO CYLINDRICAL SOLUTION

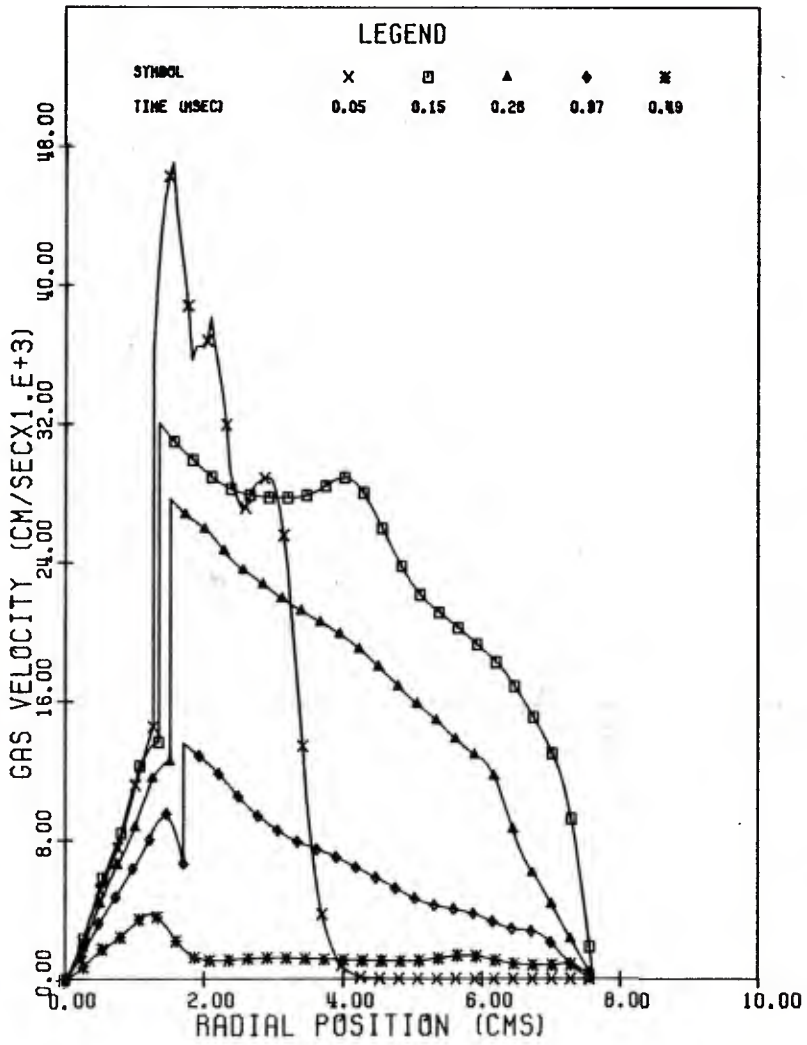

FIG.3.3.11 DISTRIBUTIONS OF GAS VELOCITY ACCORDING TO CYLINDRICAL SOLUTION

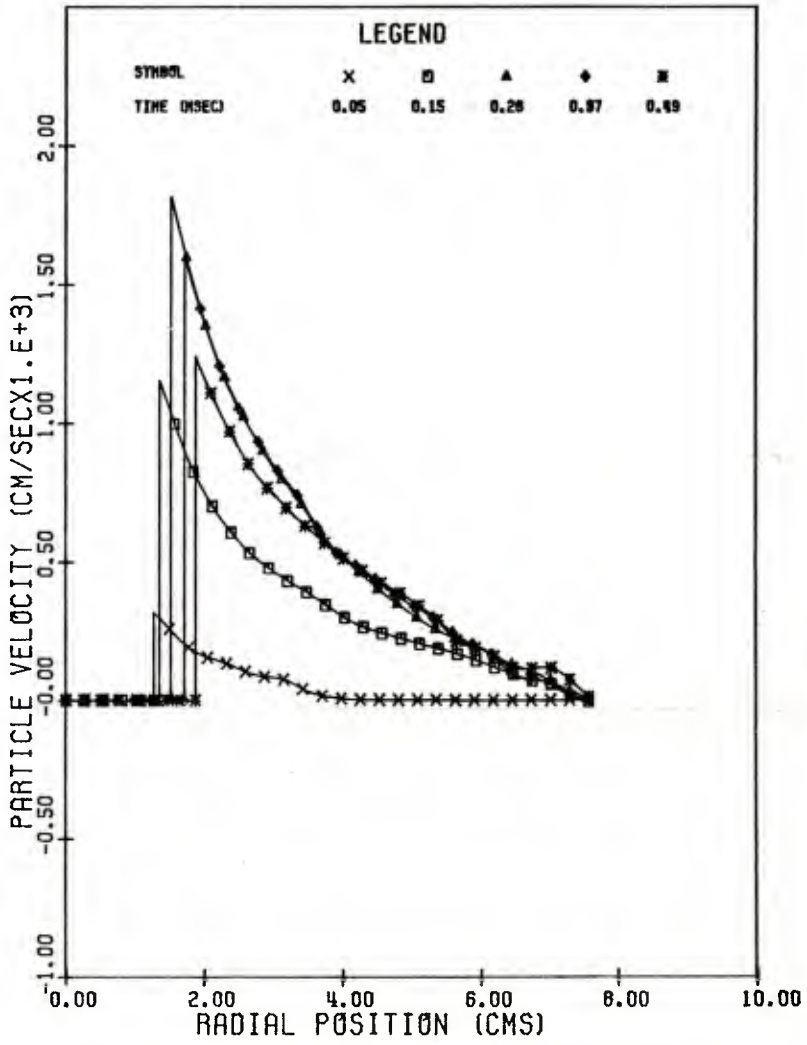

FIG.3.3.12 DISTRIBUTIONS OF SOLID VELOCITY ACCORDING TO CYLINDRICAL SOLUTION

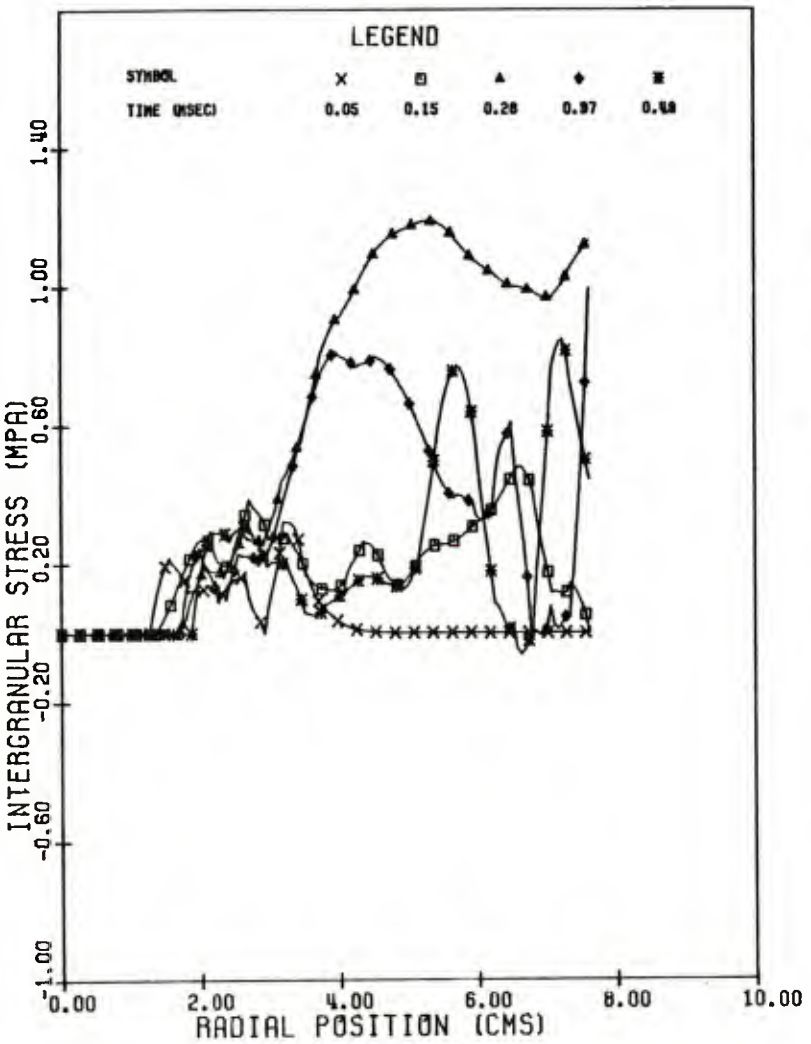

FIG.3.3.13 DISTRIBUTIONS OF GRANULAR STRESS ACCORDING TO CYLINDRICAL SOLUTION

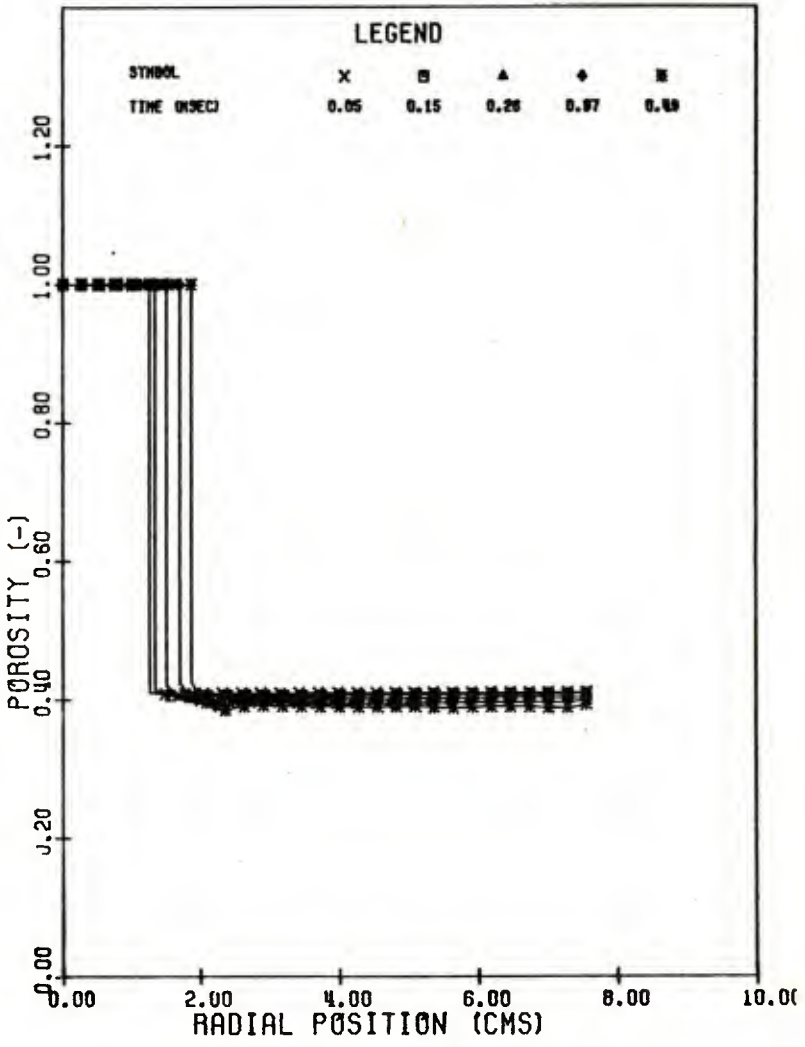

FIG.3.3.14 DISTRIBUTIONS OF POROSITY ACCORDING TO CYLINDRICAL SOLUTION

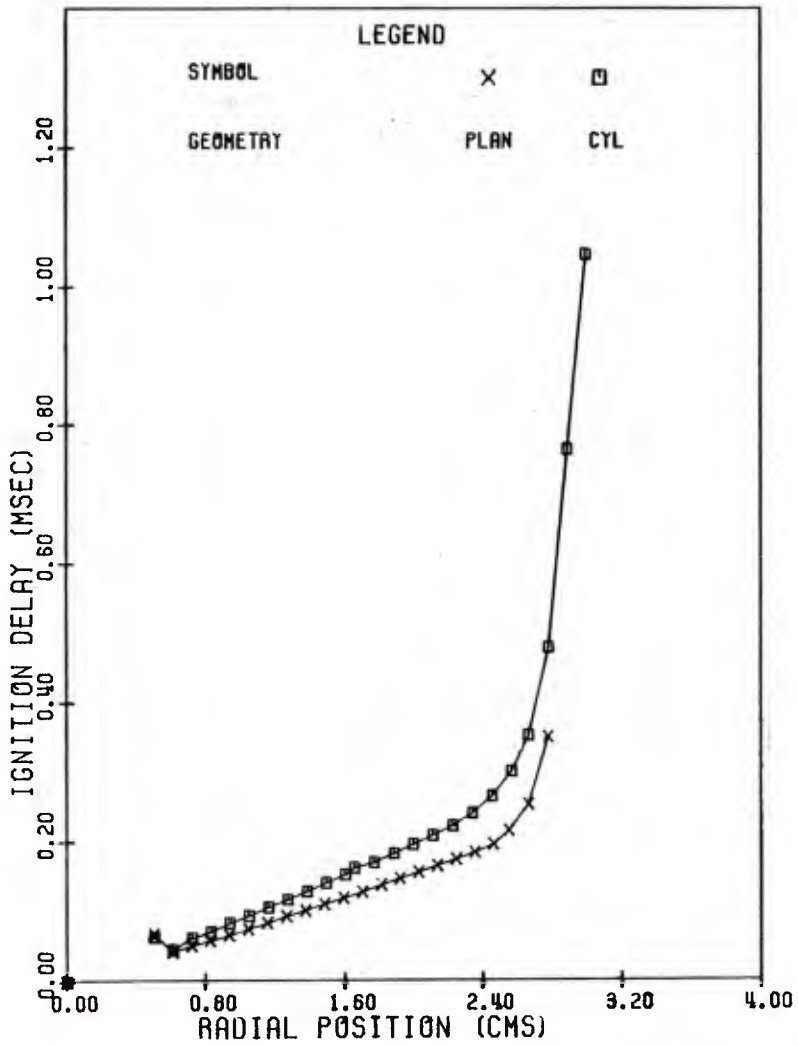

FIG.3.3.15 COMPARISON OF RATE OF FLAMESPREADING IN PLANAR AND CYLINDRICAL FLOWS

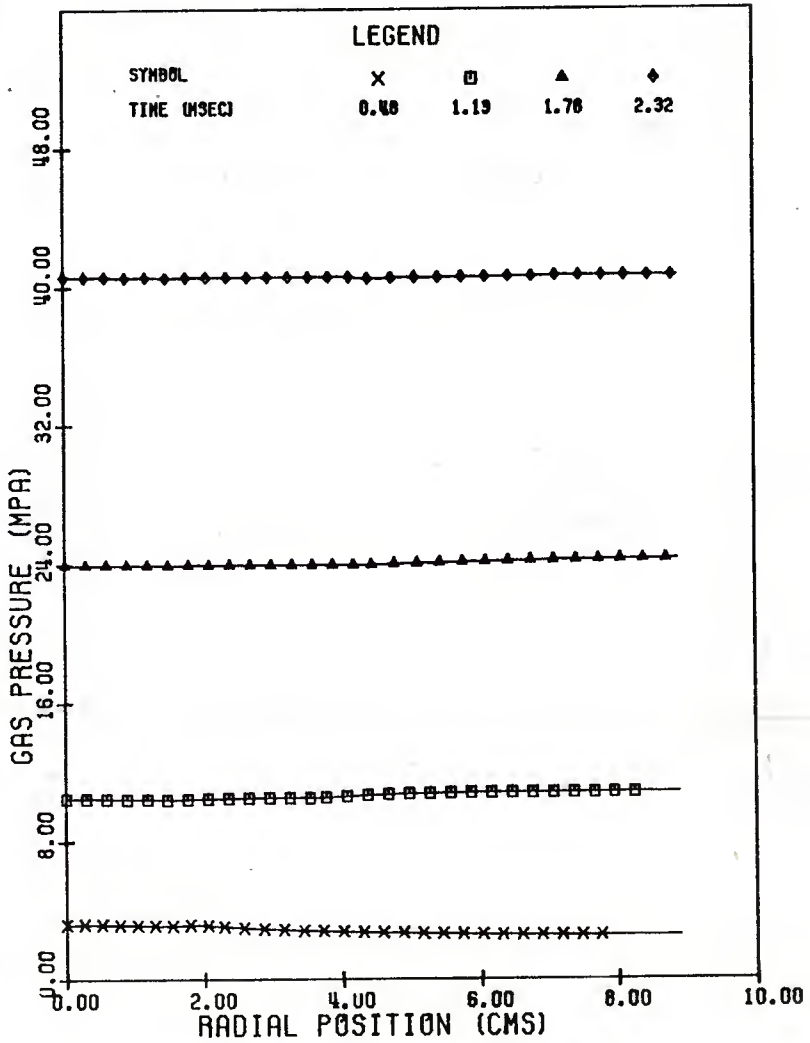

FIG.3.4.1 DISTRIBUTIONS OF PRESSURE ACCORDING TO CYLINDRICAL SOLUTION WITH 1.27 CM ULLAGE

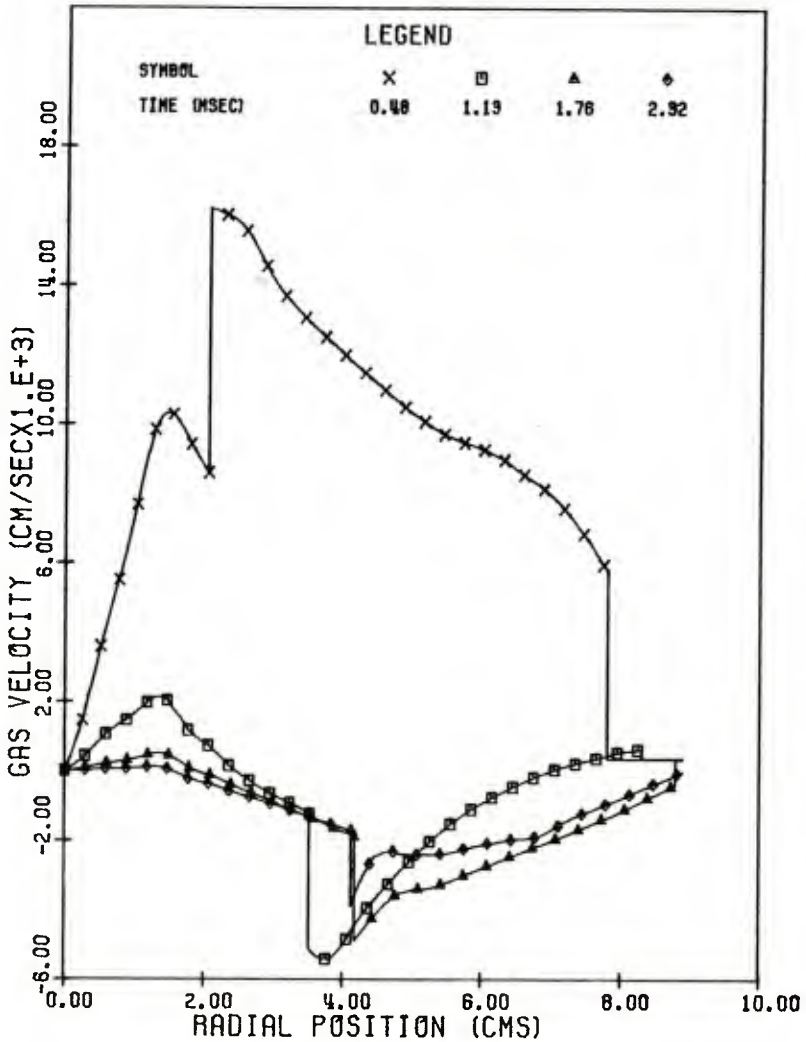

FIG.3.4.2 DISTRIBUTIONS OF GAS VELOCITY ACCORDING TO CYLINDRICAL SOLUTION WITH 1.27 CM ULLAGE

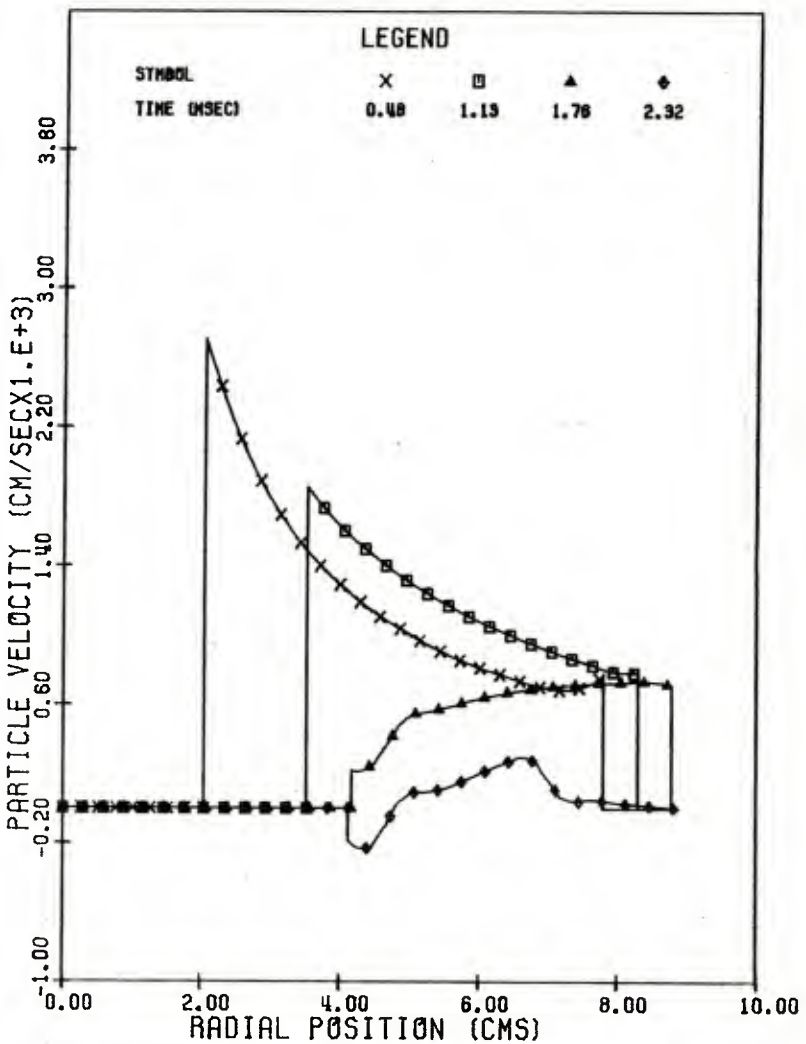

FIG.3.4.3 DISTRIBUTIONS OF SOLID VELOCITY ACCORDING TO CYLINDRICAL SOLUTION WITH 1.27 CM ULLAGE

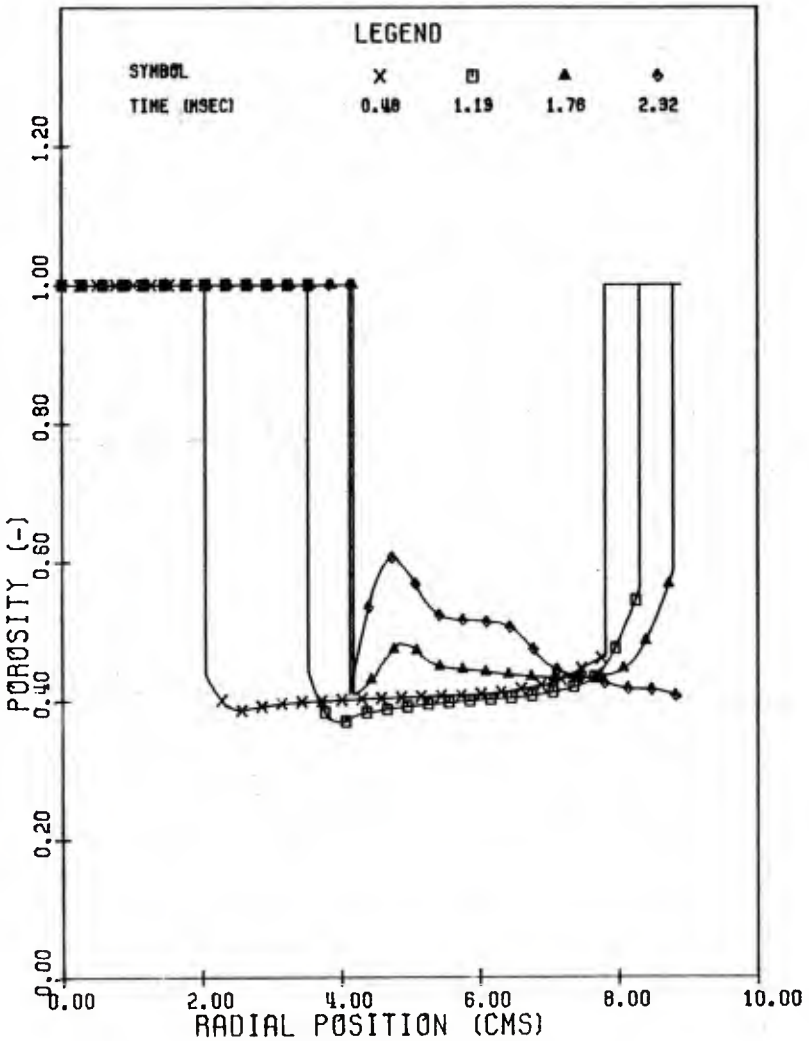

FIG.3.4.4 DISTRIBUTIONS OF POROSITY ACCORDING TO CYLINDRICAL SOLUTION WITH 1.27 CM ULLAGE

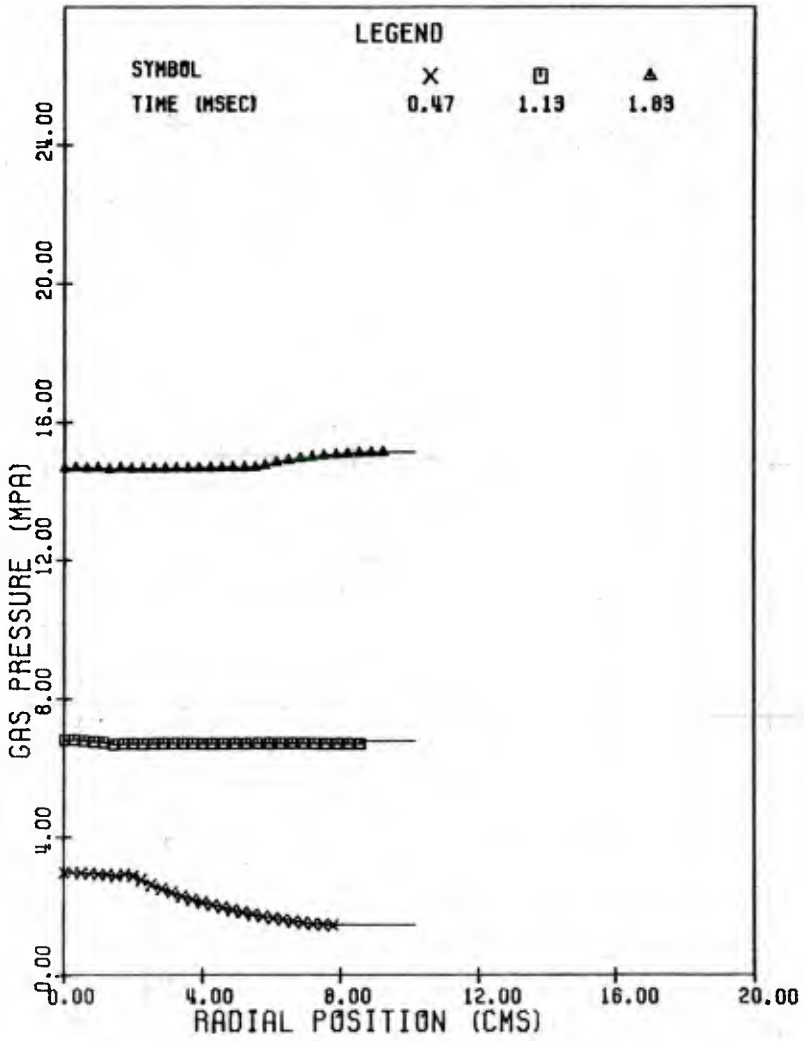

FIG.3.4.5 DISTRIBUTIONS OF PRESSURE ACCORDING TO CYLINDRICAL SOLUTION WITH 2.54 CM ULLAGE

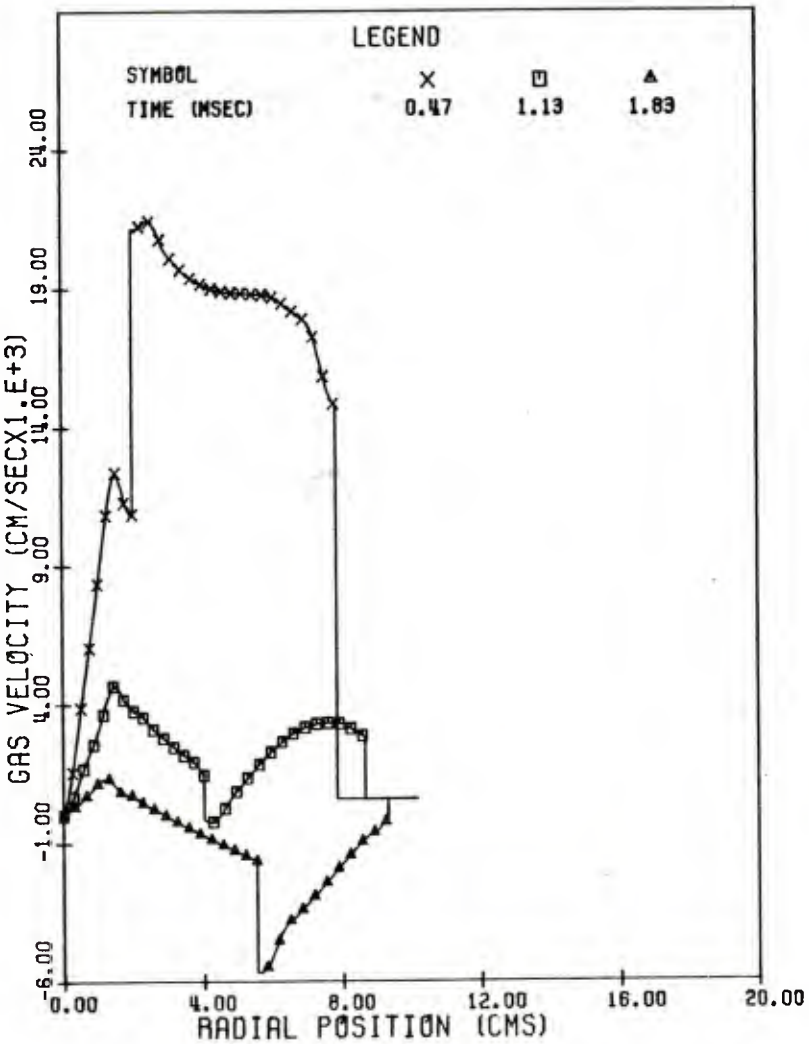

FIG.3.4.6 DISTRIBUTIONS OF GAS VELOCITY ACCORDING TO CYLINDRICAL SOLUTION WITH 2.54 CM ULLAGE

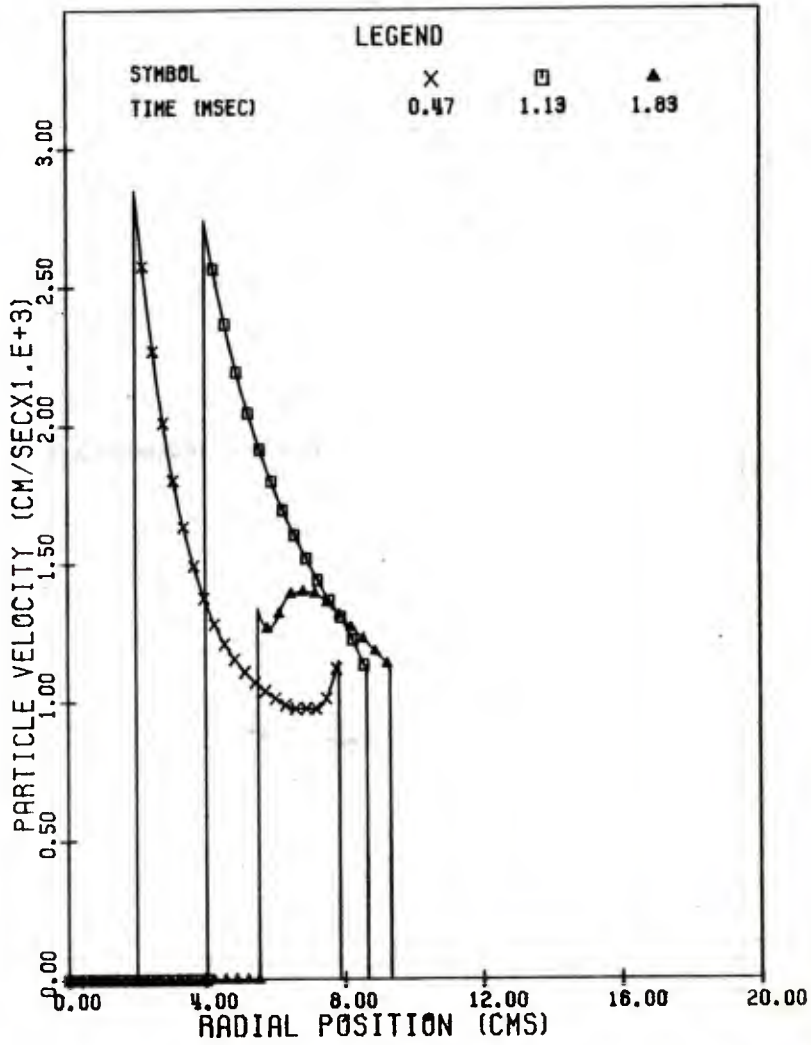

FIG.3.4.7 DISTRIBUTIONS OF SOLID VELOCITY ACCORDING TO CYLINDRICAL SOLUTION WITH 2.54 CM ULLAGE

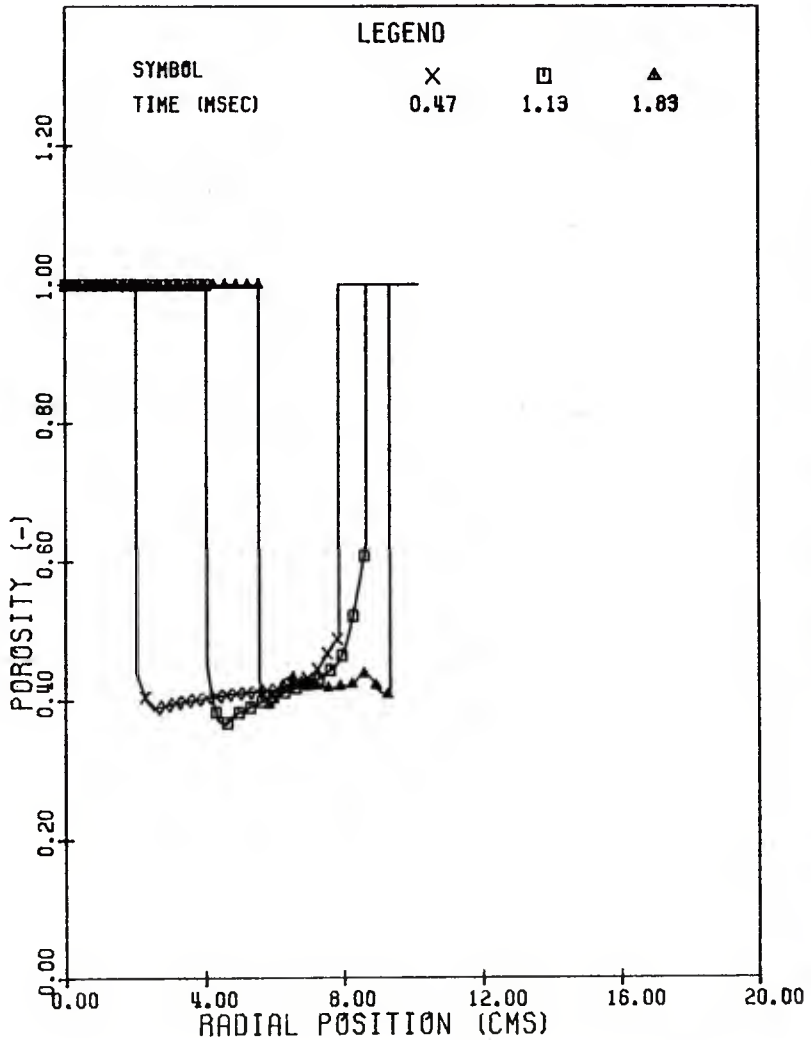

FIG.3.4.8 DISTRIBUTIONS OF POROSITY ACCORDING TO CYLINDRICAL SOLUTION WITH 2.54 CM ULLAGE

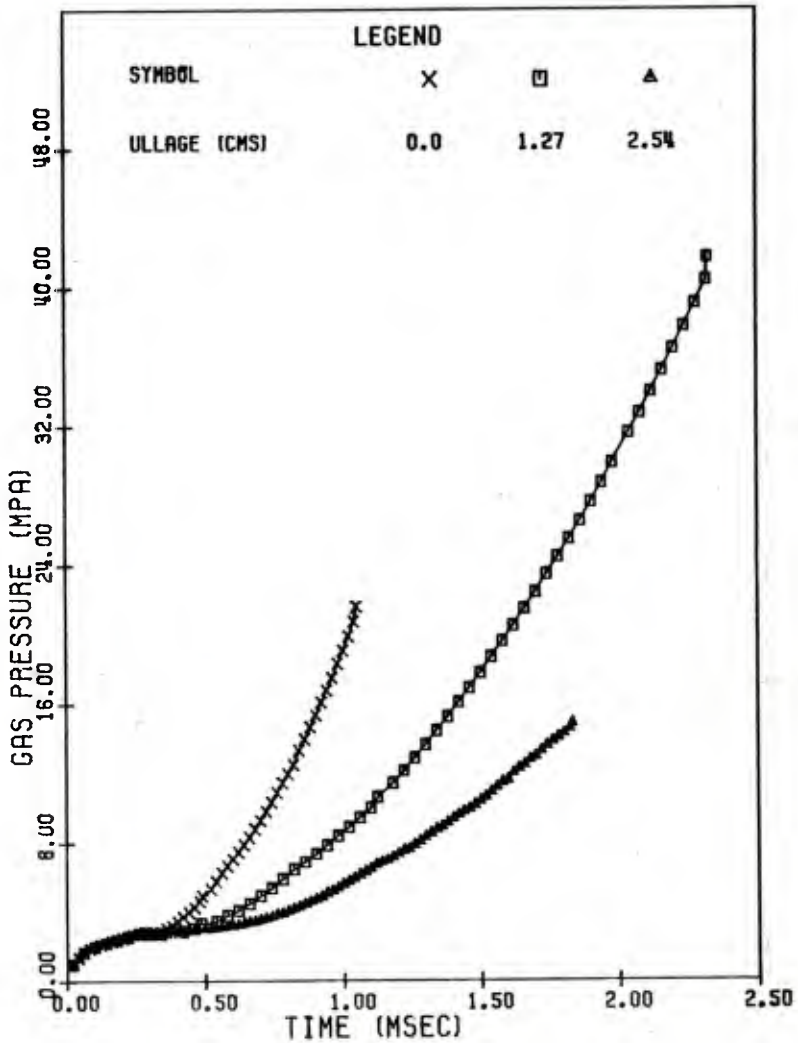

FIG.3.4.9 COMPARISON OF PRESSURE HISTORIES AT CENTER OF PROPELLANT BED FOR THREE VALUES OF EXTERNAL ULLAGE

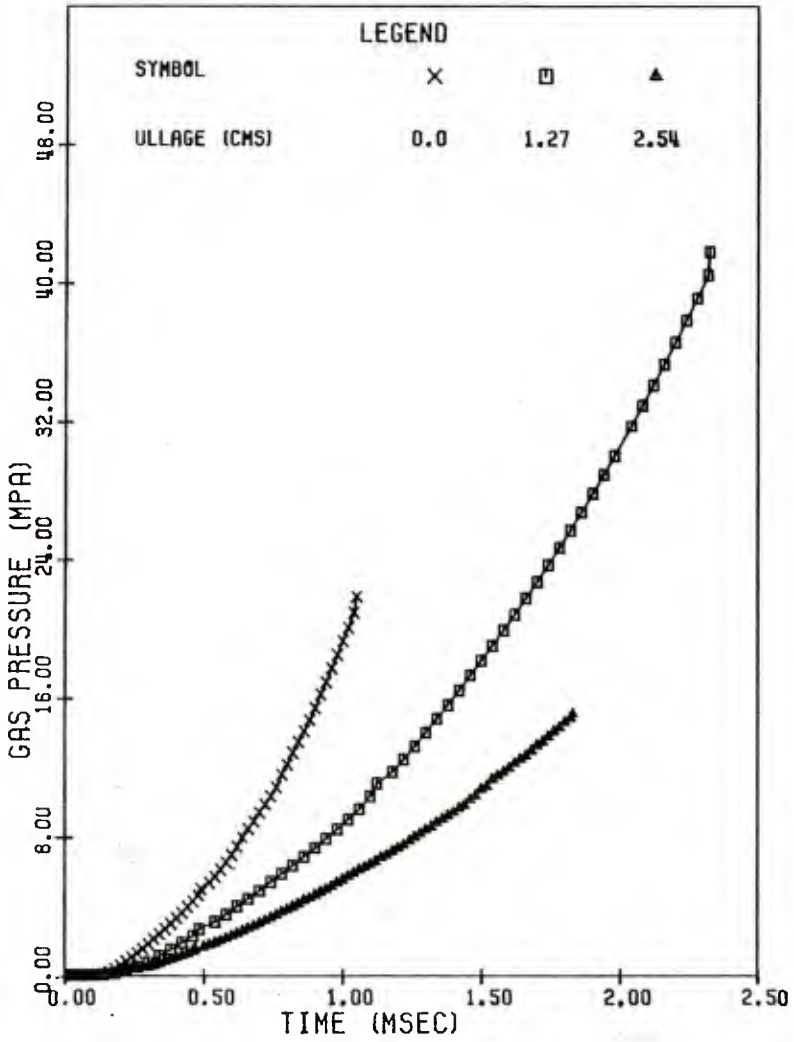

FIG.3.4.10 COMPARISON OF PRESSURE HISTORIES AT OUTSIDE OF PROPELLANT BED FOR THREE VALUES OF EXTERNAL ULLAGE

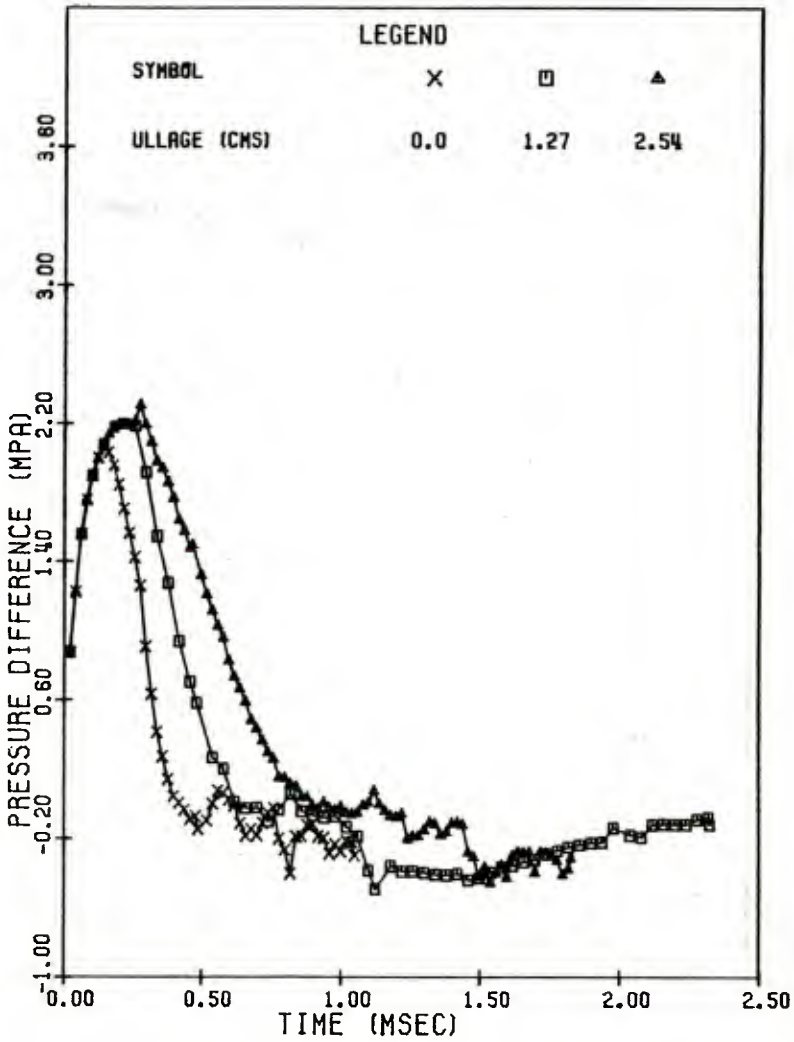

FIG.3.4.11 COMPARISON OF HISTORY OF RADIAL PRESSURE DIFFERENCE ACROSS PROPELLANT BED FOR THREE VALUES OF EXTERNAL ULLAGE

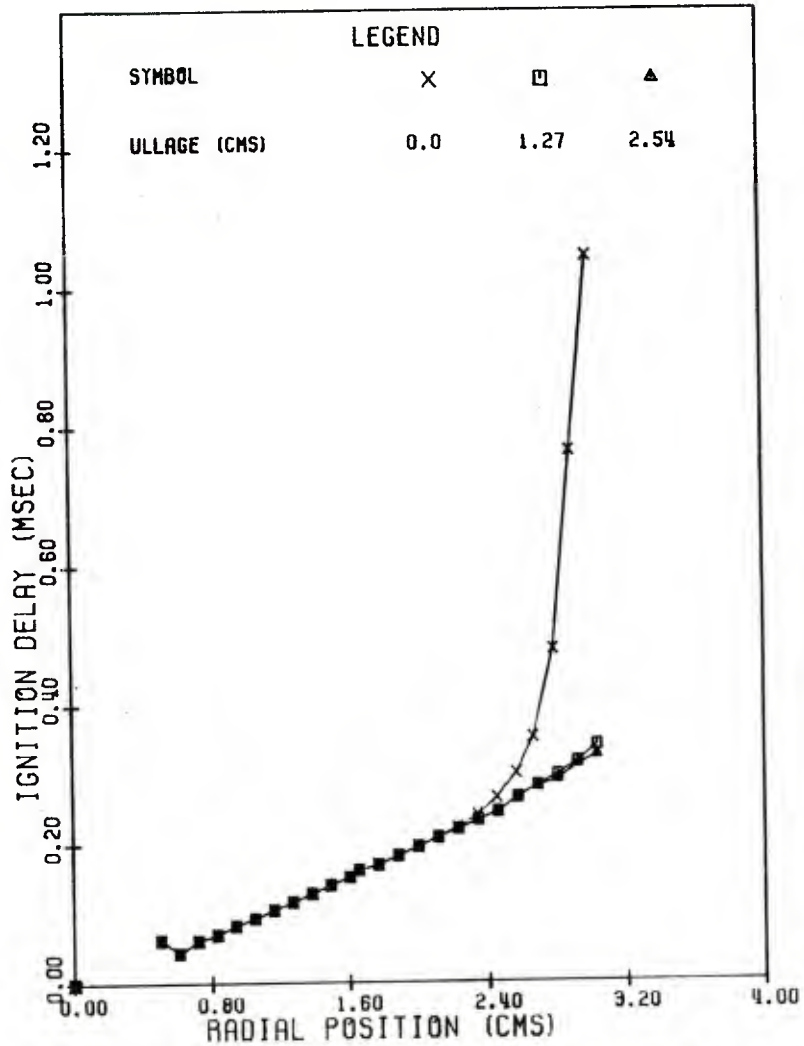

FIG.3.4.12 COMPARISON OF RATE OF FLAMESPREADING IN CYLINDRICAL PROPELLANT BED FOR THREE VALUES OF EXTERNAL ULLAGE

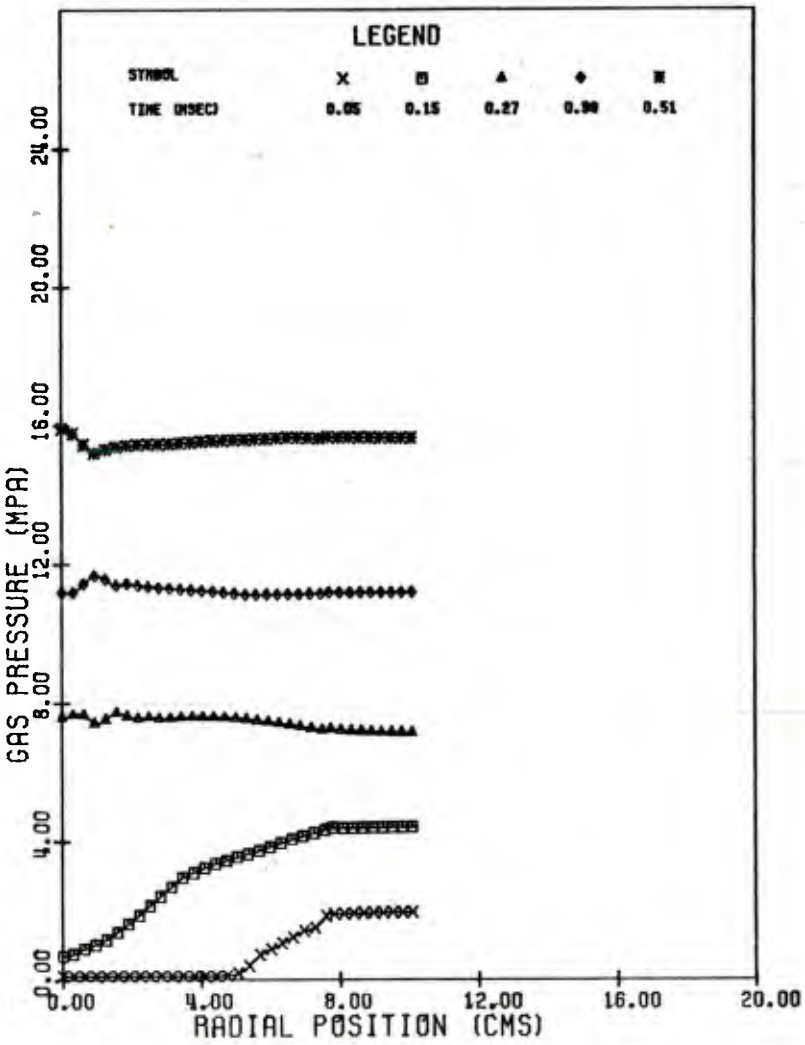

FIG.3.5.1 DISTRIBUTIONS OF PRESSURE ACCORDING TO CYLINDRICAL SOLUTION WITH 2.54 CM ULLAGE AND STRONG EXTERNAL IGNITION STIMULUS

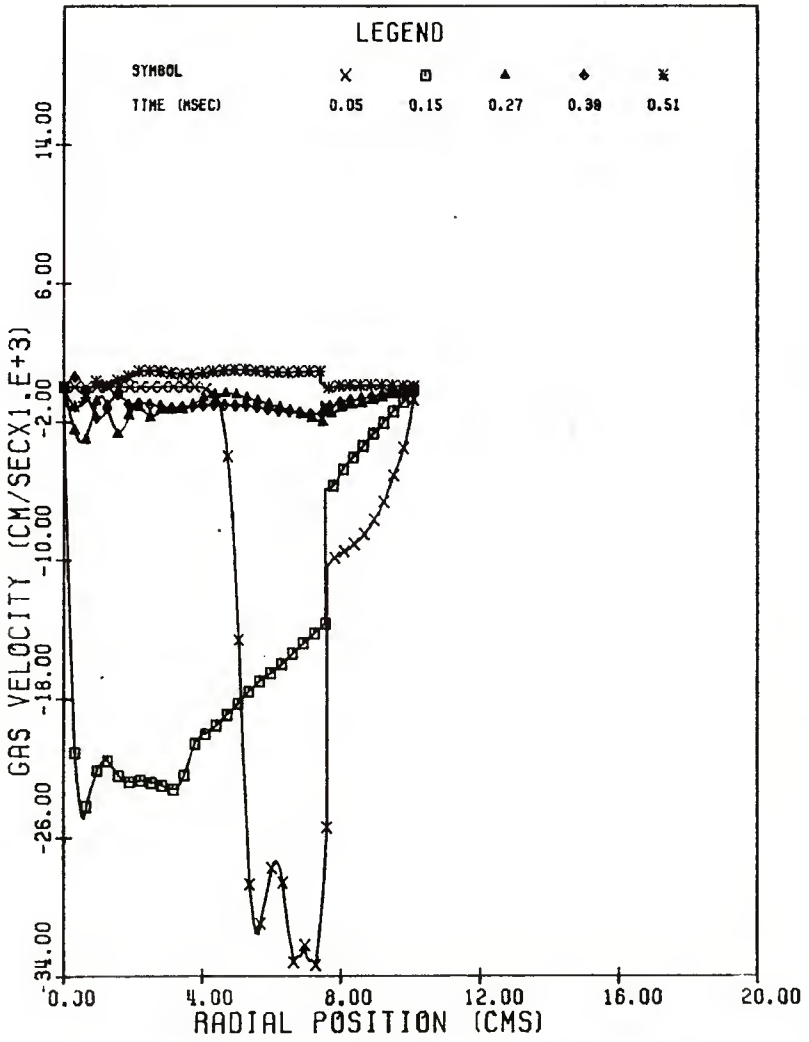

FIG.3.5.2 DISTRIBUTIONS OF GAS VELOCITY ACCORDING TO CYLINDRICAL SOLUTION WITH 2.54 CM ULLAGE AND STRONG EXTERNAL IGNITION STIMULUS

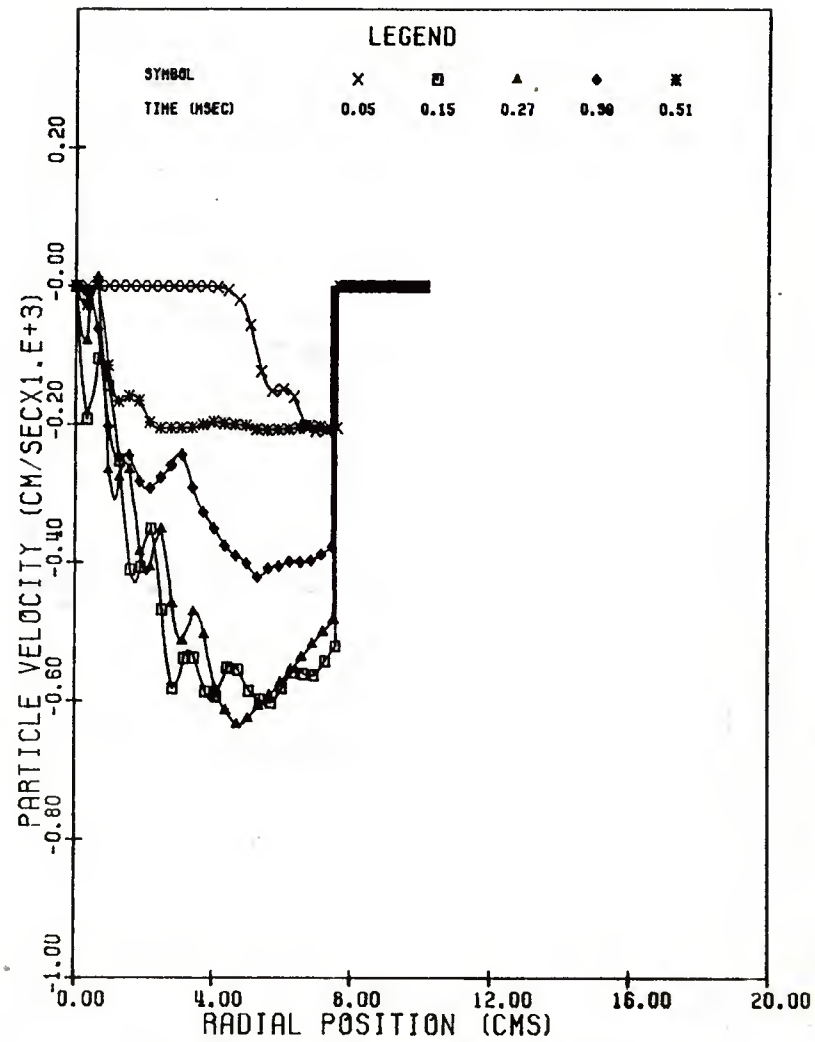

FIG.3.5.3 DISTRIBUTIONS OF SOLID VELOCITY ACCORDING TO CYLINDRICAL SOLUTION WITH 2.54 CM ULLAGE AND STRONG EXTERNAL IGNITION STIMULUS

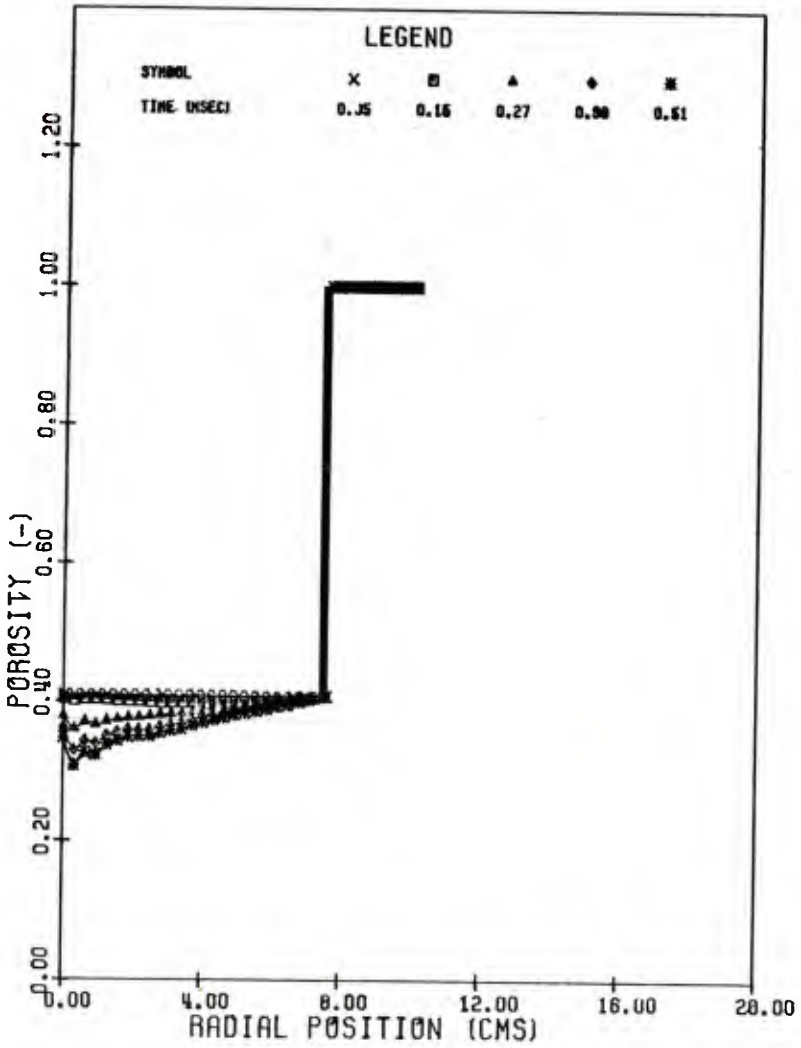

FIG.3.5.4 DISTRIBUTIONS OF POROSITY ACCORDING TO CYLINDRICAL SOLUTION WITH 2.54 CM ULLAGE AND STRONG EXTERNAL IGNITION STIMULUS

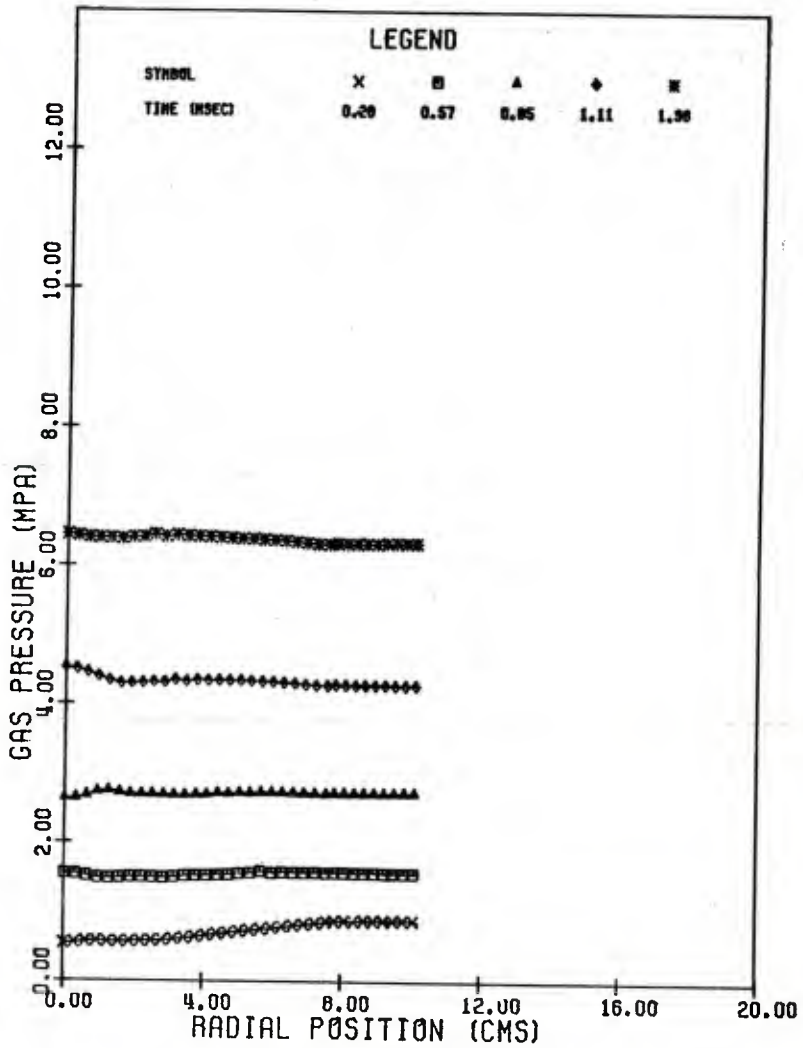

FIG.3.5.5 DISTRIBUTIONS OF PRESSURE ACCORDING TO CYLINDRICAL SOLUTION WITH 2.54 CM ULLAGE AND WEAK EXTERNAL IGNITION STIMULUS

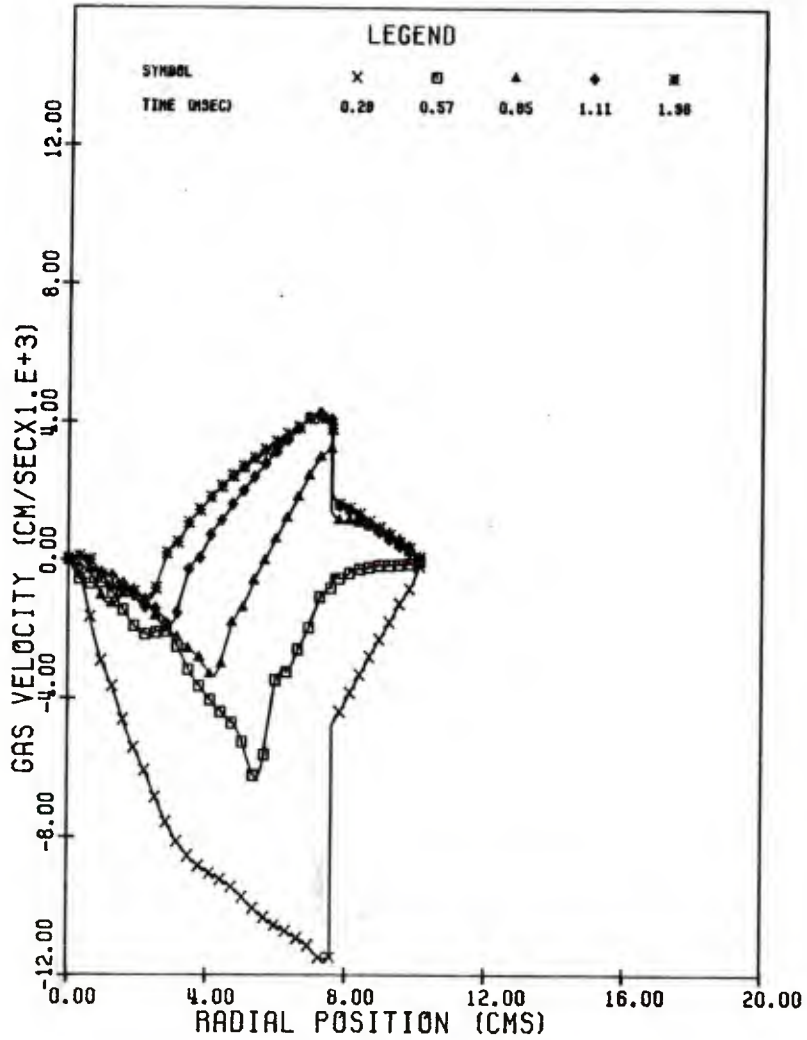

FIG.3.5.6 DISTRIBUTIONS OF GAS VELOCITY ACCORDING TO CYLINDRICAL SOLUTION WITH 2.54 CM ULLAGE AND WEAK EXTERNAL IGNITION STIMULUS

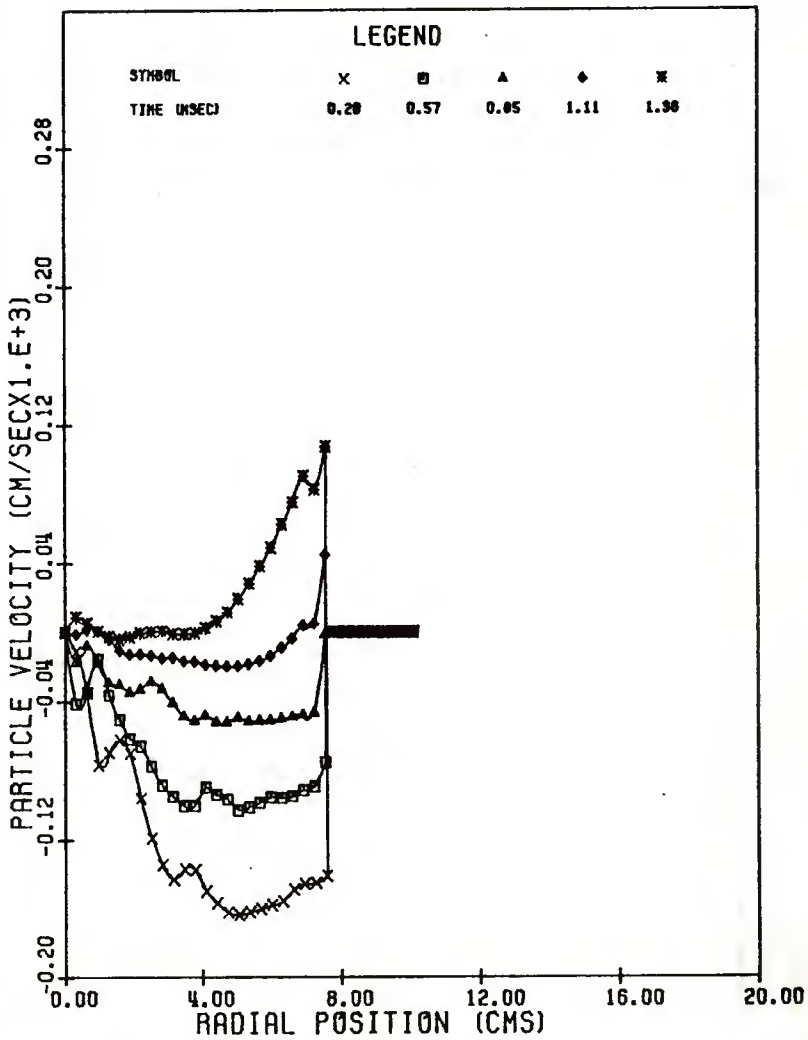

FIG.3.5.7 DISTRIBUTIONS OF SOLID VELOCITY ACCORDING TO CYLINDRICAL SOLUTION WITH 2.54 CM ULLAGE AND WEAK EXTERNAL IGNITION STIMULUS

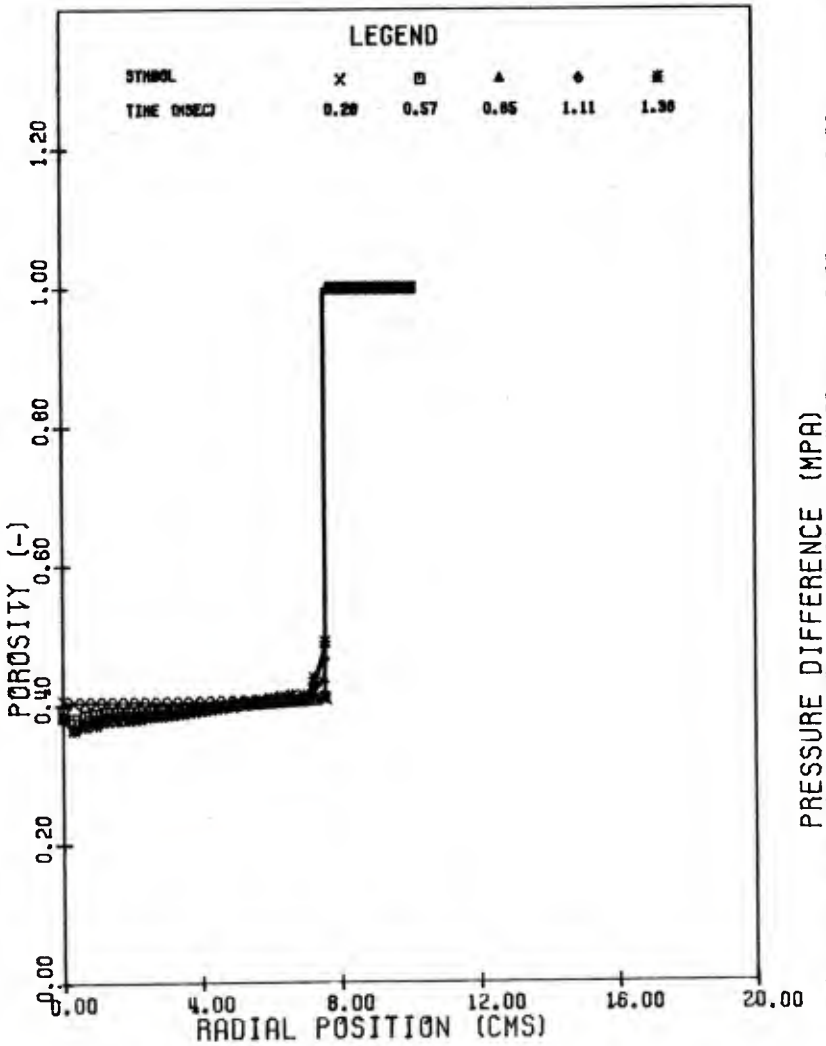

FIG.3.5.8 DISTRIBUTIONS OF POROSITY ACCORDING TO CYLINDRICAL SOLUTION WITH 2.54 CM ULLAGE AND WEAK EXTERNAL IGNITION STIMULUS

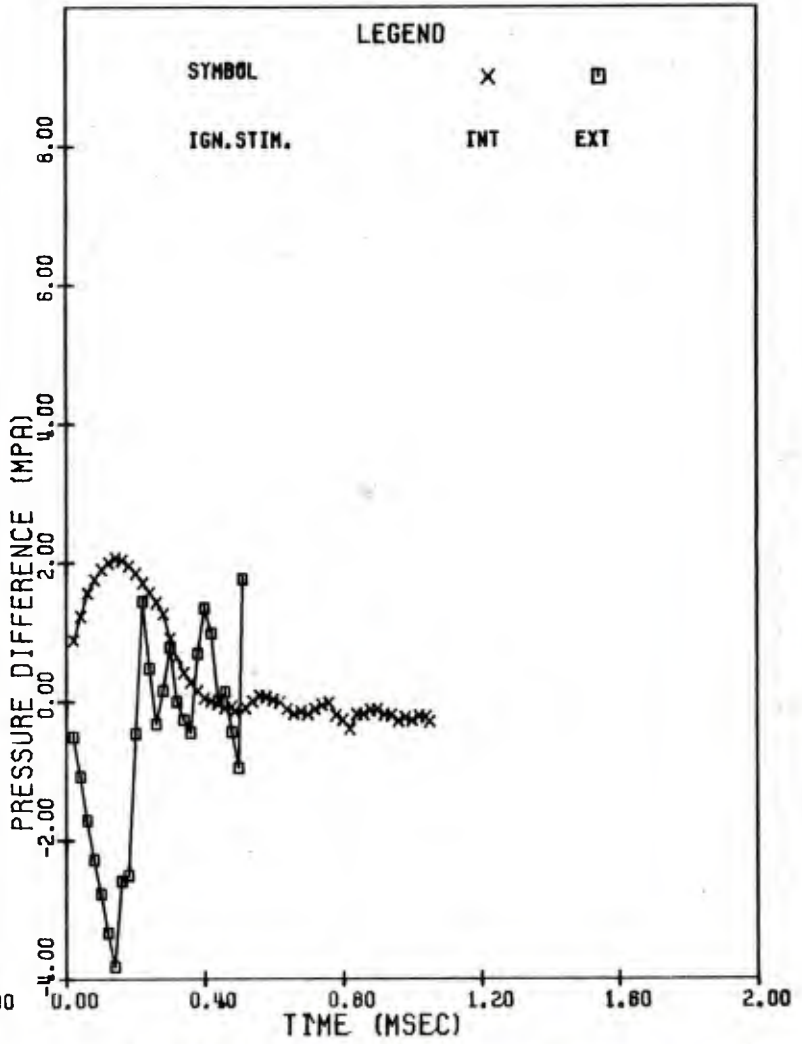

FIG.3.5.9 COMPARISON OF HISTORY OF RADIAL PRESSURE DIFFERENCE IN PROPELLANT BED INDUCED BY INTERNAL AND STRONG EXTERNAL IGNITION STIMULI

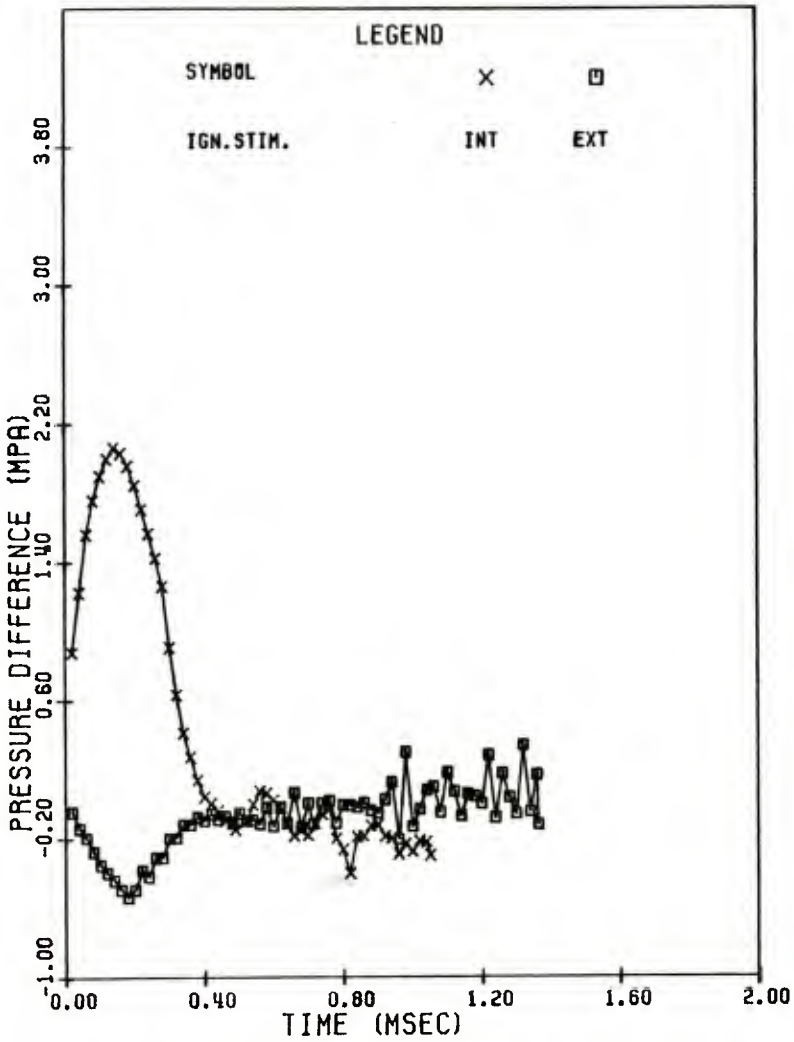

FIG.3.5.10 COMPARISON OF HISTORY OF RADIAL PRESSURE DIFFERENCE IN PROPELLANT BED INDUCED BY INTERNAL AND WEAK EXTERNAL STIMULI

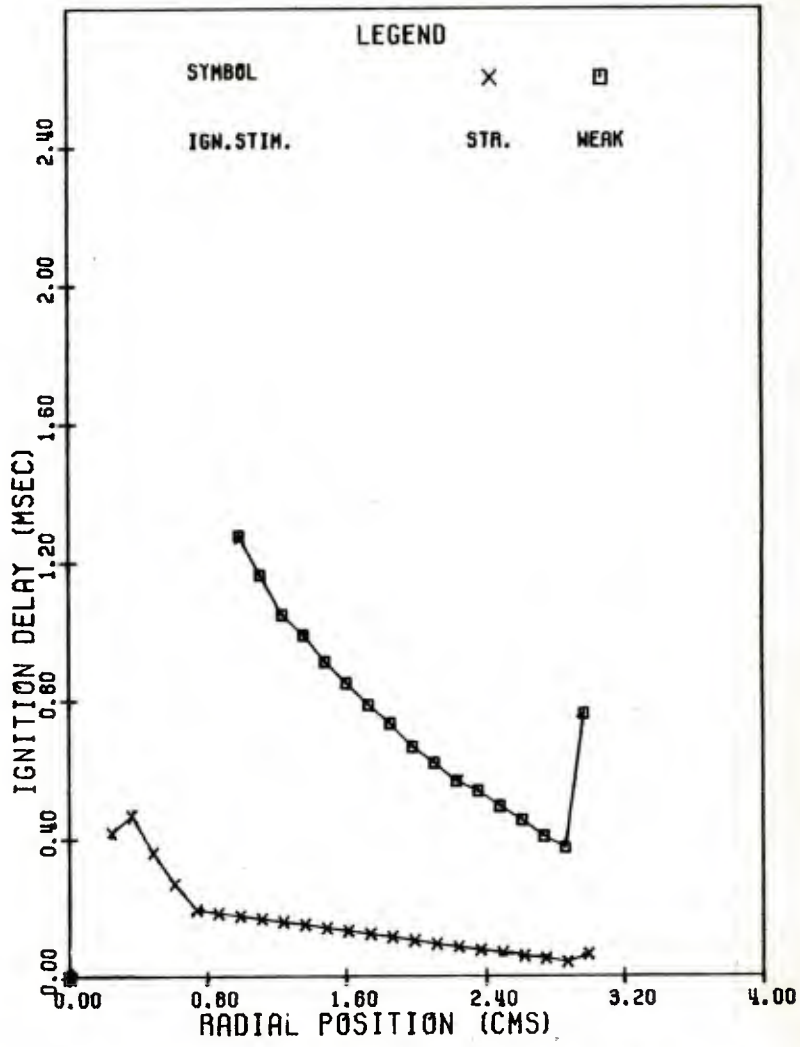

FIG.3.5.11 COMPARISON OF RATE OF FLAMESPREADING IN CYLINDRICAL PROPELLANT BED INDUCED BY STRONG AND WEAK IGNITION STIMULI

4.0 THE INFLUENCE OF ANNULAR ULLAGE AND BAG RUPTURE

In this chapter we attempt to assess the extent to which the quasi-one-dimensional approximation embedded in the NOVA code limits its predictive capacity in respect to the behaviour of a particular Army propelling charge. We do so by extending the physical model of the charge to recognize, in an approximate manner, that the propellant is initially contained within a bag, that the bag may serve as a flow impediment and that there exists, initially, a region of ullage between the cylindrical surfaces of the bag and the tube in addition to that in the breech and mouth of the chamber.

The numerical solutions are deduced from the 155mm cannon XM199 containing a charge of 10.9 kgm of seven perforation, M30A1 propellant ignited by a base bad. A solution is first generated using the present level of the NOVA code which does not recognize the annular ullage or the existence of a bag. Subsequently, the code is extended to treat the annular ullage as an axisymmetric continuum which exchanges mass with the centrally located propelling charge and with the axially distributed ullage. A model is proposed for the rate of opening of the bag and dispersal of the charge into the annular ullage. When the propellant is completely ignited, the solution is completed by means of the present version of the code. The two solutions are then compared with particular emphasis being given to the history of breech pressure, base pressure and pressure difference in the chamber.

In contrast to the previous chapter, a considerable body of analysis is required to establish what we have described in the introduction as a quasi-two-dimensional model. This is discussed in detail in section 4.1. The quasi-one-dimensional solution is presented in section 4.2. The corresponding quasi-two-dimensional solution is discussed in section 4.3 and the ballistic predictions of the two solutions are compared in section 4.4. Further discussion of these results is contained in section 6.0.

4.1 Analysis

We consider, in successive subsections, the balance equations for the two-phase flow within the bag, the balance equations for the annular and the axial regions of ullage and the constitutive laws which govern the behaviour of the bag and the mass transfer across it.

4.1.1 Balance Equations for the Two-Phase Flow within the Bag

We have previously deduced the balance equations under the assumption that the cross sectional area varied with position but not with time. In the present application we shall view the cross section of the bag as constituting the flow channel for the mixture until such time as the flow is fully fluidized and expanded to the walls of the tube. Therefore, the balance equations must be extended to reflect the time dependence of the cross sectional area. Moreover, we shall have to consider the bag as permeable to the gas phase although not to the solid phase.

Previously we deduced the quasi-one-dimensional form of the balance equations in an essentially analytical fashion, postulating a linear velocity profile in the radial direction and beginning with a three-dimensional formulation. However, in the interest of physical clarity we effect the desired extension by reference to a control volume formulation of the physical principles of conservation of mass, Newton's law of motion and the first law of thermodynamics.

4.1.1.1 Balance of Mass

It is taken for granted that our state variables will be macroscopic quantities. That is to say, they will constitute averages taken over regions large in comparison with the scale of heterogeneity of the mixture but small in comparison with the dimensions of the container. We deduce the governing equations for these average quantities by invoking the balance equations for the microscopic flow and asserting the coincidence of the local flow properties with the macroscopic value at all points within the control volume except those which lie on the interface between the media. On the interface it will be necessary to recognize the microscopic boundary condition expressed in terms of the jump conditions at a discontinuity.

Consider an arbitrary volume V bounded by the closed surface S. Let $\vec{w}$ be the velocity of a point on the surface and let $\vec{u}$ be the fluid velocity at the same point. Let ρ be the density of the substance which occupies V and let $\vec{n}$ be the outward facing normal to S. Then the principle of conservation of mass has the control volume formulation:

$$\frac{d}{dt}\int_V \rho dV = \int_S \rho(\vec{w}-\vec{u})\cdot\vec{n}da \qquad 4.1.1.1.1$$

In order to apply this principle to each of the two phases of the heterogeneous mixture, consider the sketch shown below. Let the cross sectional area of the duct be A(z,t). Let two stations be chosen, separated by a distance dz. The quantity dx is to be understood as a differential in the sense of continuum mechanics. That is to say, it represents a distance over which the average or macroscopic properties of the flow vary infinitesimally yet it is large compared with the scale of heterogeneity of the mixture. Let the volume occupied by the gas phase between the two stations be V_g and let V_p be the volume occupied by the solid phase. Let the total volume defined by the interval dz be denoted as $V = V_g + V_p$. Let the cross sectional area at each of the axial

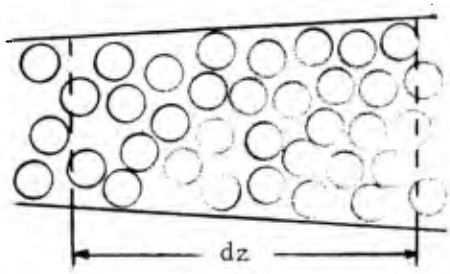

bounding surfaces be decomposed into A_g and A_p in a fashion analogous to that for the volume. Finally, denote the interface between the phases lying within dz as Σ. Evidently V_g is bounded by $A_g U \Sigma$ while V_p is bounded by $A_p U \Sigma$.

We may now state the mass balance for the gas phase by applying 4.1.1.1.1 to the control volume V_g:

$$\frac{d}{dt} \int_{V_g} \rho dV = \int_{A_g U \Sigma} \rho(\vec{w}-\vec{u})\cdot\vec{n} da \qquad 4.1.1.1.2$$

We now evaluate the terms of 4.1.1.1.2 one by one. Since the control volume is infinitesimal relative to the scale of variations of the macroscopic state variables we have:

$$\int_{V_g} \rho dV = \rho V_g = \varepsilon A \rho dz \qquad 4.1.1.1.3$$

where we have introduced the porosity:

$$\varepsilon = V_g/V \qquad 4.1.1.1.4$$

We may think of the state variables as representing microscopic quantities within the control volume law 4.1.1.1.2. However, equation 4.1.1.1.3 expresses a transformation from the microscopic to the macroscopic scale so that the resulting balance equations refer to average properties of the flow.

Accordingly, the left hand side of 4.1.1.1.2 is:

$$\frac{d}{dt} \int_{V_g} \rho dV = \frac{\partial}{\partial t} [\varepsilon A \rho] \, dz \qquad 4.1.1.1.5$$

We now turn to the evaluation of the surface integral on the right hand side. We suppose that the surface of the solid phase is regressing, due to combustion, at a rate $\dot{d}$. Therefore, on Σ we have $\vec{w} = \vec{u}_p + \vec{n}\dot{d}$. Making use of the jump condition which expresses conservation of mass at a discontinuity, we write:

$$\int_{\Sigma} \rho(\vec{w}-\vec{u})\cdot\vec{n} da = \rho_p \dot{d} \int_{\Sigma} da \qquad 4.1.1.1.6$$

The remaining integral on the right hand side of 4.1.1.1.6 is just the interphase surface area within the volume V. Taking the solid phase to consist of an aggregate of similar particles of individual surface area S_p and mass M_p we have:

$$\int_{\Sigma} da = (1-\varepsilon) \frac{S_p \rho_p}{M_p} A \, dz \qquad 4.1.1.1.7$$

Thus:

$$\int_{\Sigma} \rho(\vec{w}-\vec{u})\cdot\vec{n} da = (1-\varepsilon)\rho_p^2 \dot{d} \frac{S_p}{M_p} A \, dz \qquad 4.1.1.1.8$$

In order to evaluate the integral over A_g we assume that the porosity ε also describes the fraction of surface area available to the gas phase on both the ends and the circumferential portion of A_g. Then, using r_{bag} to denote the radius of the bag we have:

$$\int_{A_g} \rho(\vec{w}-\vec{u})\cdot\vec{n} da = - [\frac{\partial}{\partial z} \varepsilon\rho A u]dz - [2\pi r_{bag} \varepsilon dz]\dot{m}_{bag} \qquad 4.1.1.1.9$$

where we have u as the non-vanishing component of the macroscopic velocity and:

$$\dot{m}_{bag} = \rho(\vec{u}-\vec{u}_p)\cdot\vec{n} \qquad 4.1.1.1.10$$

is the mass flux per unit area across the circumferential portion of the control volume. Evidently $\dot{m}_{bag}$ represents the mass transfer between the bag and the radial ullage and will require a constitutive law which will relate it to the average conditions in the two regions. We take a positive value of $\dot{m}_{bag}$ to mean a transfer from the bag to the ullage.

By substituting 4.1.1.1.8 and 4.1.1.1.9 into 4.1.1.1.2 we have the continuity equation for the gas phase in the form:

$$\frac{\partial}{\partial t} \varepsilon A\rho + \frac{\partial}{\partial z} \varepsilon A\rho u = (1-\varepsilon)\rho_p^2 \frac{S_p}{M_p} A\dot{d} - 2\pi\varepsilon r_{bag} \dot{m}_{bag} \qquad 4.1.1.1.11$$

We have not considered the influence of the primer in the derivation of 4.1.1.1.11. As in previous work, we will represent the primer by a predetermined source term which we will incorporate in section 4.1.1.4 when we summarize the balance equations.

The balance of mass of the solid phase follows in an essentially analogous fashion. However, there is no transport of the solid phase across the circumferential portion of the control volume. Therefore, we have:

$$\frac{\partial}{\partial t}(1-\varepsilon)A + \frac{\partial}{\partial z}(1-\varepsilon)Au_p = -(1-\varepsilon)\rho_p \frac{S_p}{M_p}\dot{A}d \qquad 4.1.1.1.12$$

in which the assumption ρ_p = constant has been incorporated.

4.1.1.2 Balance of Momentum

The momentum balance for the gas phase within V_g may be stated analytically as:

$$\frac{d}{dt}\int_{V_g}\rho\vec{u}dV = \int_{A_g U\Sigma}\overleftrightarrow{\sigma}\cdot\vec{n}da + \int_{A_g U\Sigma}\rho\vec{u}(\vec{w}-\vec{u})\cdot\vec{n}da \qquad 4.1.1.2.1$$

where our nomenclature conforms with that of the previous section and we have introduced the stress tensor $\overleftrightarrow{\sigma}$. As in the previous section, we evaluate the terms one by one. Evidently, confining our attention to the axial component of velocity:

$$\frac{d}{dt}\int_{V_g}\rho\vec{u}_z dV = \frac{\partial}{\partial t}[\varepsilon A\rho u]dz \qquad 4.1.1.2.2$$

In order to evaluate the stress integral we suppose that the stress is everywhere hydrostatic and equal to the average gas pressure except on Σ where the influence of the boundary layer due to relative motion makes itself felt. We set:

$$\overleftrightarrow{\sigma} = -p\overleftrightarrow{I} + \overleftrightarrow{\sigma}' \qquad 4.1.1.2.3$$

where $\overleftrightarrow{\sigma}'$ may be thought of as a stress fluctuation tensor and is zero except within the boundary layer around each particle. We use $\overleftrightarrow{I}$ to signify the unit tensor of rank two. Evidently:

$$\int_{A_g U\Sigma}\overleftrightarrow{\sigma}\cdot\vec{n}da = \int_{\Sigma}\overleftrightarrow{\sigma}'\cdot\vec{n}da - \int_{A_g U\Sigma}p\vec{n}da \qquad 4.1.1.2.4$$

We assume that the first integral on the right hand side reflects the influence of drag and is a function of the relative velocity of the phases. It is to be resolved by reference to empirical data. As for the remaining term, we assume the pressure to be a smooth function of position so that using the divergence theorem and treating $\frac{\partial p}{\partial z}$ as constant throughout V_g we have:

$$\int_{A_g U \Sigma} (\overleftrightarrow{\sigma} \cdot \vec{n})_z da = - A f_s dz - \varepsilon A \frac{\partial p}{\partial z} dz \qquad 4.1.1.2.5$$

where f_s is understood to represent the velocity dependent interphase drag per unit volume.

Finally, referring to 4.1.1.2.1, we see that we must evaluate the momentum flux integral. On Σ we may apply the jump condition at a discontinuity in the form:

$$\rho \vec{u}_z (\vec{w}-\vec{u}) \cdot \vec{n} = \rho_p u_p \dot{d} + \Delta p \qquad 4.1.1.2.6$$

where Δp is the pressure jump and is negligible in all problems of interest to the interior ballistician. Thus using 4.1.1.2.6 and the nomenclature of the preceding section to describe the mass flux through the circumferential boundary of V_g we have:

$$\int_{\Sigma U A_g} \rho \vec{u}_z (\vec{w}-\vec{u}) \cdot \vec{n} da = (1-\varepsilon)\rho_p^2 \frac{S_p}{M_p} A \dot{u}_p dz - \frac{\partial}{\partial z}[\varepsilon A \rho u^2] dz$$

$$- [2\pi r_{bag} \varepsilon dz] u \dot{m}_{bag} \qquad 4.1.1.2.7$$

Here we have assumed $\dot{m}_{bag} > o$. If $\dot{m}_{bag} < o$, the corresponding momentum flux will involve u_g rather than u, where u_g is the gas velocity in the region of annular ullage. We will proceed under the assumption $\dot{m}_{bag} > o$ and note the revisions required when $\dot{m}_{bag} < o$ in section 4.1.1.4.

Thus combining 4.1.1.2.1, 4.1.1.2.2, 4.1.1.2.5 and 4.1.1.2.7 we see that:

$$\frac{\partial}{\partial t}[\varepsilon A \rho u] + \frac{\partial}{\partial z}[\varepsilon A \rho u^2] + \varepsilon A \frac{\partial p}{\partial z} = - A f_s$$

$$+ (1-\varepsilon)\rho_p^2 \frac{S_p}{M_p} A \dot{u}_p - 2\pi \varepsilon u r_{bag} \dot{m}_{bag} \qquad 4.1.1.2.8$$

If the left hand side is expanded and use is made of the continuity equation 4.1.1.1.11 we have the gas phase momentum equation in the form:

$$\varepsilon\rho\left[\frac{\partial u}{\partial t} + u\frac{\partial u}{\partial z}\right] + \varepsilon\frac{\partial p}{\partial z} = - f_s + (1-\varepsilon)\rho_p{}^2 \frac{S_p}{M_p}\dot{d}\,(u_p - u) \qquad 4.1.1.2.9$$

The derivation of the momentum equation for the solid phase is essentially similar to that for the gas phase. Indeed, when the solid phase is dispersed so that the average pressure in the particles is the same as in the ambient gas, the only differences arise from the fact that the exterior of the bag, by definition, is impermeable to the solid phase and the sign of f_s is opposed to that in equation 4.1.1.2.8. Thus the momentum equation for the dispersed solid phase may be deduced from 4.1.1.2.8 by replacing u by u_p throughout, setting $\dot{m}_{bag} = 0$, changing the sign of f_s and finally, replacing ε by $1-\varepsilon$, the corresponding quantity for the solid phase.

However, when the solid phase is packed we may not assume that the average stress is the same as that in the gas. We must consider that:

$$\overleftrightarrow{\sigma}_p = \overleftrightarrow{\sigma} - \overleftrightarrow{RI} \qquad 4.1.1.2.10$$

where R is the (hydrostatic) pressure due to contacts among the particles. Moreover, contributions to R can arise only on A_p since on Σ the jump condition for momentum applies. We assume that the reaction against the bag, or the wall of the tube, is similar in nature to that of the gas pressure. Therefore, the porosity will appear inside the derivative of the granular stress term, but the cross sectional area will not. Thus the solid phase momentum equation is:

$$(1-\varepsilon)\rho_p\left[\frac{\partial u_p}{\partial t} + u_p\frac{\partial u_p}{\partial z}\right] + (1-\varepsilon)\frac{\partial p}{\partial z} + \frac{\partial}{\partial z}(1-\varepsilon)R = f_s \qquad 4.1.1.2.11$$

The constitutive law for R will be discussed in detail in section 4.1.3.2.

4.1.1.3 Balance of Energy

As in previous work[1-5], we consider it necessary only to deduce an energy equation for the gas phase. Using e to denote the internal energy per unit mass and $\vec{q}$ to denote the heat flux we may state the first law of thermodynamics for the control volume V_g in the form:

$$\frac{d}{dt}\int_{V_g}\rho\left(e+\frac{u^2}{2}\right)dV = \int_{A_g U\Sigma}\rho\left(e+\frac{p}{\rho}+\frac{u^2}{2}\right)(\vec{w}-\vec{u})\cdot\vec{n}da - \int_{A_g U\Sigma}p\vec{w}\cdot\vec{n}da$$

4.1.1.3.1

$$- \int_{A_g U\Sigma}\vec{q}\cdot\vec{n}da + \int_{A_g U\Sigma}\overleftrightarrow{\sigma'}\cdot\vec{u}\cdot\vec{n}da$$

The procedure should be clear by now. The term on the left hand side will produce a partial derivative with respect to time of the total energy in the differential control volume V_g. The first term on the right hand side will provide a partial derivative with respect to z of the total enthalpy together with a source term due to combustion on Σ and a loss due to efflux over the circumferential boundary of A_g. The third term will involve a contribution only on Σ and will be interpreted as the interphase heat transfer, a quantity to be resolved empirically. The fourth term represents the rate of work done by the drag force and is readily stated in terms of f_s. Finally, the second term on the right hand side may be interpreted as the work to expand the control volume and may be resolved as:

$$\int_{A_g U\Sigma}p\vec{w}\cdot\vec{n}da = p\frac{\partial}{\partial t}A\varepsilon dz \qquad 4.1.1.3.2$$

The energy equation is thus determined to be:

$$\frac{\partial}{\partial t}\left[\varepsilon A\rho\left(e+\frac{u^2}{2}\right)\right] + \frac{\partial}{\partial z}\left[\varepsilon A\rho u\left(e+\frac{p}{\rho}+\frac{u^2}{2}\right)\right] + p\frac{\partial}{\partial t}\left[A\varepsilon\right]$$

$$= - Au_p\cdot f_s - (1-\varepsilon)\rho_p\frac{S_p}{M_p}Aq_s + (1-\varepsilon)\rho_p{}^2\frac{S_p}{M_p}A\dot{d}\left[e+\frac{p}{\rho_p}+\frac{u_p{}^2}{2}\right.$$

$$\left. - 2\pi r_{bag}\varepsilon\dot{m}_{bag}\left[e+\frac{p}{\rho}+\frac{u^2}{2}\right]\right. \qquad 4.1.1.3.3$$

If we expand the differentials on the left hand side and make use of the gas phase continuity and momentum equations we will have:

$$\varepsilon A\rho\left[\frac{\partial e}{\partial t} + u\,\frac{\partial e}{\partial z}\right] + \varepsilon A p\,\frac{\partial u}{\partial z} + p\left[\frac{\partial A\varepsilon}{\partial t} + u\,\frac{\partial \varepsilon A}{\partial z}\right]$$

$$= (u-u_p) f_s A - (1-\varepsilon)\rho_p \frac{S_p}{M_p} A q_s$$

$$+ (1-\varepsilon)\rho_p{}^2 \frac{S_p}{M_p} A\,\dot{d}\,\left[e_p + \frac{p}{\rho_p} - e + \tfrac{1}{2}(u-u_p)^2\right]$$

$$- 2\pi r_{bag}\,\varepsilon\,\frac{p}{\rho}\,\dot{m}_{bag} \qquad 4.1.1.3.4$$

4.1.1.4 Summary of Balance Equations

We now summarize the balance equations in a form suitable for comparison with earlier work[1-5]. It will be necessary to incorporate the influence of the primer. Moreover, a transformation to convective coordinates will be required, as described in chapter 2.0. We find:

Balance of Mass of Gas Phase:

$$\frac{\partial \varepsilon\rho}{\partial t} + \frac{u-\eta}{z_B}\,\frac{\partial}{\partial \zeta}\,\varepsilon\rho + \frac{\varepsilon\rho}{A z_B}\,\frac{\partial}{\partial \zeta}\,Au = (1-\varepsilon)\rho_p{}^2 \frac{S_p}{M_p}\,\dot{d} + \psi\left(1 - \frac{\varepsilon\rho}{\rho_{IG}}\right)$$

$$- \frac{2\varepsilon}{r_{bag}}\,\dot{m}_{bag} - \frac{\varepsilon\rho}{A}\left[\frac{\partial A}{\partial t} - \frac{\eta}{z_B}\,\frac{\partial A}{\partial \zeta}\right] \qquad 4.1.1.4.1$$

where we have assumed $A = \pi r_{bag}^2$ and ψ represents the action of the primer which we treat as injected without axial momentum. Moreover, we restrict our considerations to a single granular specie.

Balance of Momentum of Gas Phase:

$$\varepsilon\rho\left[\frac{\partial u}{\partial t} + \frac{u-\eta}{z_B}\,\frac{\partial u}{\partial \zeta}\right] + \frac{\varepsilon g_o}{z_B}\,\frac{\partial p}{\partial \zeta} = -f_s - \psi u + (1-\varepsilon)\rho_p{}^2 \frac{S_p}{M_p}\,\dot{d}\,(u_p - u) \qquad 4.1.1.4.2$$

Here we have neglected the influence of virtual mass[5] and incorporated the dimensional constant g_o. We have assumed $\dot{m}_{bag}$ to be positive.

Balance of Energy of Gas Phase:

$$\varepsilon\rho\left[\frac{\partial e}{\partial t} + \frac{u-\eta}{z_B}\frac{\partial e}{\partial \zeta}\right] + p\left[\frac{\partial \varepsilon}{\partial t} + \frac{u-\eta}{z_B}\frac{\partial \varepsilon}{\partial \zeta}\right] + \frac{\varepsilon p}{Az_B}\frac{\partial Au}{\partial \zeta}$$

$$= \frac{f_s}{g_o}(u-u_p) - (1-\varepsilon)\rho_p \frac{S_p}{M_p} q_s - \frac{\varepsilon p}{A}\left[\frac{\partial A}{\partial t} - \frac{\eta}{z_B}\frac{\partial A}{\partial \zeta}\right]$$

$$+ \psi\left[e_{IG} + \frac{p}{\rho_{IG}}(1-\varepsilon) - e + \frac{u^2}{2g_o}\right] - \frac{2\varepsilon}{r_{bag}}\dot{m}_{bag}\frac{p}{\rho}$$

$$+ (1-\varepsilon)\rho_p^2 \frac{S_p}{M_p}\dot{d}\left[e_p - e + \frac{p}{\rho_p} + \frac{(u-u_p)^2}{2g_o}\right] \qquad 4.1.1.4.3$$

Again, the effect of virtual mass has been neglected and we have assumed $\dot{m}_{bag} > 0$.

Balance of Mass of Solid Phase:

$$\frac{\partial \varepsilon}{\partial t} + \frac{u_p-\eta}{z_B}\frac{\partial \varepsilon}{\partial \zeta} - \frac{(1-\varepsilon)}{Az_B}\frac{\partial}{\partial \zeta}Au_p = (1-\varepsilon)\rho_p \frac{S_p}{M_p}\dot{d} + \frac{(1-\varepsilon)}{A}\left[\frac{\partial A}{\partial t} - \frac{\eta}{z_B}\frac{\partial A}{\partial \zeta}\right]$$

$$+ \psi(1-\varepsilon)/\rho_{IG} \qquad 4.1.1.4.4$$

Balance of Momentum of Solid Phase:

$$\rho_p(1-\varepsilon)\left[\frac{\partial u_p}{\partial t} + \frac{u_p-\eta}{z_B}\frac{\partial u_p}{\partial \zeta}\right] + (1-\varepsilon)\frac{g_o}{z_B}\frac{\partial p}{\partial \zeta} + \frac{g_o}{z_B}\frac{\partial}{\partial \zeta}(1-\varepsilon)R = f_s \qquad 4.1.1.4.5$$

It has been assumed throughout the preceding development that $\dot{m}_{bag}$ is positive, corresponding to a transfer from the bag to the annular ullage. We must also allow for the possibility of reversed flow. If $\dot{m}_{bag}$ is negative, 4.1.1.4.1, 4.1.1.4.4 and 4.1.1.4.5 will be unchanged. However, 4.1.1.4.2 will exhibit a source term involving $\dot{m}_{bag}$ and the velocity difference (u_g-u) where u_g is the axial velocity of the entering gas. Similarly, 4.1.1.4.3 will involve, as a coefficient of $\dot{m}_{bag}$, the expression $(e_g + p_g/\rho_g + (u_g-u)^2/2g_o - e)$ where the subscript g has been used to designate properties of the region of ullage.

4.1.2 Balance Equations for Regions of Ullage

Two distinct formulations are required to describe the regions of ullage. The annular ullage which arises due to the gap between the bag and the cylindrical walls of the tube is treated as a continuum so that axial transport can be studied. However, the axial ullage due to spaces in the breech and mouth of the chamber is treated according to a lumped parameter formulation throughout the period in which annular ullage exists. Once the radial gap has closed, our earlier formulation is adopted as described in chapter 2.0. Accordingly, the axial ullage is subject to a continuum representation, if sufficiently large, and provided that the annular ullage has disappeared.

The two subsequent subsections summarize the balance equations for the annular and axial ullage respectively.

4.1.2.1 Region of Annular Ullage

The balance equations for this region view the flow as that of an inviscid single phase substance subject to mass addition, or loss, as a consequence of transfers between the gap and the bag. The mass transfer is taken to be positive when the bag is the donor and the gap is the receiver. For computational reasons, we retain the balance equations in divergence form.

We note that:

$$\frac{1}{z_B}\frac{\partial}{\partial\zeta}[\psi(u-\eta)] = -\frac{\eta}{z_B}\frac{\partial\psi}{\partial\zeta} + \frac{1}{z_B}\frac{\partial\psi u}{\partial\zeta} - \psi\frac{\dot{z}_B}{z_B} \qquad 4.1.2.1.1$$

where ψ is an arbitrary quantity. Then by analogy with 4.1.1.1.11 and using 4.1.2.1.1 we have:

Balance of Mass

$$\frac{\partial}{\partial t}(A_g\rho_g z_B) + \frac{\partial}{\partial\zeta}[A_g\rho_g(u_g-\eta)] = 2\pi\varepsilon r_{bag}\dot{m}_{bag}z_B \qquad 4.1.2.1.2$$

We have used the subscript g to denote properties of the annular gap. The value of porosity on the right hand side refers to the properties of the bag at the same axial station.

Balance of Momentum

$$\frac{\partial}{\partial t}[A_g\rho_g u_g z_B] + \frac{\partial}{\partial\zeta}[A_g\rho_g u_g(u_g-\eta)] + g_o A_g\frac{\partial p_g}{\partial\zeta} = 2\pi\varepsilon u r_{bag}\dot{m}_{bag}z_B \qquad 4.1.2.1.3$$

Balance of Energy

$$\frac{\partial}{\partial t}\left[A_g\rho_g\left(e_g + \frac{u_g^2}{2g_o}\right)z_B\right] + \frac{\partial}{\partial \zeta}\left[A_g\rho_g\left(e_g + \frac{u_g^2}{2g_o}\right)(u_g - \eta)\right]$$

$$+ z_B p_g\left[\frac{\partial A_g}{\partial t} - \frac{\eta}{z_B}\frac{\partial A_g}{\partial \zeta}\right] + \frac{\partial}{\partial \zeta}\left(A_g u_g p_g\right) = 2\pi\varepsilon r_{bag}\dot{m}_{bag} z_B\left[e + \frac{p}{\rho} + \frac{u^2}{2g_o}\right]$$

4.1.2.1.4

It should be noted that in the foregoing we have assumed $\dot{m}_{bag}$ to be positive and the coefficients have therefore been designated as properties of the bag. If $\dot{m}_{bag}$ is negative the coefficients must naturally correspond to the properties of the region of ullage.

4.1.2.2 Region of Axial Ullage

The regions of axial ullage are treated according to a lumped parameter formulation during the period in which the annular ullage exists. Therefore, the balance equations for each such region consist of statements of mass and energy conservation; a momentum equation is not required. The equations must reflect mass transfer between the region of axial ullage and both the bag and the annular ullage. In addition, mass generation within the ullage may occur as a consequence of primer venting.

Using a subscript c to designate the properties of the lumped parameter region and using $\dot{m}_i$ to denote an entering mass flux and $\dot{m}_o$ to denote an exiting flux we have:

Rate of Change of Volume

$$\frac{dV_c}{dt} = \frac{\dot{m}_s}{\rho_{IG}} + A_R\dot{z}_R - A_L\dot{z}_L \qquad 4.1.2.2.1$$

where z_L, z_R are the left and right hand boundaries and A_L, A_R are the corresponding cross sectional areas of the tube. We also have:

$$\dot{m}_s = \int_{z_L}^{z_R} \psi A dz \qquad 4.1.2.2.2$$

Balance of Mass

$$\frac{d\rho_c}{dt} = \frac{1}{V_c}\left[\dot{m}_s\left(1-\frac{\rho_c}{\rho_{IG}}\right) + \Sigma\dot{m}_i - \Sigma\dot{m}_o + \rho_c(A_L\dot{z}_L - A_R\dot{z}_R)\right] \qquad 4.1.2.2.3$$

where the summations are over all entering and exiting fluxes.

Balance of Energy

$$\frac{de_c}{dt} = \frac{1}{\rho_c V_c}\left[\dot{m}_s(e_{IG} - e_c) + \Sigma\dot{m}_i\left(e_i + \frac{p_i}{\rho_i} + \frac{(u_i-u_c)^2}{2g_o} - e_c\right)\right.$$

$$\left. - \frac{p_c}{\rho_c}\Sigma\dot{m}_o + p_c(A_L\dot{z}_L - A_R\dot{z}_R)\right] \qquad 4.1.2.2.4$$

In the sum over the entering fluxes, the coefficients involve the properties of either the annular ullage or the bag according to the source of $\dot{m}_i$.

4.1.3 Constitutive Laws

In the two preceding sections we have considered those balance equations which are either new or modified as a consequence of the present study. It should be noted that the NOVA code does contain other balance equations[5] such as those for the compactible filler elements or for the heat conduction in the tube walls or the solid phase. However, we pay no attention to them here. Similarly, when we turn to the constitutive laws we cite only the new or modified laws associated with the present enquiry. We will discuss, in the subsequent subsections, the assumed behaviour of the bag, the granular stress law, the radial motion of the bed and, finally, mass exchange between the bag and the ullage.

4.1.3.1 Behaviour of Bag

With the exception of the work of Fisher[18], little appears to be known about the behaviour of the bag used to contain the charge, at least in the sense defined by the requirements of the present study. In general, the bag may be viewed as a thin structural member whose properties are uniform throughout its thickness. Therefore, it may be viewed as a membrane whose inertia may be neglected but whose strength and/or permeability may be important.

As a provisional measure, we adopt the following model of the behaviour of the bag. We assume that if the pressure outside the bag, within the region of annular ullage, exceeds the pressure within the bag, then the bag acts as an impermeable boundary whose motion is governed by the

compactability of the propelling charge. Thus we suppose that the excess external pressure is transmitted through the flexible cloth into the solid phase which takes up the load. The impermeability reflects the intrusion of the material into the intergranular interstices.

However, the situation is quite different when the bag is subjected to an excess of internal gas pressure. No external support exists, unless the bag is in contact with the tube, a case which we do not consider. Accordingly, the pressure differential must be supported by the hoop stress within the bag. As the bag cannot be expected to be particularly strong, rupture must occur under a relatively small load. Once this rupture load is exceeded we expect the bag material to be blown aside and the boundary between the mixture and the ullage to become fully permeable. Initially, we felt that it would be appropriate to neglect entirely the strength of the bag and to allow rupture to occur as soon as the internal pressure exceeded the external pressure. However, we found that the assumption of a small but non-zero strength was necessary to filter out the influence of numerical noise which precipitated what seemed to be premature rupture under pressure differentials whose magnitude corresponded to truncation errors.

On the basis of the data of Fisher[18] we assumed tentatively that the bag could support a radial pressure differential of 0.035 Mpa. This followed from Fisher's value of ~ 0.26 Mpa-cm for the shear strength of a typical material, the assumption that the tensile strength would be similar and the thin pressure vessel formula $\sigma = pr/t$ where r is the radius and t the thickness. However, the strength of the end closures was neglected altogether.

In the following sections we will note the influence of the assumed model of bag behaviour on the constitutive laws for granular stress, radial motion of the bed, and mass transfer.

4.1.3.2 Granular Stress Law

As described in chapter 2.0 we customarily use the constitutive law:

$$\frac{D}{Dt}_p (1-\varepsilon)R = - \frac{\rho_p a^2}{g_o} \frac{D\varepsilon}{Dt}_p \qquad \text{if } \frac{D\varepsilon}{Dt}_p \leq 0 \qquad 4.1.3.2.1$$

and:

$$R = 0 \qquad \text{if } \frac{D\varepsilon}{Dt}_p > 0 \qquad 4.1.3.2.2$$

Therefore, granular stresses are considered to occur in the solid phase only during loading. The functional dependence on porosity of the rate

of propagation of granular disturbances is:

$$a(\varepsilon) = \begin{cases} a_1 \dfrac{\varepsilon}{\varepsilon_o} & \text{if } \dfrac{D\varepsilon}{Dt_p} \leq o \quad \varepsilon \leq \varepsilon_o \\ a_1 \exp\left[-\kappa[\varepsilon-\varepsilon_o]\right] & \text{if } \dfrac{D\varepsilon}{Dt_p} \leq o, \ \varepsilon_o \leq \varepsilon \leq \varepsilon_1 \\ 0 & \text{if } \varepsilon > \varepsilon_1 = \varepsilon_o + \dfrac{\ell n 1000}{\kappa} \end{cases} \qquad 4.1.3.2.3$$

where ε_o is the settling porosity, a_1 the corresponding value of a and κ is the stress attenuation factor.

It must be recognized that this constitutive law is predicated on the assumption that the stress in the solid phase, due to granular contacts, is hydrostatic or isotropic in nature. This is tantamount to assuming that the granular aggregate has negligible shear strength or resistance to deformation. A natural consequence of this point of view is the fact that the normal reaction of the solid phase against the circumferential boundary must be equal to the granular stress just as is the case with the gas pressure. This fact is incorporated into the balance equation for the momentum equation for the solid phase, as described in section 4.1.1.2. In previous work the circumferential boundary was taken to be the wall of the gun tube. However, in the present study, the circumferential boundary is initially defined by the configuration of the bag which fails to provide the same constraint on lateral motion as the tube.

Accordingly, we must assume that if the bag is ruptured, no granular stress can arise until the solid phase has expanded to the wall of the tube. On the other hand, if the bag is sealed and the external pressure exceeds the internal pressure, we have the condition of radial equilibrium:

$$(1-\varepsilon)R = p_g - p \qquad 4.1.3.2.4$$

During the period in which the bag is sealed, 4.1.3.2.4 combines with the constitutive law to define the variation in porosity of the charge. Thus:

$$\frac{D\varepsilon}{Dt_p} = \begin{cases} -\dfrac{g_o}{\rho_p a^2} \dfrac{D}{Dt_p}(p_g - p) & \text{, loading} \\ 0 & \text{, unloading} \end{cases} \qquad 4.1.3.2.5$$

As we discuss, in the next section, this result may be combined with the continuity equation to enable a determination of the cross sectional area of the bag.

4.1.3.3 Radial Motion of Bag

When the bag is sealed the cross sectional area follows from 4.1.1.4.4 as:

$$\frac{\partial A}{\partial t} = \frac{\eta}{z_B}\frac{\partial A}{\partial \zeta} + \frac{A}{1-\varepsilon}\left[\frac{D\varepsilon}{Dt_p} - \frac{(1-\varepsilon)}{Az_B}\frac{\partial}{\partial \zeta} Au_p - (1-\varepsilon)\rho_p \frac{S_p}{M_p}\dot{d} - \frac{\psi}{\rho_{IG}}(1-\varepsilon)\right] \qquad 4.1.3.3.1$$

where $D\varepsilon/Dt_p$ is evaluated according to 4.1.3.2.5. The radius of the bag follows from the simple relationship $A = \pi r_{bag}^2$.

When the bag has ruptured, we assume that the motion of the radial boundary is driven by the interphase drag associated with the mass transfer. As an approximation, we assume that the high Reynolds number version of the Ergun correlation[8] can be used to describe the relationship. Therefore, the radial component of the drag is given by:

$$f_{s,r} = 1.75\,\frac{(1-\varepsilon)}{D_p}\,\frac{\dot{m}_{bag}^2}{\rho} \qquad 4.1.3.3.2$$

where D_p is the effective particle diameter $D_p = 6M_p/S_p\rho_p$. The radial equation of motion may be expressed by:

$$\frac{\partial u_{p,r}}{\partial t} + u_p\frac{\partial u_{p,r}}{\partial z} = \frac{f_{s,r}}{\rho_p(1-\varepsilon)} \qquad 4.1.3.3.3$$

which is just the solid phase momentum equation in the absence of radial gradients. The bag radius itself follows from:

$$\frac{\partial r_{bag}}{\partial t} + u_p\frac{\partial r_{bag}}{\partial z} = u_{p,r} \qquad 4.1.3.3.4$$

4.1.3.4 Mass Exchange Between Bag and Ullage

As in previous work, we suppose that the mass transfer can be described by the isentropic relations for an ideal gas. Thus we have:

$$\dot{m} = A_e \sqrt{\frac{\gamma g_o}{R_g}} \frac{p_2}{\sqrt{T_1}} \left(\frac{p_1}{p_2}\right)^{\frac{\gamma-1}{2\gamma}} \left[\frac{2}{\gamma-1}\left(\left(\frac{p_1}{p_2}\right)^{\frac{\gamma-1}{\gamma}} - 1\right)\right]^{\frac{1}{2}} \qquad 4.1.3.4.1$$

where the subscripts 1 and 2 refer to the donor and receiver sides respectively. However, the mass flow rate may not exceed:

$$\dot{m}_* = A_* \left\{\frac{\gamma g_o}{R_g}\left(\frac{2}{\gamma+1}\right)^{\frac{\gamma+1}{\gamma-1}}\right\}^{\frac{1}{2}} \frac{p_1}{\sqrt{T_1}} \qquad 4.1.3.4.2$$

where A_* is the minimum flow area between 1 and 2 and A_e is the flow area on the receiving side. Thus:

$$\dot{m}_{bag} = \min\ (\dot{m}, \dot{m}_*) \qquad 4.1.3.4.3$$

In the case of transfer to or from the radial ullage A_* is taken to be equal to ε. The value of A_{ext} is equal to 1 if flow is directed towards the ullage and ε if reversed. The static pressures are used to evaluate p_1 and p_2, the axial motion being treated as essentially uncoupled. In the case of transfer to or from the axial ullage these values of A_* and A_{ext} are multiplied by the value of the cross sectional area of the tube. However, the value of p_1 is based on the isentropic stagnation pressure on the donor side while p_2 is still taken to be the static value on the receiver side.

4.1.4 Computational Considerations

As far as the flow within the bag is concerned we simply note that the previously developed methodology[5] is followed here with a suitable allowance for the additional terms. In brief, the balance equations for the two-phase flow are updated using the MacCormack scheme supported by the method of characteristics at the boundaries. The axial ullage is represented according to a lumped parameter formulism and is updated by means of a predictor/corrector scheme simultaneously with the determination of the boundary values for the mixture.

The region of annular ullage, which has a continuum formulation, is also updated by means of a two-step explicit scheme. However, we decided to use the Richtmyer version[28] of the Lax-Wendroff scheme rather than that of MacCormack. We felt that the mass transfer from the bag might be a rather irregular function of position and that the smoothing effect of the predictor step, based on the diffusive Lax scheme, would be beneficial. The boundary values for the region of annular ullage were deduced according to the method of characteristics.

---

28. *Richtmyer, R.D. and Morton, K.W.*
"Difference Methods for Initial Value Problems"
Interscience *1967*

Both the two-phase flow and the flow in the annular ullage are required to be compatible, in some physical sense, with the state of the axial ullage at each end of the chamber. Conceptually, therefore, we are presented with a computational problem analogous to that previously solved in the case of ullage occurring between two bags of propellant[5]. That is to say, we must simultaneously update the lumped parameter region together with the boundary values of two contiguous continuum regions. An existing subroutine was modified for this purpose.

4.2 Quasi-One-Dimensional Solution

The data base for the analysis of the 155mm Howitzer was essentially the same in the two calculations, the only differences being associated with the representation of the initial distribution. The data are given in Tables 4.2.1 through 4.2.4. It may be seen that we are considering the same physical problem as that described by Nelson[29] and also by ourselves[5]. The following points are noteworthy.

[1] The value of the settling porosity corresponds to the initial condition for the quasi-two-dimensional calculation in which the bag radius is assumed to be 7.49 cms. Since, in the one-dimensional representation we take the bag as initially expanded to the walls of the tube, the initial value of the porosity in the present calculation is substantially larger than the settling porosity. Accordingly, the present calculation views the charge as dispersed. This assumption affects the magnitude of the granular stress, since the bed is compactible, and it affects the interphase drag, which is reduced as the bed is fluidized.

[2] In contrast to earlier analyses of this problem[5,29], the initial condition takes no account of the presence of the salt bag at the front end of the charge. We had previously noted[5] that the manner of representation of the salt bag was open to criticism since it was treated as a compactible filler element whose stiffness corresponded to the adiabatic compression of the column of air between it and the base of the projectile. Moreover, the flow of gas around it was neglected.

We desired to have as much compatibility as possible between the two present calculations. Since, therefore, we felt that flow from the annular ullage into the forward region would play an important role and since there was no obvious way to incorporate this effect simultaneously with an analysis of the salt bag, the salt bag was neglected altogether in both calculations.

The phenomenology of this problem, as perceived by a quasi-one-dimensional formulation, has been discussed in detail elsewhere[5]. In brief, venting of the igniter in the region of rear ullage causes ignition in the rear of the charge and monotonic flamespreading to the front. The bag is accelerated forward and, following ignition, also expands rearward. Stagnation of the forward boundary against the projectile base is closely associated with the formation of a reverse pressure gradient and is followed by stagnation at the breech. Separation of the forward boundary occurs following motion of the projectile.

29. Nelson, C.W.
"Some Simulations of a 155mm Howitzer with the NOVAE Code"
BRL IMR 451 November 1975

Table 4.2.1 Thermophysical Data Used to Simulate 155mm Howitzer

(1)	General Properties of Initial Ambient Gas:	
	Initial Temperature (°K)	294.4
	Initial Pressure (atm)	1.0
	Molecular Weight (gm/gm-mol)	29.0
	Ratio of Specific Heats (-)	1.4
(2)	General Properties of Propellant Bed:	
	Initial Temperature (°K)	294.4
	Virtual Mass Constant (-)	0.
	Rate of Propagation of Intergranular Stress in Settled Bed (m/sec)	442.
	Settling Porosity of Bed (-)	0.4094
(3)	Properties of Propellant:	
	Left Hand Boundary (cms)	5.08
	Right Hand Boundary (cms)	71.12
	Mass (kgm)	10.886
	Density (gm/cm^3)	1.583
	Outside Diameter (cms)	1.0528
	Perforation Diameter (cms)	0.0813
	Length (cms)	2.413
	Number of Perforations (-)	7
	Solid Phase Thermochemical Data:	
	Burning Rate Additive Constant	0.
	Burning Rate Pre-exponential factor ($cm/sec/(Mpa)^n$)	4.567
	Burning Rate Exponent (-)	0.67
	Ignition Temperature (°K)	450.
	Thermal Conductivity (J/cm-sec-°K)	2.661×10^{-2}
	Thermal Diffusivity (cm^2/sec)	8.677×10^{-4}
	Emmissivity Factor (-)	0.6
	Gas Phase Thermochemistry:	
	Chemical Energy Released in Burning (J/gm)	4426
	Molecular Weight (gm/gm-mol)	23.46
	Ratio of Specific Heats (-)	1.24
	Covolume (-)	26.15
(4)	Properties of Primer:	
	Chemical Energy Released in Burning (J/gm)	3465
	Ratio of Specific Heats (-)	1.24
	Molecular Weight (gm/gm-mol)	22.40
(5)	Projectile and Rifling Characteristics:	
	Initial Position of Base of Projectile (cms)	82.194
	Mass of Projectile (kg)	43.545
	Polar Moment of Inertia ($kg-cm^2$)	40.969
	Angle of Rifling (rad)	0.1047

Table 4.2.2 Tabular Values Used to Specify Internal Radius of Tube of 155mm Howitzer*

Distance From Breech (cms)	Radius (cms)
0	8.890
82.194	7.620
596.900	7.620

Table 4.2.3 Tabular Values Used to Specify Bore Resistance in 155mm Howitzer*

Distance From Breech (cms)	Resistive Pressure** (Mpa)
82.194	8.274
86.004	105.076
89.814	82.737
596.900	82.737

Table 4.2.4 Tabular Values Used to Specify Rate of Discharge of Igniter*

	Rate of Discharge (kg/cm/sec)***		
Position (cms)	0.	5.08	5.105
Time (msec)			
0	0.2857	0.2857	0.
50.	0.2857	0.2857	0.

* Values linearly interpolated

** Multiplied by Factor $14.7V_p^{-0.6}$ if V_p, projectile velocity, $\geq$ 8.2 m/sec

** Interpolated first spacewise then timewise

The numerical solution is illustrated in figures 4.2.1 through 4.2.6 which present distributions corresponding to the period of flamespreading. In spite of the difference in the treatment of the forward boundary condition they are quite close in appearance to those of reference 5 and require little discussion. In fact, it was asserted in reference 5 that this would be the case since the salt bag was found to be blown forward quite rapidly. The only point deserving a comment here relates to figures 4.2.1 and 4.2.6. We draw attention to the large jumps in pressure and temperature which occur at the forward boundary of the bed.

4.3 Quasi-Two-Dimensional Solution

Except that the propellant is explicitly represented as being contained in a bag whose initial radius is 7.49 cms, the data base for this solution is identical to that discussed in the previous section. The solution, during flamespreading, is exhibited in figures 4.3.1 through 4.3.11. Two things are immediately apparent from an inspection of these figures: the solution, within the bag, is completely different from that deduced according to the one-dimensional approximation and, the quality of the numerical solution is not as satisfactory.

As a consequence of the venting of the igniter, the propellant at the rear boundary of the bag is quickly ignited, just as it was in the one-dimensional representation. However, the presence of the annular ullage causes the flame to stall for some time. Burning continues at the boundary but the flame does not penetrate the bed appreciably. Instead, the products of combustion are found to vent around the bag. The converging cross sectional area soon results in a choked condition at the forward boundary of the region of annular ullage. This tends to limit the rate of loss somewhat and flamespreading through the bed resumes at the rear. Since the bag is treated as impermeable from without prior to rupture, there is no mass exchange between the bag and the annular ullage at this time. Rather, the bag is compressed due to the pressure differential and granular stresses of the order of a few Mpa are observed.

Meanwhile the forward region of ullage is filled with gas venting around the bag. Since the forward end of the bag is represented as permeable, a reversed flow occurs at the forward end. The rate of convection increases in vigor until ignition occurs at the forward end and flamespreading now proceeds in two regions, one at each end of the bag. As the two convective flames approach each other the regions in which ignition has occurred soon develop an excess of pressure with respect to the annular ullage. The bag ruptures in these stations, venting occurs and bag expansion commences. Eventually, the two flames coalesce, flamespreading is complete and the calculation is concluded by means of a quasi-one-dimensional formulism.

The manner of flamespreading is evident by reference to figure 4.3.1 in which the positions of the two flame fronts are apparent from the

pressure distributions. These distributions also reveal numerical wiggles which are not seen in the quasi-one-dimensional calculation. These are probably associated to a certain extent with the added structure of the flow field. However, the principal contribution is thought to arise from the mass transfer to the annular ullage. This turned out to have considerable stiffness, as we discuss further and, moreover, to have considerable variation with position, as we anticipated.

Figure 4.3.2 presents the density in the bag. The very large density just ahead of the flame fronts is due to local pressure equilibration superimposed on a sharp temperature gradient and is analogous to the density variation in a thermal boundary layer.

Figure 4.3.3 presents distributions of porosity. The local maximum at the left hand boundary of the bag is due to the early ignition at this point. We believe that the adjacent minimum represents a numerical anomaly although a careful check of the coding did not reveal any errors.

The distributions of gas and solid phase velocities are shown in figures 4.3.4 and 4.3.5. The loss of quality of the numerical solution can be ascertained by comparing figures 4.2.4 and 4.3.4. The multiform structure of the convective flame and the mass transfer to the annulus results in numerical wiggles which are not seen in the one-dimensional case. Figure 4.3.6 presents distributions of temperature within the bag and exhibits clearly the presence of the two separate flames.

The behaviour of the gas in the region of annular ullage is contained in figures 4.3.7 through 4.3.10. The pressure distributions, figure 4.3.7, are, of course, much smoother than their counterparts within the bag. The wiggles seen in the later distributions are not instabilities; they represent points at which the bag is freshly ruptured. It should be noted that at the later times, the static pressure at the forward boundary is almost continuous even though the flow is choked. This is due to the fact that the pressure within the bag is close to that in the region of axial ullage due to the large connecting flow area and that, following rupture, the pressure in the annular ullage must also approximate that within the bag as a consequence of mass transfer. The choking of the flow from the annular ullage into the region of axial ullage follows from a consideration of the stagnation pressure at the forward boundary, which is considerably larger than the static pressure.

The strong positive gradient of the gas velocity in the annular ullage is seen in figure 4.3.9. Figure 4.3.8 presents distributions of density, which are seen to be smooth. The temperature is seen in figure 4.3.10 and exhibits sharp variations in the vicinity of the freshly ruptured bag material.

Finally, figure 4.3.11 presents the distributions of bag radius at various times. It is noteworthy that the calculation represents this quantity as nearly constant. While surprising, this is in accord with the findings of the previous chapter.

We conclude this section with a discussion of the behaviour of the radial mass transfer which is the driving mechanism for radial bed expansion.

From a computational viewpoint, the mass transfer between the bag and the annular ullage proved to be quite troublesome. We found that an extremely small time step was required to assure numerical stability in the sense of an ordinary differential equation. Moreover, the pressure difference between the bag and the surrounding ullage tended to be so small that the mass transfer oscillated substantially between predictor and corrector steps. Probably, an operator splitting procedure would have to be incorporated if future calculations of this type are desired. That is to say, the mass transfer would be deduced according to a finer mesh spacing than the convective processes.

4.4 Comparison of Ballistic Predictions

In figures 4.4.1 through 4.4.3 we present comparisons of the predictions of breech and base pressure and of pressure difference between the breech and mouth of the chamber. It is evident that although the two solutions are completely different in respect to the manner of flamespreading, the overall effect on the chamber and base pressures is small, amounting to little more than a bias in time. Generally speaking, it appears that the neglect of the radial ullage results in an overestimate of the strength of pressure transients. This is borne out by a consideration of figure 4.4.3.

The reduction in pressure wave amplitude is a consequence of the tendency of the annular ullage to effect pressure equilibration throughout the chamber. This, too, results in a much reduced forward momentum of the propelling charge during flamespreading. We might also mention that the predicted values of muzzle velocity were very close being 769.4 m/sec and 771.8 m/sec for the quasi-one-dimensional and quasi-two-dimensional calculations respectively.

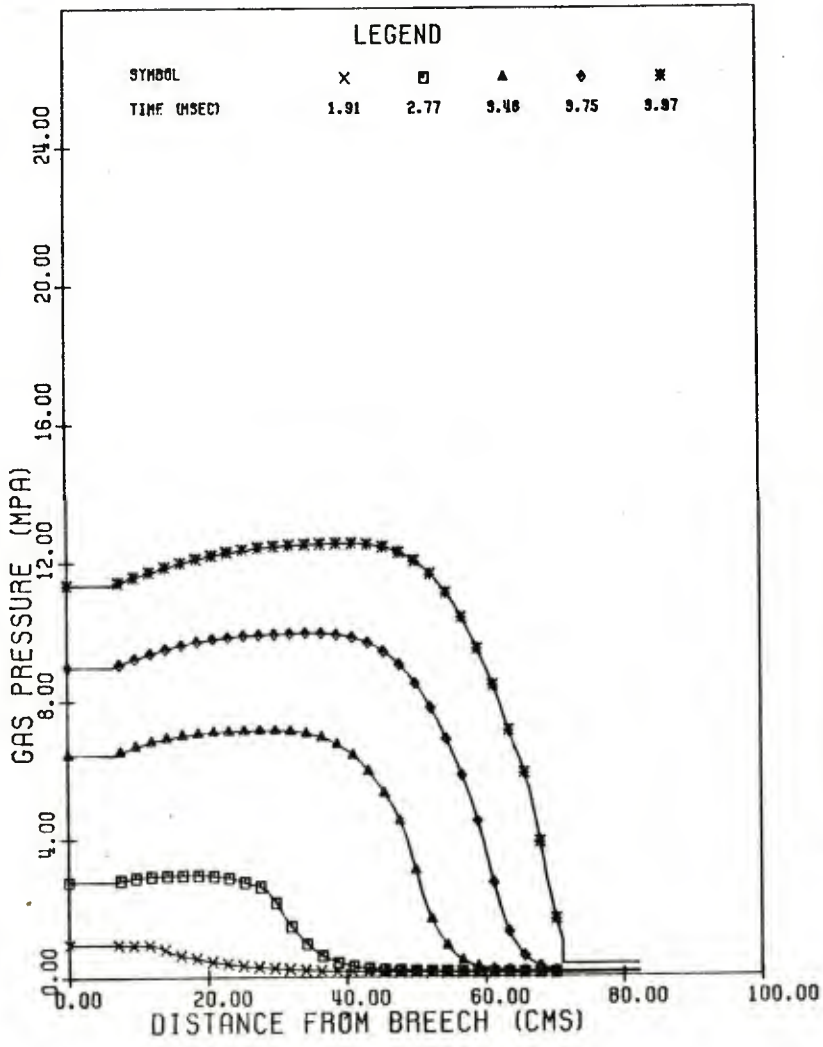

FIG.4.2.1 DISTRIBUTIONS OF PRESSURE IN 155MM HOWITZER ACCORDING TO QUASI-ONE-DIMENSIONAL CALCULATION.

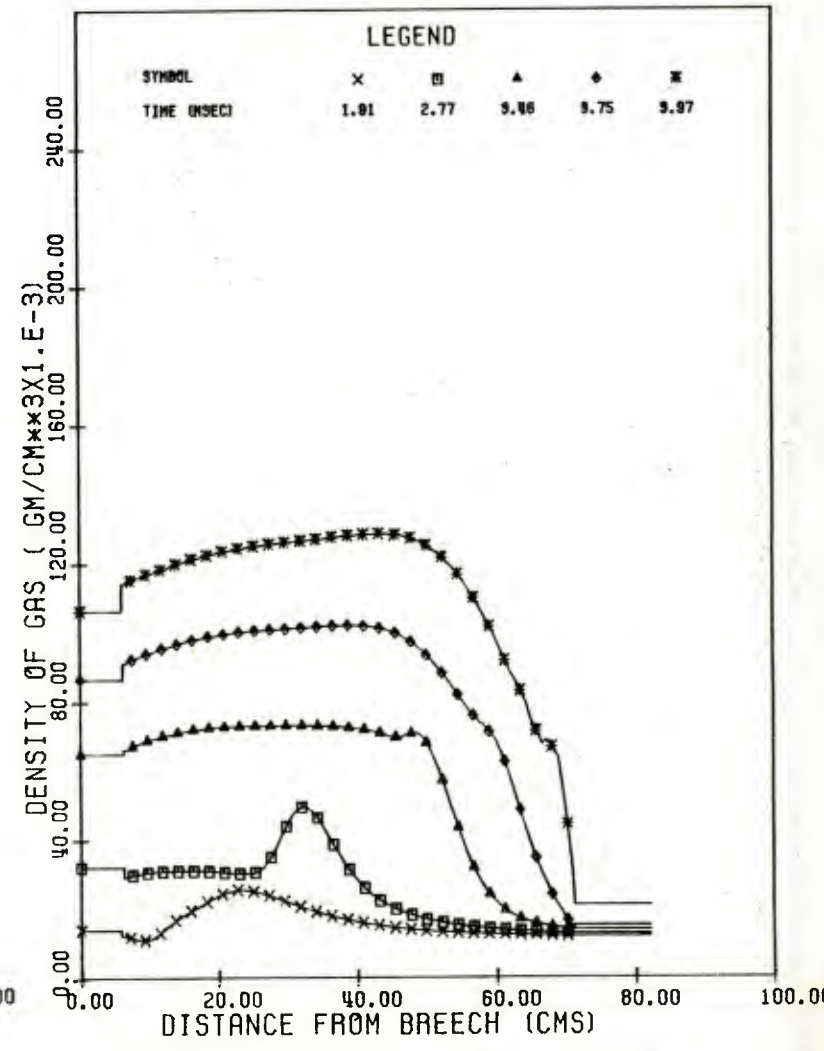

FIG.4.2.2 DISTRIBUTIONS OF DENSITY IN 155MM HOWITZER ACCORDING TO QUASI-ONE-DIMENSIONAL CALCULATION.

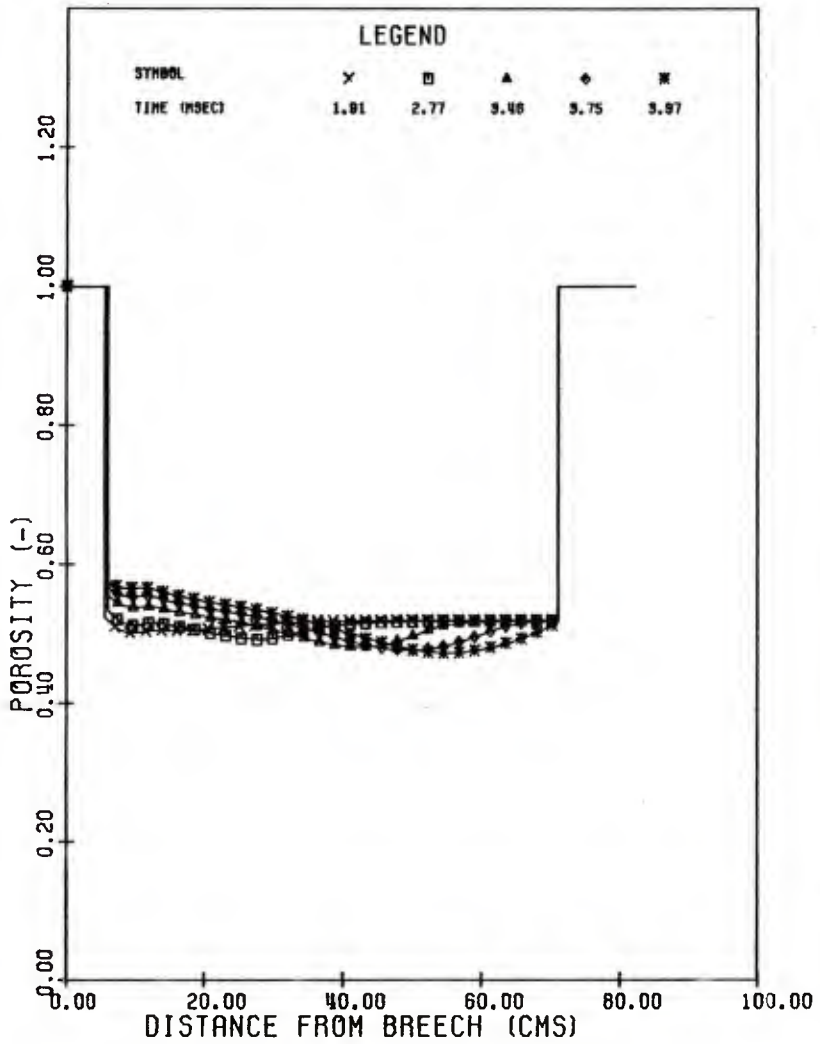

FIG.4.2.3 DISTRIBUTIONS OF POROSITY IN 155MM HOWITZER ACCORDING TO QUASI-ONE-DIMENSIONAL CALCULATION.

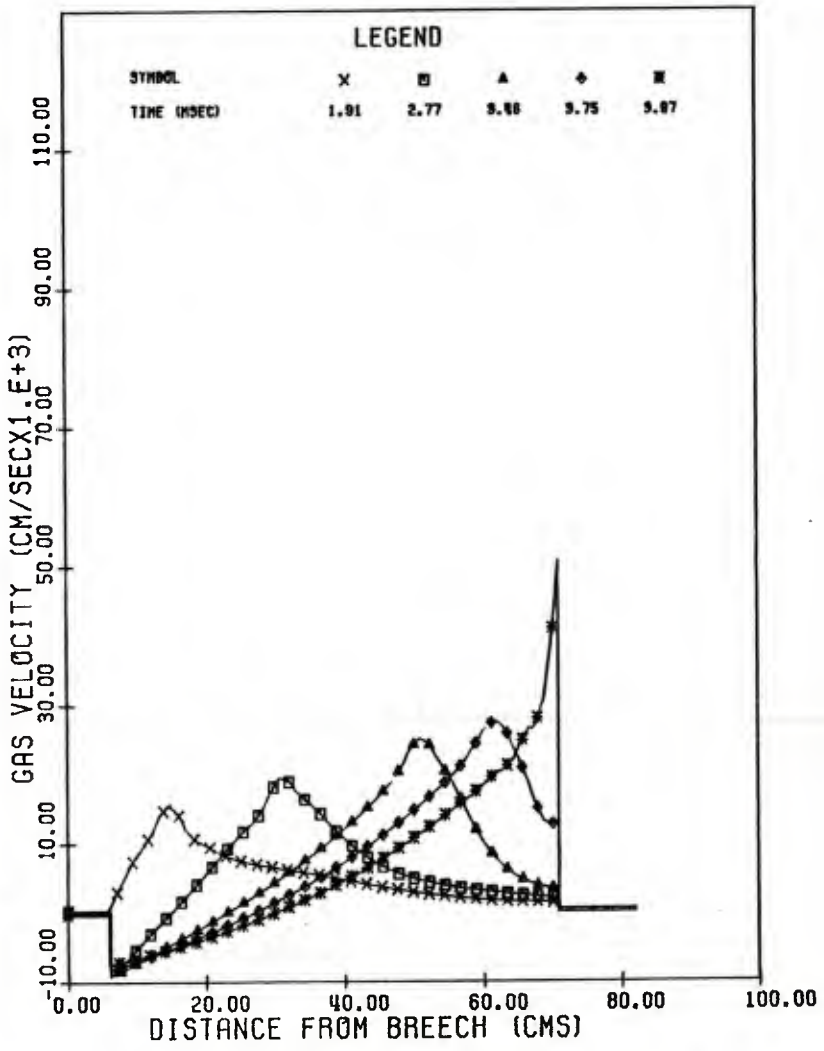

FIG.4.2.4 DISTRIBUTIONS OF GAS VELOCITY IN 155MM HOWITZER ACCORDING TO QUASI-ONE-DIMENSIONAL CALCULATION.

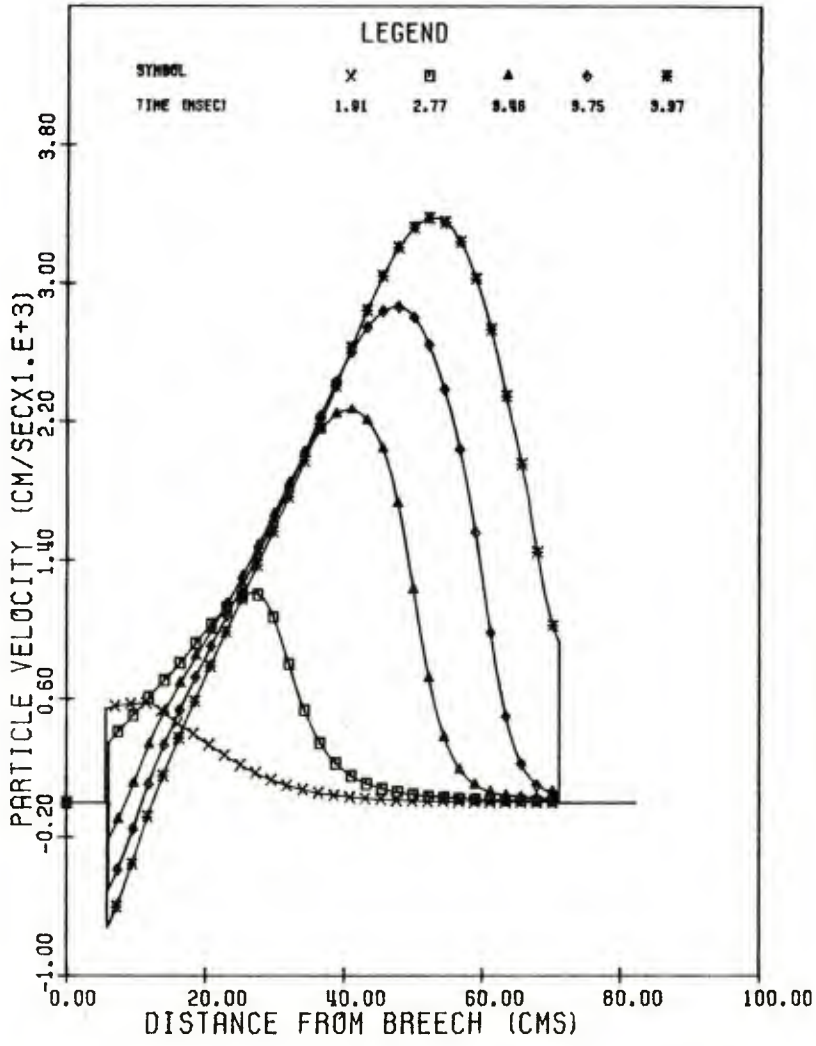

FIG.4.2.5 DISTRIBUTIONS OF SOLID VELOCITY IN 155MM HOWITZER ACCORDING TO QUASI-ONE-DIMENSIONAL CALCULATION.

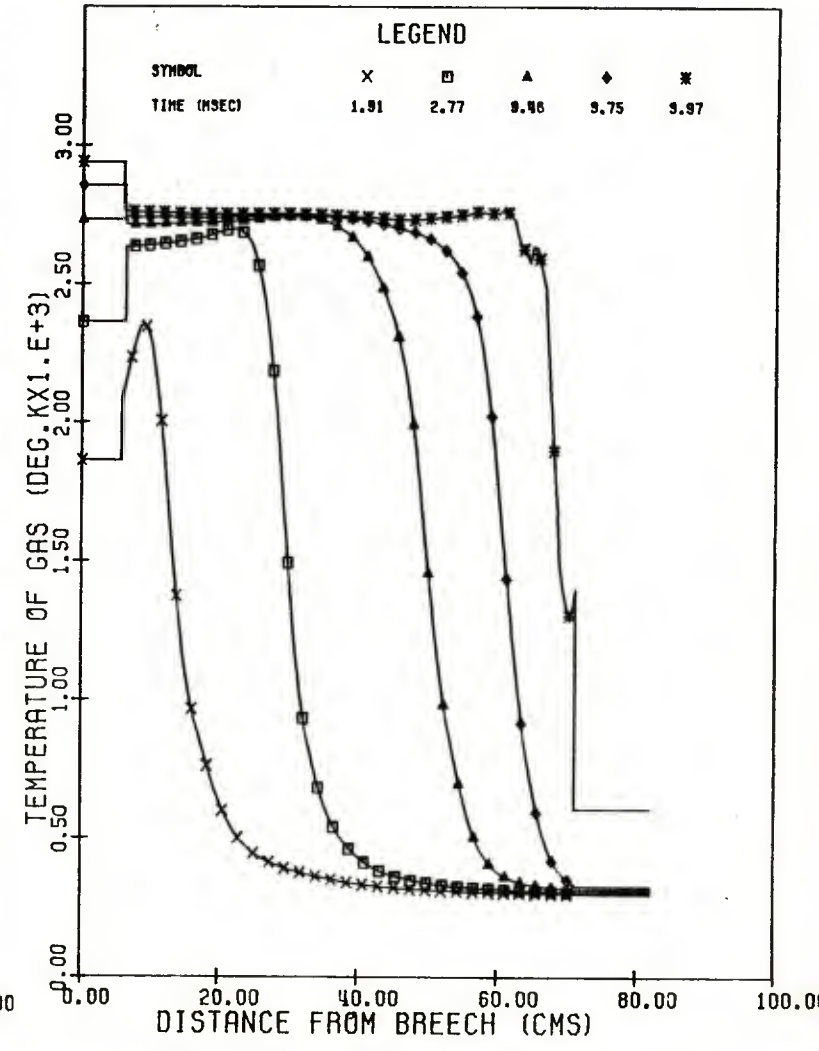

FIG.4.2.6 DISTRIBUTIONS OF TEMPERATURE IN 155 MM HOWITZER ACCORDING TO QUASI-ONE-DIMENSIONAL CALCULATION.

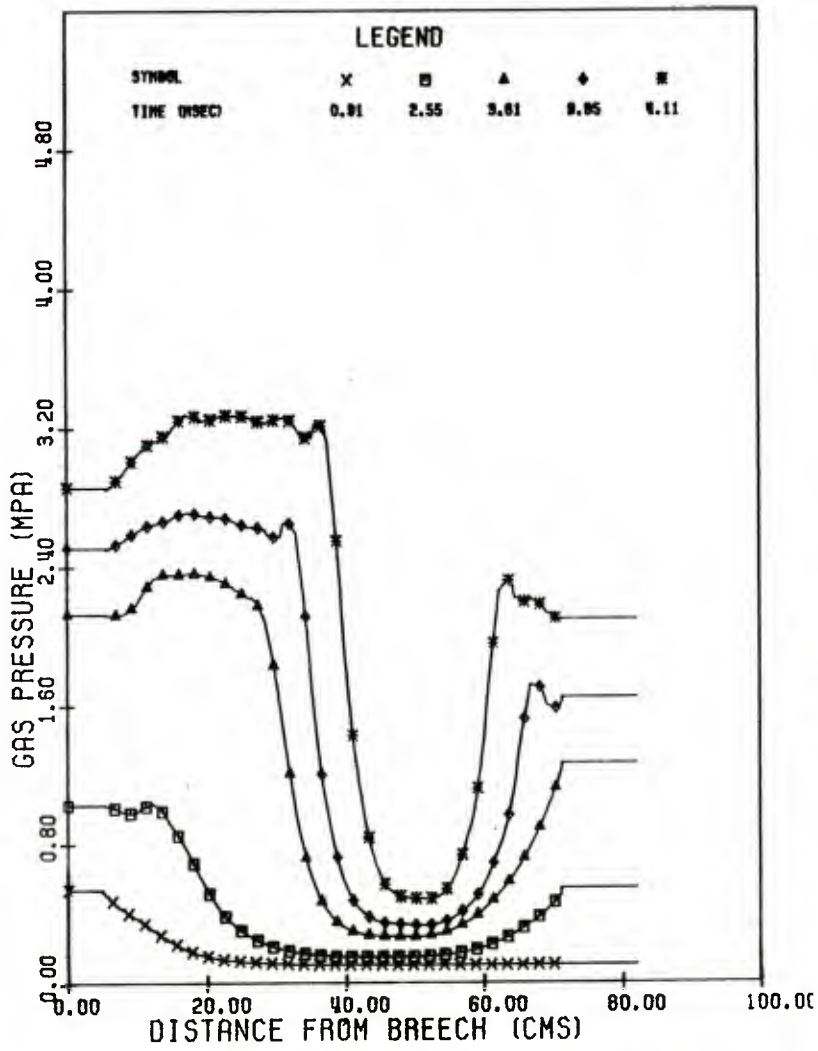

FIG.4.3.1 DISTRIBUTIONS OF BAG PRESSURE IN 155 MM HOWITZER ACCORDING TO QUASI-TWO-DIMENSIONAL CALCULATION.

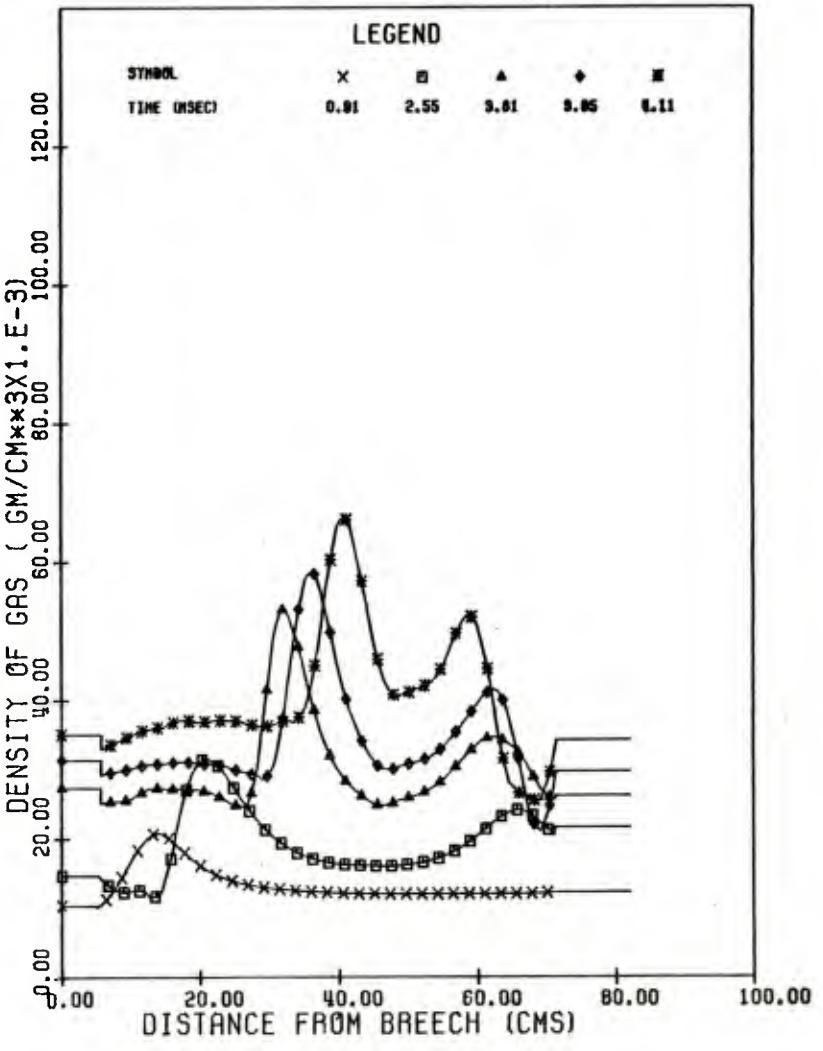

FIG.4.3.2 DISTRIBUTIONS OF BAG DENSITY IN 155 MM HOWITZER ACCORDING TO QUASI-TWO-DIMENSIONAL CALCULATION.

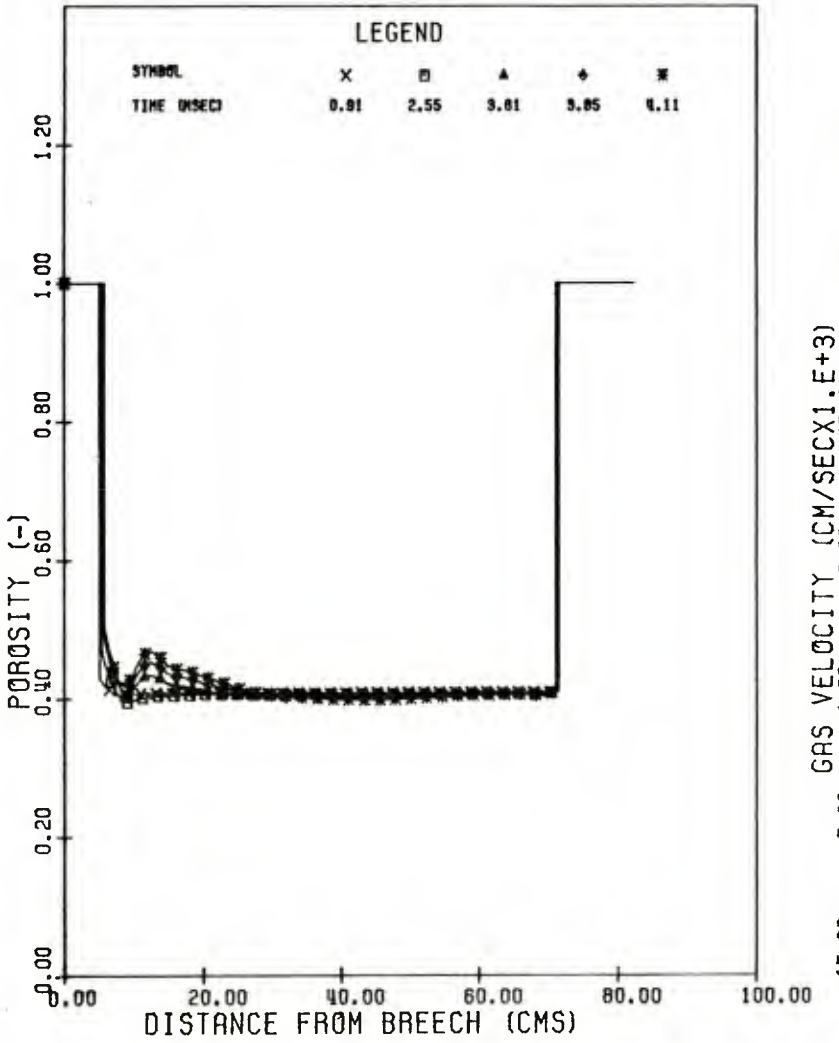

FIG.4.3.3 DISTRIBUTIONS OF BAG POROSITY IN 155 MM HOWITZER ACCORDING TO QUASI-TWO-DIMENSIONAL CALCULATION.

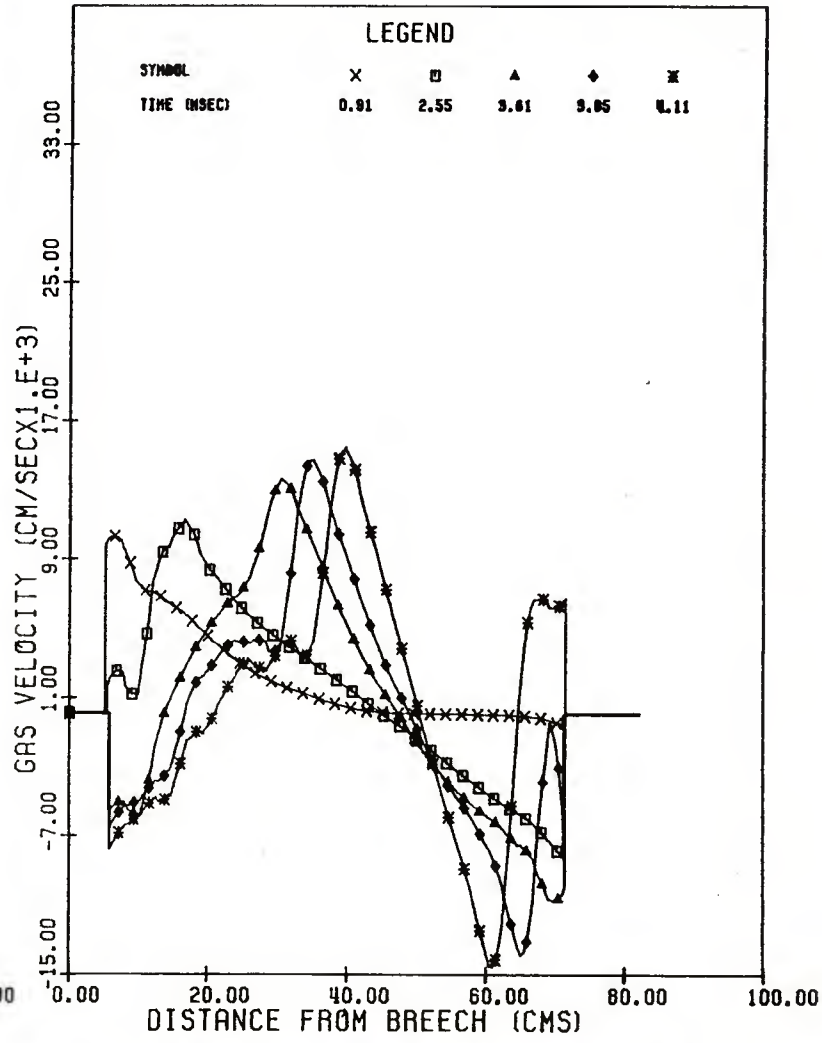

FIG.4.3.4 DISTRIBUTIONS OF BAG GAS VELOCITY IN 155MM HOWITZER ACCORDING TO QUASI-TWO-DIMENSIONAL CALCULATION.

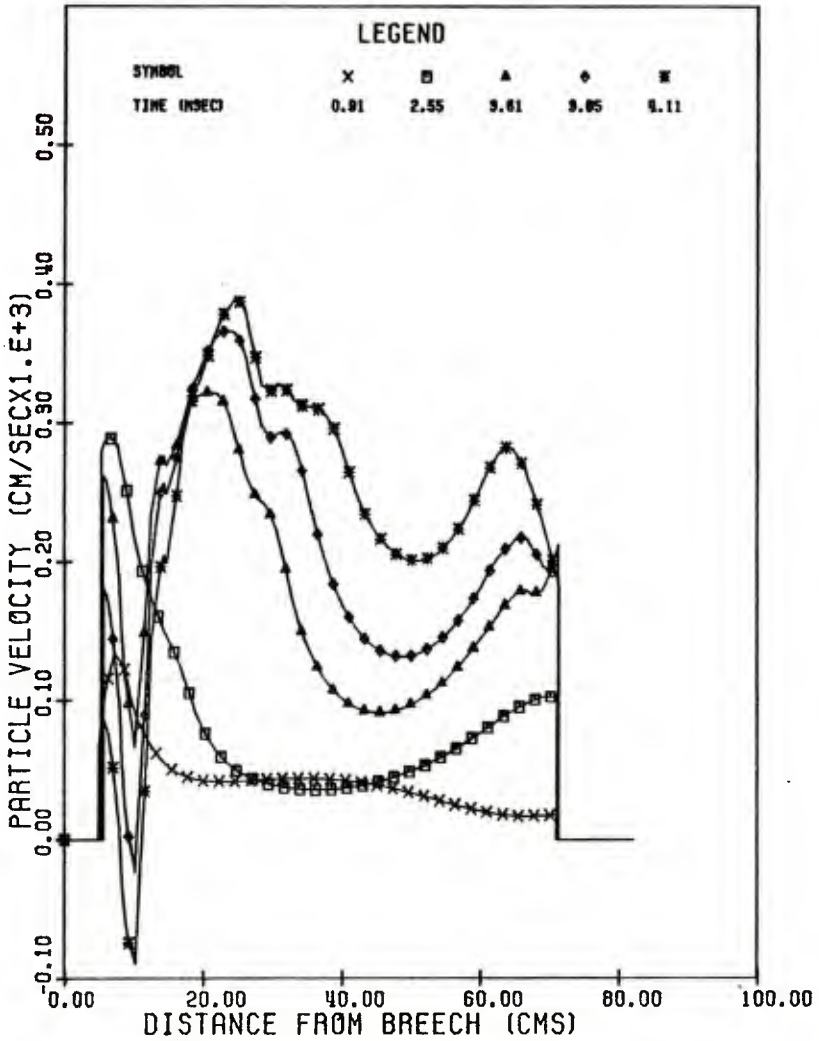

FIG.4.3.5 DISTRIBUTIONS OF SOLID VELOCITY IN 155 MM HOWITZER ACCORDING TO QUASI-TWO-DIMENSIONAL CALCULATION.

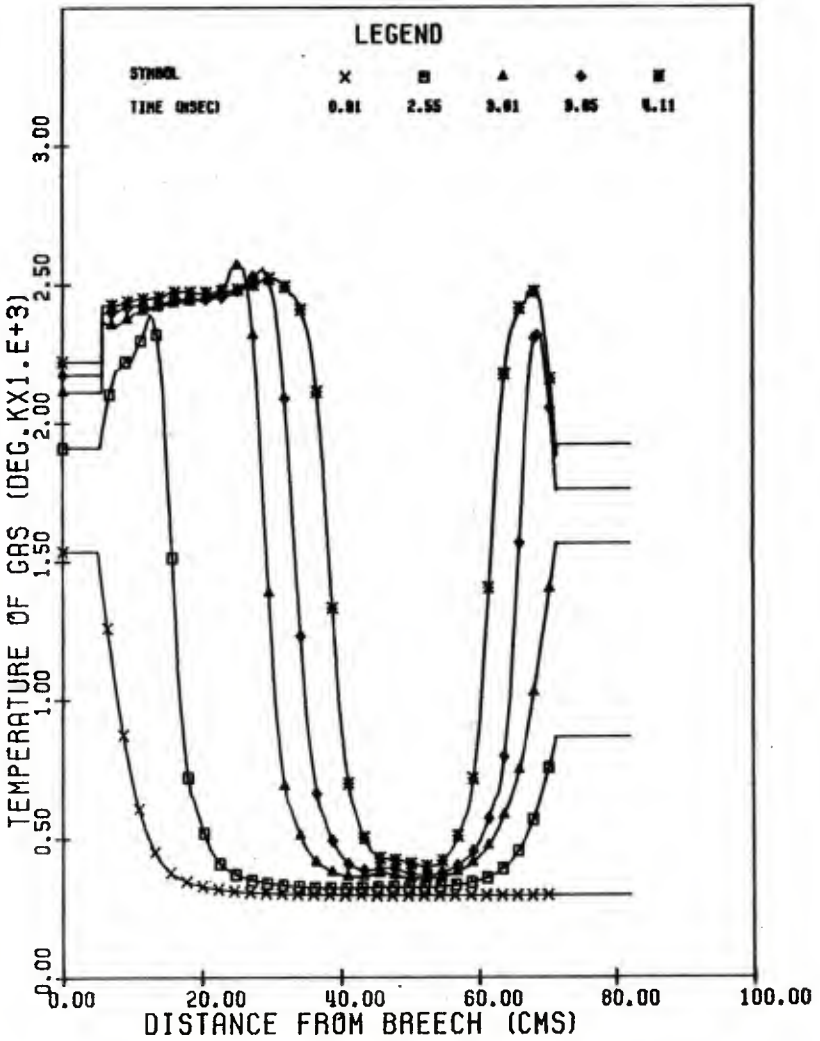

FIG.4.3.6 DISTRIBUTIONS OF BAG TEMPERATURE IN 155 MM HOWITZER ACCORDING TO QUASI-TWO-DIMENSIONAL CALCULATION.

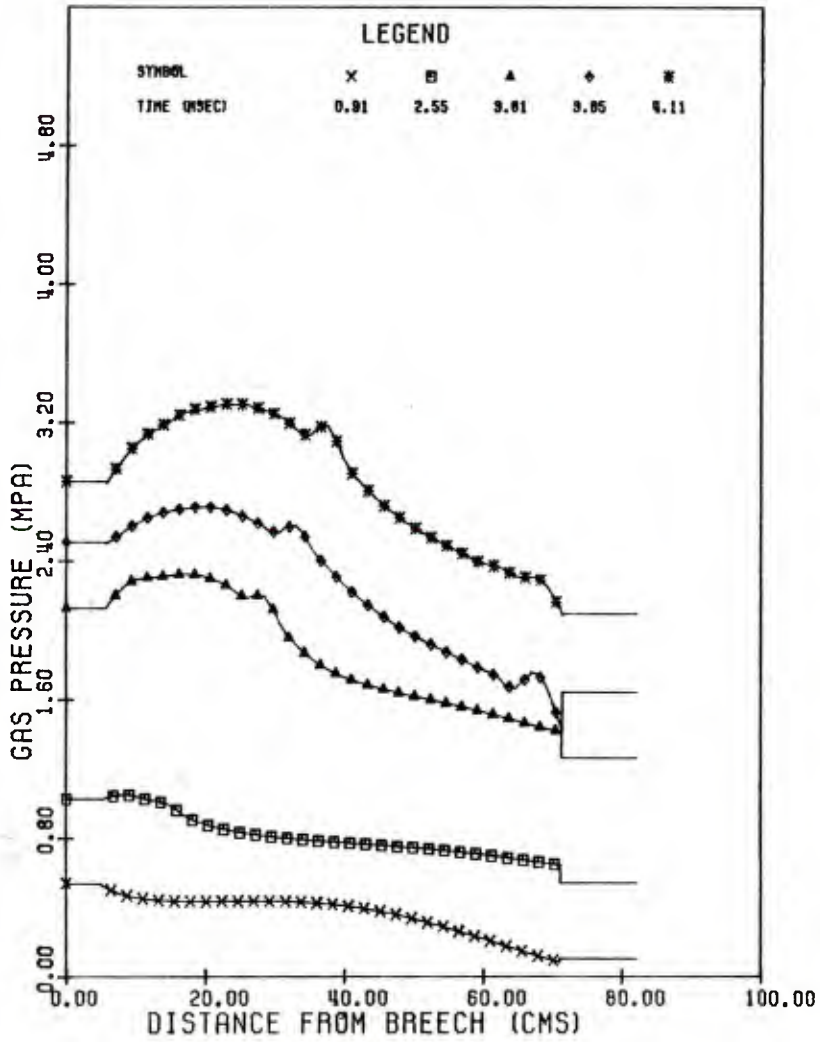

FIG.4.3.7 DISTRIBUTIONS OF GAP PRESSURE IN 155 MM HOWITZER ACCORDING TO QUASI-TWO-DIMENSIONAL CALCULATION.

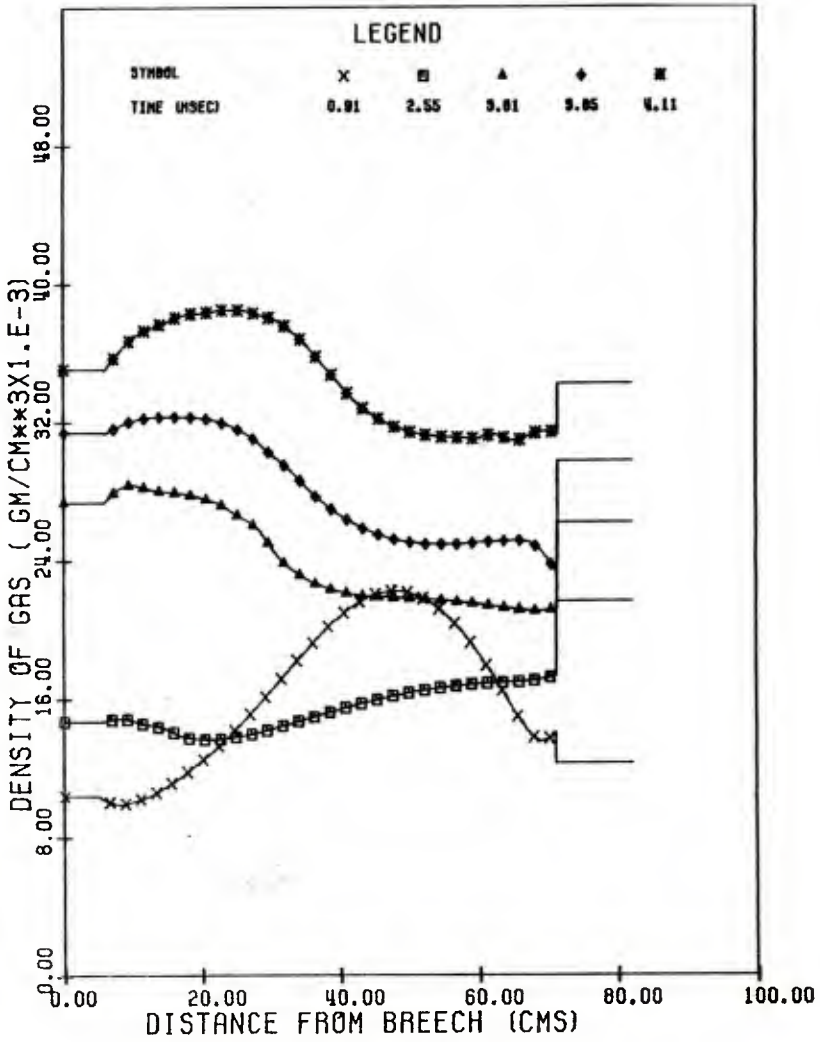

FIG.4.3.8 DISTRIBUTIONS OF GAP DENSITY IN 155 MM HOWITZER ACCORDING TO QUASI-TWO-DIMENSIONAL CALCULATION.

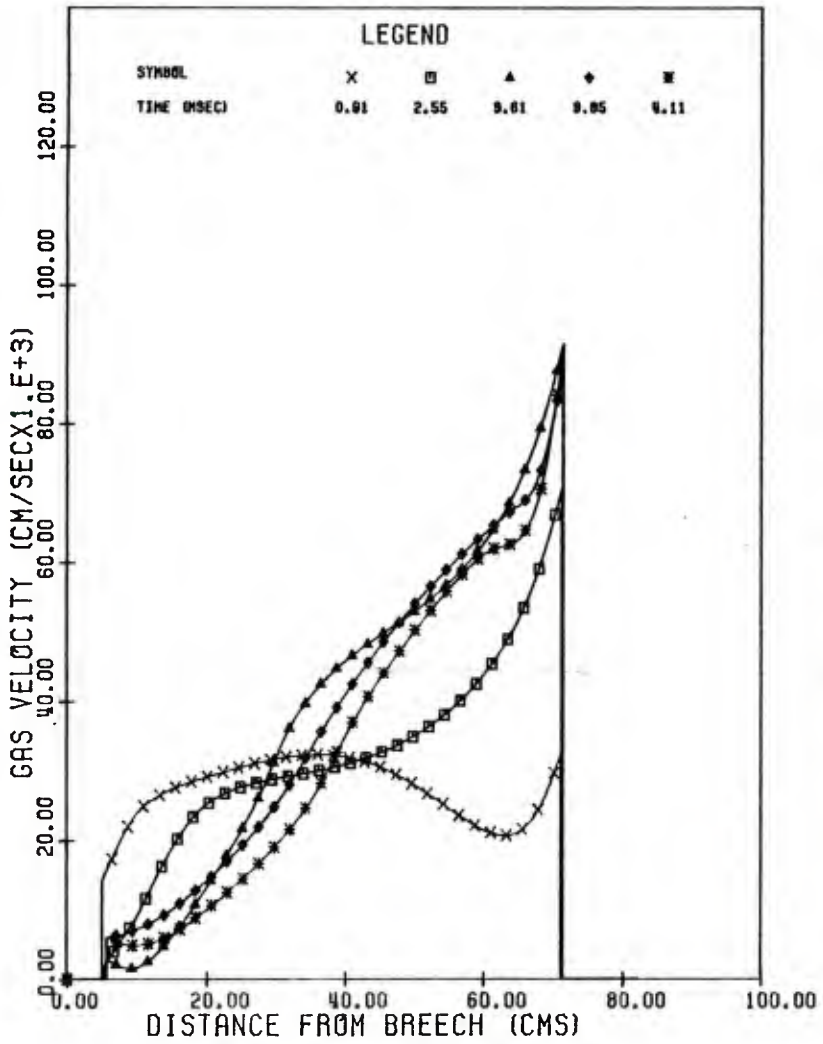

FIG.4.3.9 DISTRIBUTIONS OF GAP GAS VELOCITY IN 155MM HOWITZER ACCORDING TO QUASI-TWO-DIMENSIONAL CALCULATION.

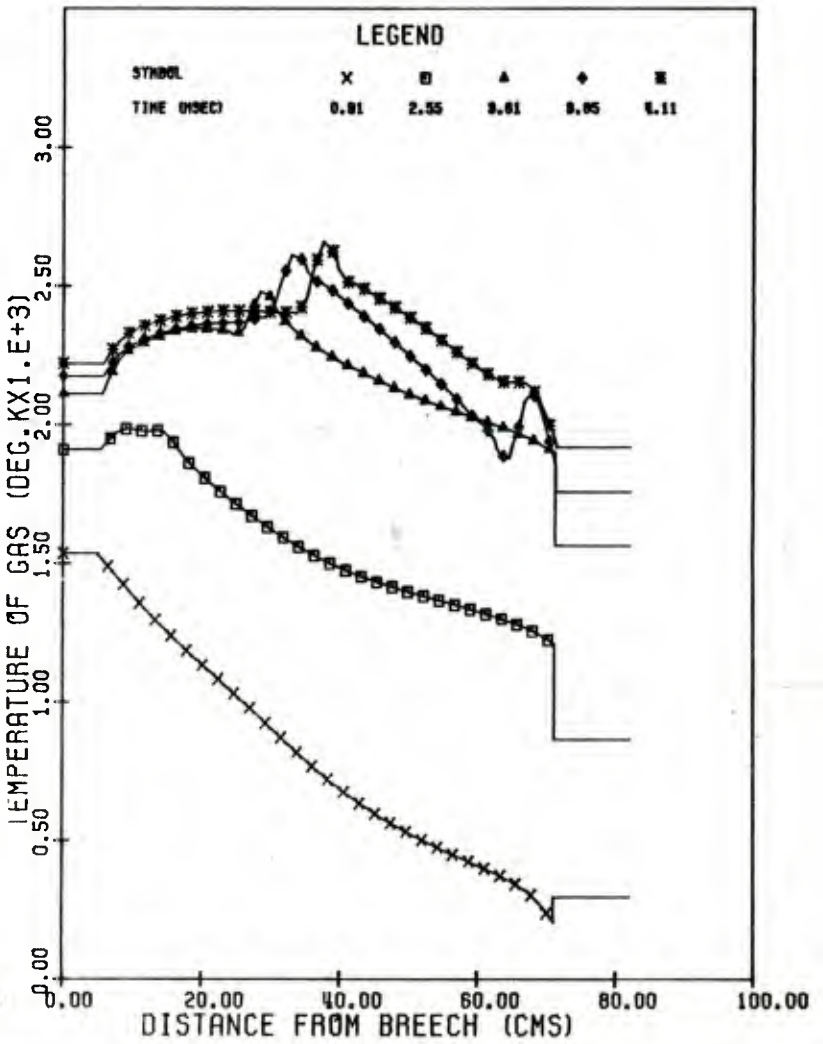

FIG.4.3.10 DISTRIBUTIONS OF GAP TEMPERATURE IN 155MM HOWITZER ACCORDING TO QUASI-TWO-DIMENSIONAL CALCULATION.

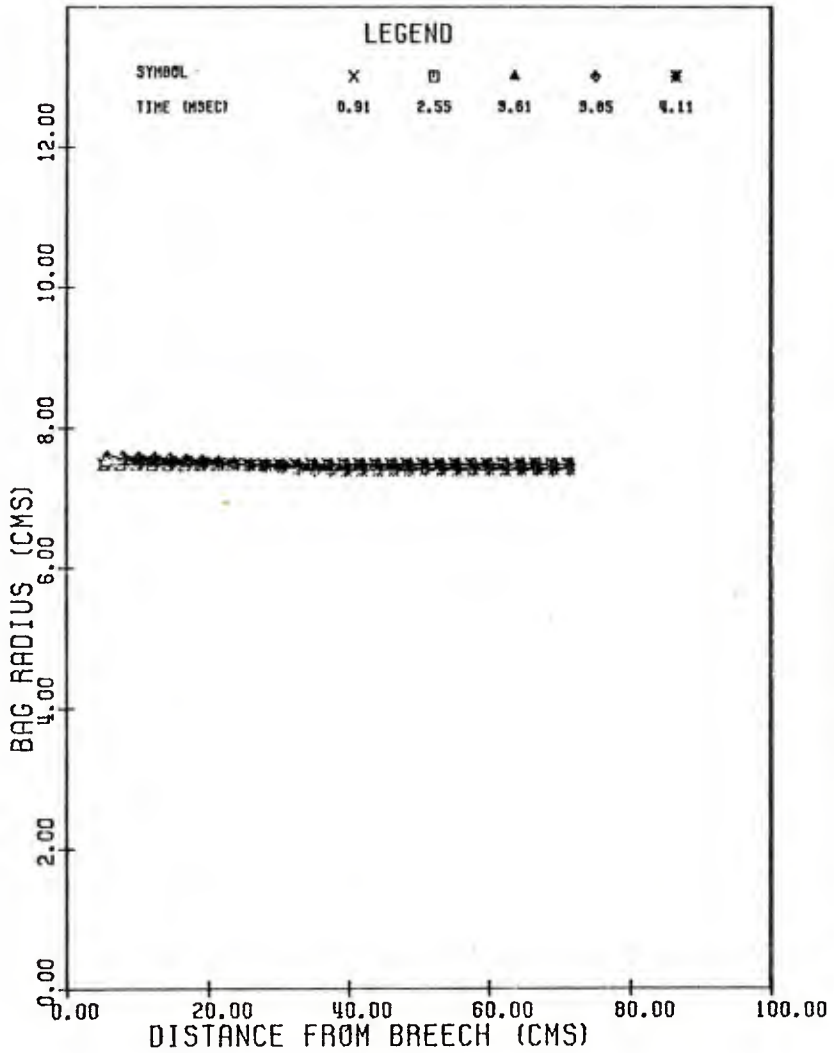

FIG.4.3.11 DISTRIBUTIONS OF BAG RADIUS IN 155 MM HOWITZER ACCORDING TO QUASI-TWO-DIMENSIONAL CALCULATION.

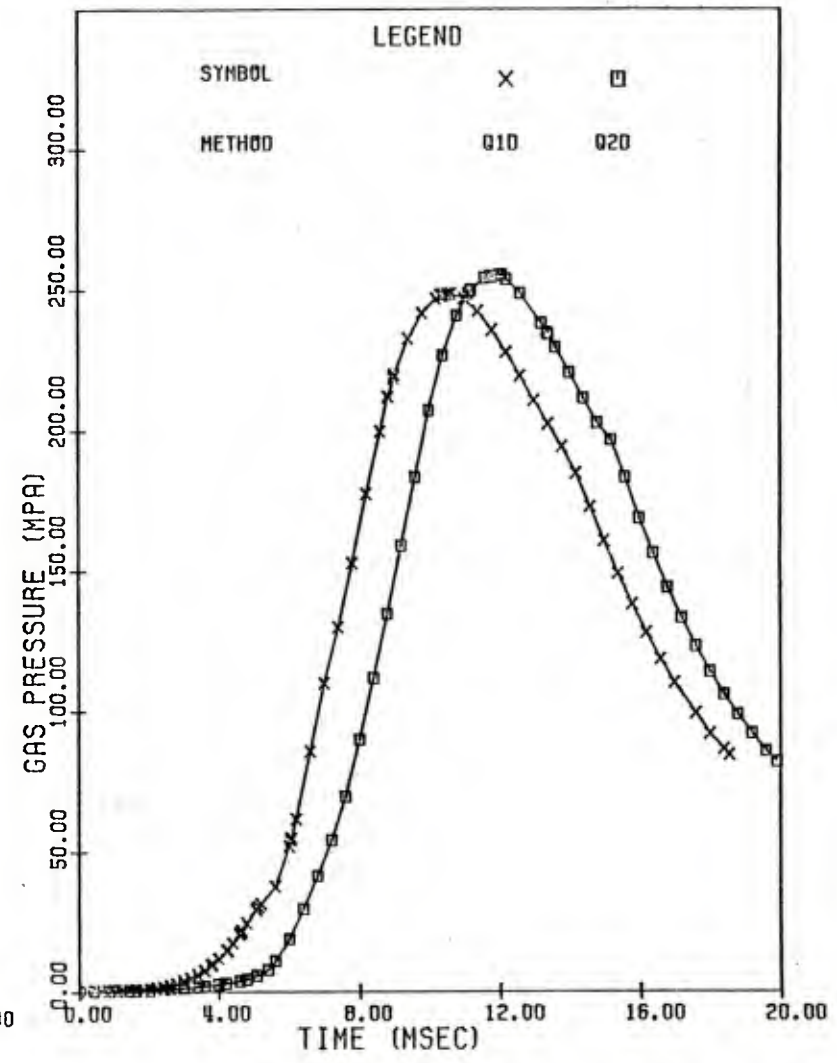

FIG.4.4.1 COMPARISON OF PREDICTIONS OF BREECH PRESSURE IN 155 MM HOWITZER ACCORDING TO QUASI-ONE -DIMENSIONAL AND QUASI-TWO-DIMENSIONAL CALCULATIONS.

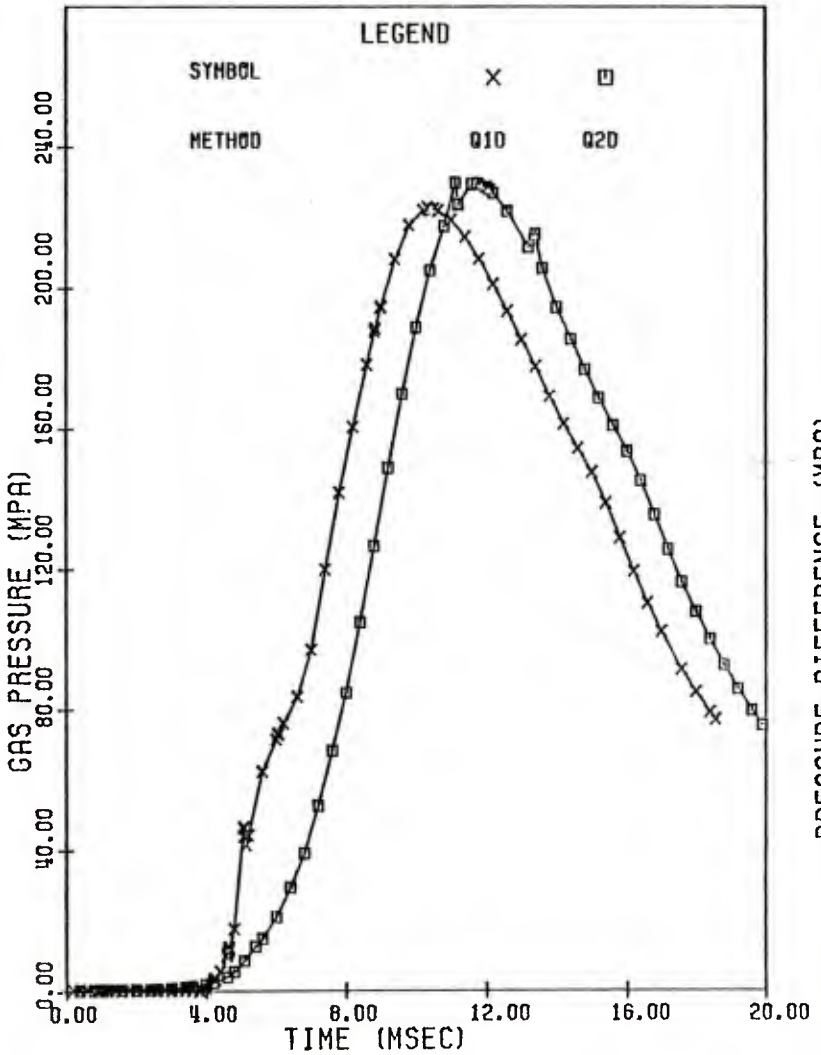

FIG.4.4.2 COMPARISON OF PREDICTIONS OF BASE PRESSURE IN 155 MM HOWITZER ACCORDING TO QUASI-ONE-DIMENSIONAL AND QUASI-TWO DIMENSIONAL CALCULATIONS.

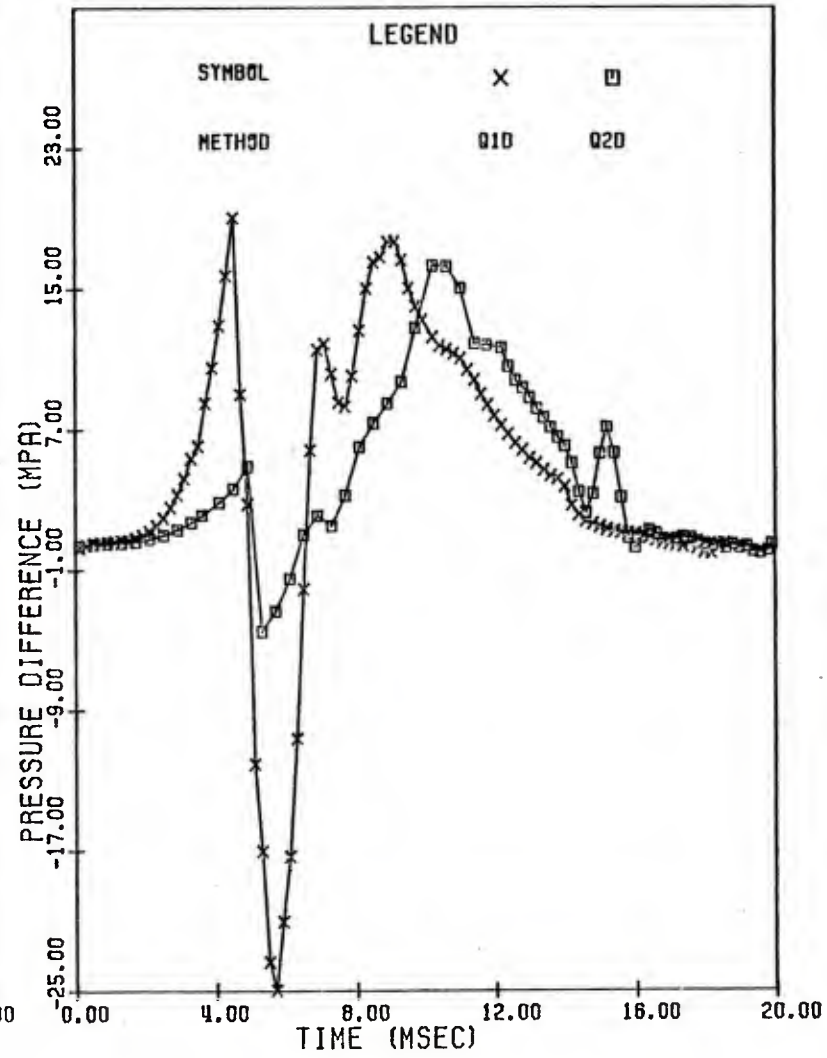

FIG.4.4.3 COMPARISON OF PREDICTIONS OF PRESSURE DIFFERENCE HISTORY IN 155 MM HOWITZER ACCORDING TO QUASI-ONE-DIMENSIONAL AND QUASI-TWO-DIMENSIONAL CALCULATIONS.

5.0 OBSTRUCTED QUASI-ONE-DIMENSIONAL FLAMESPREADING

In this chapter we perform a study of the ballistic consequences of an obstruction to one-dimensional flamespreading in a typical gun propelling charge. Such an obstruction may be visualized as arising in a charge consisting of two or more zoned bags and for which the center core igniter fails to function. In such a case, breech end ignition would produce an axially propagating convective deflagration wave whose passage from zone to zone would be impeded to a certain extent by the presence of the bag material. Since this would result in an increased lack of simultaneity of ignition of the overall charge it would be expected that the amplitude of ignition related pressure waves would also be increased.

The scope of the study is as follows. We consider a propelling charge based on the properties of the 155mm Howitzer with 10.9 kg of M30A1 propellant. A nominal solution is generated taking the ignition stimulus to be due to a base pad. Subsequently, we generate a solution in which part of the charge, at the front end, is isolated from the flame by an impermeable membrane. The membrane is presumed to transmit stress to the forward portion but does not admit the passage of the gas phase.

Following a predetermined delay the membrane is assumed to have been destroyed as a consequence of thermal and mechanical attack and the previously insulated propellant is represented as pressurized and burning. Three separate solutions are obtained based upon different values of the ignition delay introduced by the obstructing material. Complete interior ballistic cycles are determined and the results are compared with those for the nominal case with particular reference to the history of pressure difference between stations located in the breech and the mouth of the chamber.

In section 5.1 we describe such analysis as was required by the present study. The behaviour of a charge in which the forward region is insulated is discussed in section 5.2 and the influence of the ignition delay due to obstruction is assessed in section 5.3. Further discussion of these results in a broader context is given in chapter 6.0. The nominal charge configuration for this study is that described in the previous chapter and requires no further attention here.

5.1 Analysis

As we have described in the introduction, the principal task required of the analysis is the modification of the existing methodology for the filler elements to embed the mechanical characteristics of the solid propellant. In section 5.1.1 we present the required analysis . We discuss the sources for the choice of ignition delays due to flow obstruction in section 5.1.2. In section 5.1.3 we comment on the method of solution.

5.1.1 Governing Equations for Insulated Region

The governing equations consist solely of statements of continuity, conservation of momentum and the constitutive law for the solid phase. However, the balance equations are not stated in the usual Eulerian form. Indeed, we do not express them as differential equations at all. Instead, we pass directly to the difference equations. Following our previous treatment of the inert filler elements we establish nomenclature in accordance with the sketch below.

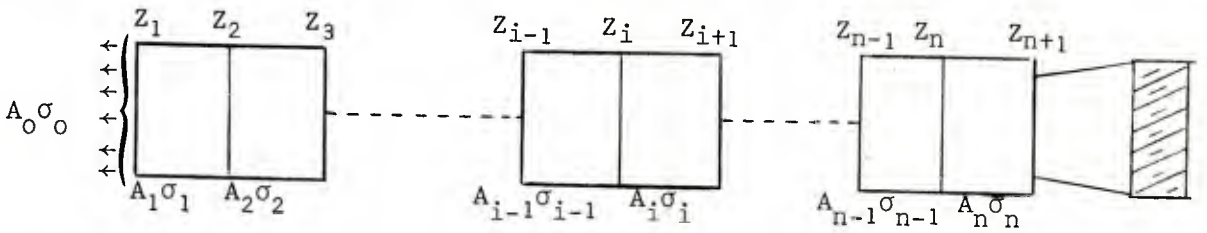

We set M_i equal to the mass of element i, Z_i the position of its left hand boundary, A_i the cross sectional area of the tube at the center of element i and σ_i the stress (positive in tension) at the center of element i. The subscript o denotes the boundary condition at the adjacent region of the two-phase flow. Subscript n+1 refers to the projectile.

It must be noted that the granular stress is assumed to be isotropic or hydrostatic. Accordingly, the solid phase only experiences stress when it is confined radially. Thus we must suppose that the propellant fills each cross section of the tube in which it resides or we must assume that it is stress-free. Here we take the propellant to occupy completely the cross section and to experience a reaction due to the wall. Rather than incorporate the wall reaction explicitly as we have done previously for incompressible elements[5] we embed it implicitly by constructing the momentum balance as follows:

$$\frac{1}{2g_o}\left[\frac{M_i}{A_i}+\frac{M_{i-1}}{A_{i-1}}\right]\ddot{Z}_i = \sigma_{i+1}-\sigma_i \qquad 5.1.1.1$$

Thus 5.1.1.1 expresses a momentum balance per unit cross sectional area for one half of element i plus one half of element i-1. At the endpoints i=1 and n+1 we proceed as previously[5], respectively taking a balance for one half of element 1 and one half of element n plus the rigid projectile.

The equation of continuity may be expressed simply in the algebraic form:

$$\varepsilon_i = 1 - \frac{M_i}{\rho_p A_i (Z_{i+1}-Z_i)} \qquad 5.1.1.2$$

where ρ_p is the density of the solid propellant which, as usual, we take to be a constant. The constitutive law assumes irreversible compaction of the solid phase. We have:

$$\sigma_i = f(\varepsilon) - f(\varepsilon_1) \qquad 5.1.1.3$$

and

$$f(\varepsilon) = \begin{cases} -(1-\varepsilon)\dfrac{a_1^2 \rho_p}{2g_o \kappa} e^{-2\kappa(\varepsilon-\varepsilon_o)} & , \varepsilon \geq \varepsilon_o \\ -(1-\varepsilon)\dfrac{a_1^2 \rho_p}{g_o}\left[\dfrac{1}{2\kappa} + \varepsilon_o^2\left(\dfrac{1}{\varepsilon} - \dfrac{1}{\varepsilon_o}\right)\right] & , \varepsilon < \varepsilon_o \end{cases} \qquad 5.1.1.4$$

where ε_1 is the initial porosity of the insulated section and ε_o is the settling porosity of the propellant bed. Equation 5.1.1.3 is valid provided $\varepsilon \leq \varepsilon_1$ and $\dot{\varepsilon} < o$. When the bed is unloading we assume $\dot{\varepsilon} = o$ since there are no forces available to expand the bed. This condition of unloading is expressed in the form:

$$\dot{Z}_i A_{i_L} = \dot{Z}_{i+1} A_{i_R} \qquad 5.1.1.5$$

where A_{i_L}, A_{i_R} are the cross sections of the tube at the left and right hand sides of element i respectively.

It should be noted that this constitutive law is somewhat different from that which we have used in the past. Previously we have set $\sigma = o$ on unloading and then to increase according to $d\sigma = -\rho_p a^2 d\varepsilon / g_o$ during reloading. The present constitutive law assumes no further compaction on reloading until the stress level at which unloading occurred is once again established. The present law is thought to represent more accurately the behaviour of the granular bed. It is, moreover, better behaved from a computational point of view and its implementation into the NOVA code would be desirable.

It should also be noted that by differentiating 5.1.1.5 along the element pathline we can show that for an unloading element:

$$\ddot{Z}_i = \alpha_i \ddot{Z}_{i+1} + \beta_i \qquad 5.1.1.6$$

where

$$\alpha_i = A_{i_R} / A_{i_L} \qquad 5.1.1.7$$

$$\beta_i = (A'_{i_R} \dot{Z}_{i+1}^2 - A'_{i_L} \dot{Z}_i^2) / A_{i_L} \qquad 5.1.1.8$$

5.1.2 Ignition Delay Due to Flow Obstruction

We now comment on the ignition delay associated with burnthrough of the impeding material. According to Fisher and Graves[18], studies of the attack of a Mortar bag by the high pressure jet issuing from the boom yielded the following observations:

(i) Penetration of bag after ~0.12 msec
(ii) Possible ignition by ~0.18 msec
(iii) Massive bag failure after 0.30 msec
(iv) Pressure of jet ~80 Mpa
(v) Bag heat transfer rate α $p^{\frac{1}{2}}$

Studies of the nominal solution which we described in section 4.2 show the gas pressure at the flow obstruction to be much lower than that observed by Fisher, being typically 10 Mpa. Moreover, the nominal solution shows that ~0.2 msec is required for the flame to spread through the forward region.

Thus assuming that Fisher's relationship for the heat transfer rate is applicable, we find that a delay of roughly 0.5 - 0.8 msec is required for ignition of the propellant and massive failure of the impeding material. Since there will be a delay of roughly 0.2 msec to spread the flame through the previously insulated region, it follows that a nominal estimate of the ignition delay due to the flow obstruction will be 1 msec.

5.1.3 Method of Solution

The method of solution is as follows. The determination of the nominal solution requires no comment here since it is performed with previously established methods. Concerning the inhibited solution, we proceed in three steps. The problem is first represented in terms of a two-phase flow analysis of the rear portion of the charge which is initially separated from the projectile by a series of inert and compactible elements. We took a total of six elements in the present study. Five of these represented the propellant and the sixth represented the space between the forward end of the bag and the base of the projectile.

The solution of the balance equations of section 5.1.1 proceeded in the fashion we have described previously[4,5]. At any stage in the analysis the boundary value of the stress, σ_o, is always known. It is assumed that all elements are loading whereupon all stresses are determined and the values of Z_i, $\dot{Z}_i$ may be updated. It is then verified that each element is indeed in a loading condition. If not, the integration is repeated with the relevant value of σ_i taken as indeterminate. The value of σ_i is eliminated by using the unloading condition 5.1.1.6 and adding the balance equations which involve this term. The iteration is continued until a self consistent solution is established.

The second step of this solution is implemented following the delay for ignition due to flow obstruction. At this point the problem is transformed so that a two-phase flow analysis may be conducted for the forward region of propellant.

The third and final step is conducted using the existing coding. The propelling charge is treated as a multibag configuration with internal ullage.

5.2 Solution with Forward Region Obstructed

The position of the flow obstruction was taken to be 10.67 cm from the leading edge of the charge. Thus approximately 17% of the charge is located in the insulated region. The solution which we present here is continued for 6.28 msec and forms the basis for the subsequent studies of the influence of bag rupture, ignition and pressurization of the insulated region. In all other respects the data base for this problem was that described in section 4.2 for the nominal case.

In figures 5.2.1 through 5.2.4 we present some distributions of presure, porosity, gas velocity and particle velocity at various times. Figures 5.2.5 and 5.2.6 compare the histories of breech and "base" pressure in the nominal and insulated configurations. These latter figures illustrate the fraction of the interior ballistic cycle for which the insulation is presumed to operate. It may be seen from 5.2.5 that the effect on the breech pressure of insulating the forward region is very mild; a noticable deviation between the two calculations occurs only after about 6 msec.

Figure 5.2.6 requires some explanation. The base pressure for the nominal solution corresponds to that detected by a gage mounted on the base of the projectile. Such a gage would, in the insulated region, register only ambient or possibly a modest increase over ambient pressure due to adiabatic compression of the air in the forward ullage. The base pressure plotted for the insulated configuration corresponds to that observed by a gage mounted in the rear face of the insulated region. It is interesting to observe the plateau which extends for about 1 msec. This corresponds to the period in which the insulated region is being propelled towards the base of the projectile. It is terminated by the impact of the bag against the base; the subsequent rise looks quite similar to that in the nominal configuration.

The full sequence of events captured by the present solution is as follows. As in the nominal configuration, ignition occurs first in the breech and subsequently in the interior of the bed as a consequence of an axially propagating convective deflagration wave. Of course, the flame is unable to penetrate the flow obstruction located some 10 cms from the forward end. Prior to the arrival of the flame at this internal boundary, the pressure exerted by the gas on the insulated region causes it to be propelled forward, separating from the permeable part of the charge. At the same time, the region is compacted.

The location of the insulated region at several times can be seen in figure 5.2.2 which provides some distributions of the porosity. The regions of ullage are denoted by the concomitant value of unity which

characterizes the porosity as well as the sharp discontinuities in this quantity which are recognized by the method of solution. The figure shows quite clearly the compaction of the insulated region as it is pushed forward. Subsequently, when the insulated region impacts against the base of the projectile, an extraordinary degree of compaction is observed. The porosity is reduced to ~0.15. This extremely low value reflects in part the relatively large velocity which the propellant acquires prior to impact, namely ~200 m/sec. It also reflects the absence of a buffering effect by the gas phase which characterizes the impact of a fully permeable region. In addition, since the boundary is impermeable, once the bag has collapsed against the projectile, the entire force due to the pressure of the gas must be supported by the intergranular stress. Accordingly, the solid phase is found to experience stresses of the order of 70 Mpa towards the end of the present solution.

This stress level is so intense as to throw certain of our assumptions into doubt. The constitutive law for the granular stress is purely speculative in this regime; it is entirely possible that even greater degrees of consolidation would be developed than those deduced here. Moreover, the assumption that the grains will not fracture becomes difficult to defend, in general.

Figure 5.2.1 presents the distributions of pressure at various times. We see that only a mild reverse gradient is associated with the sudden change in gas velocity at the boundary corresponding to the flow obstruction when the bag strikes the projectile. Figures 5.2.3 and 5.2.4 present the distributions of gas and particle velocity at various times. In figure 5.2.4 we can see quite clearly the variation in particle velocity at the earliest time while compaction of the insulated region is in progress. Subsequently, the velocity in this region is nearly uniform, reflecting the strong consolidation of the propellant.

5.3 Influence of Ignition Delay Due to Obstruction

In this section we study the consequences of assuming the flow obstruction suddenly to disappear at various times and the previously insulated region to be ignited and pressurized. The solution of the preceding section is transformed to a multi-bag problem at three times, namely; 4.45 msec, 5.51 msec and 6.07 msec. These correspond to ignition delays due to the obstruction equal to 0.62 msec, 1.68 msec and 2.23 msec respectively. The delays have been predicated on the nominal estimate. However, the specific values have also been influenced by the desire to allow ignition at certain interesting stages of the solution.

The first choice provides ignition as the forward region is being propelled towards the base of the projectile. The second provides ignition shortly after the impact and compaction of the forward region against the base of the projectile. The final choice provides ignition only after the rear portion of the bag has moved forward and has impacted onto the forward region so that there is ullage only in the breech of the chamber at the instant of ignition.

Distributions of pressure, porosity, gas velocity and particle velocity are contained in figures 5.3.1 through 5.3.4 for the first case, 5.3.5 through 5.3.8 for the second and 5.3.9 through 5.3.12 for the third. Finally, in figures 5.3.13 through 5.3.15 we compare the histories of pressure in the breech and mouth of the chamber and the difference of these quantities for each of the three cases and for the nominal configuration.

We begin by examining the comparative histories. Figure 5.3.13 makes it quite clear that this propelling charge is astonishingly tolerant of variations from the nominal path of burning. As far as the breech pressure is concerned the effect of insulating part of the charge for some time is similar to inhibiting the grains themselves. A somewhat lower maximum pressure is achieved. There is no evidence in this figure of increased wave structure due to the increased velocity of the leading edge of the charge or due to the combustion of the strongly consolidated forward region.

Figure 5.3.14 essentially corroborates this picture. It should be noted that the differences here at the early times are due to a gage uncovering effect modeled by the code. The gage at the mouth of the chamber registers ambient pressure until the forward region is ignited and pressurized.

In order to study the structure of the pressure waves we turn to figure 5.3.15 which presents the difference between the values of pressure in the breech and the mouth of the chamber. The figure shows considerable differences in the first maximum; however, this is associated with the effect of uncovering the gage in the mouth and is not intrinsic to the pressure wave itself. The first minimum is seen to be influenced by the ignition delay. However, a significant difference is seen only for the third case, in which the forward region is trapped between the projectile and the rear part of the charge without ullage interposed. Moreover, the excursion is rapidly damped and the subsequent history of pressure difference is virtually uninfluenced by the presence of a flow obstruction.

The reason for the strong tolerance of the flow to the presence of a flow obstruction whose effect is to delay ignition and compress the forward region seems to be associated with the rapid recovery of the forward region once ignition occurs. It is true that the region becomes overpressured due to the low voidage. But the result of the overpressurization is to force a rapid expansion of the previously insulated region. Only a modest increase in size is required to relax the porosity to a value close to that experienced in the nominal solution at a comparable stage of the interior ballistic process. The pressure excursion is no longer fed by enhanced combustion in a confined volume and the transient is dissipated rapidly.

Thus the situation here is apparently different from that associated with fracture of the grains as studied by Horst[16]. Once the grains are broken, producing increased surface area, relaxation of the flow to the nominal condition is not so readily accomplished. The increased surface area will be persistent and will be able to support a pressure excursion in spite of local expansion of the bed. Accordingly, there is little doubt in our mind that the results of the present study would have been quite different had we allowed for fragmentation of the insulated region.

The rapid relaxation of the flow following ignition of the forward region can be seen in the distributions of porosity in figures 5.3.2, 5.3.6 and 5.3.10. Figures 5.3.6 and 5.3.10 correspond to the cases in which the insulated region is allowed to impact upon the base of the projectile prior to ignition. These show that within a millisecond after rupture and ignition occur, the porosity in the forward region has resumed values typical of the nominal solution.

It is emphasized that the recovery does not represent an elastic effect. There are no appreciable intergranular stresses in the bed following ignition. The expansion is due to the drag exerted by the products of combustion expelled from the compacted region. The distributions of gas velocity are seen in figures 5.3.3, 5.3.7 and 5.3.11. It is particularly interesting to note how the distributions at the latest time presented in these figures shows very little trace of the preceding departure from nominal combustion. A similar comment is true of the distributions of particle velocity, figures 5.3.4, 5.3.8 and 5.3.12.

Finally, in figures 5.3.1, 5.3.5 and 5.3.9 we have the distributions of pressure. Only figure 5.3.9 reveals an appreciable reverse gradient. But this is only momentary and quickly dissipates due to the failure of the combustion process to feed it adequately.

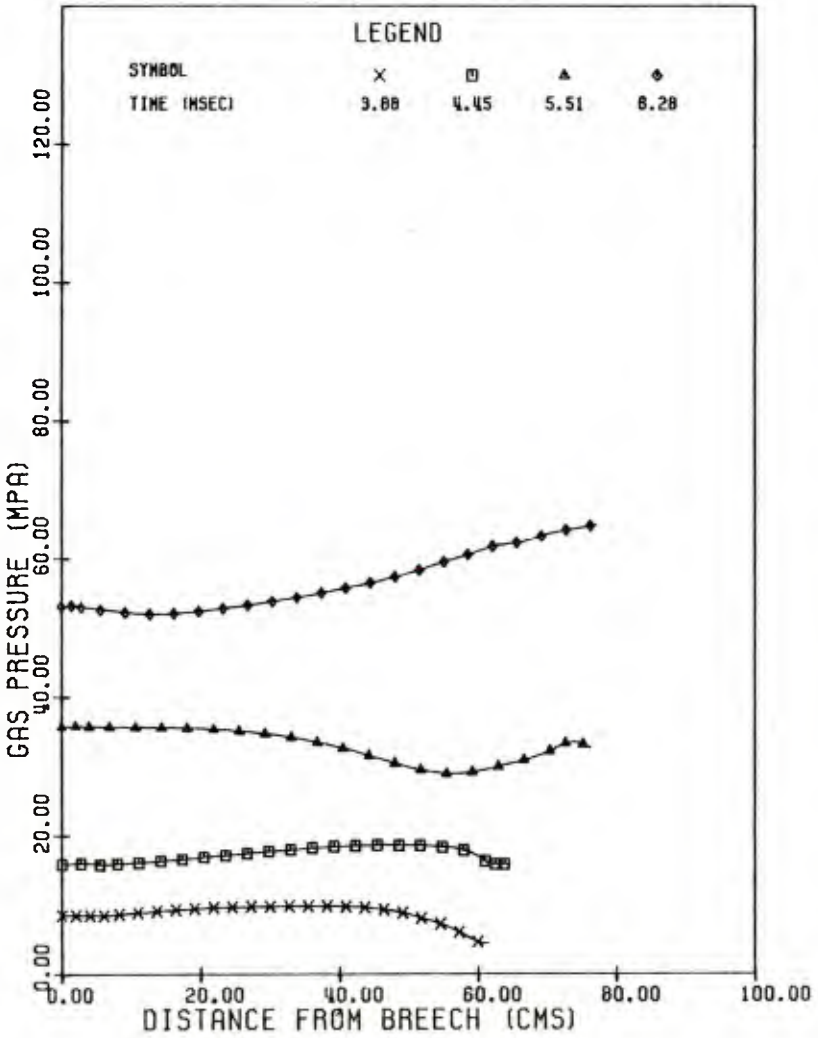

FIG.5.2.1 DISTRIBUTIONS OF PRESSURE FOR INSULATED CONFIGURATION PRIOR TO FAILURE OF INSULATING LAYER

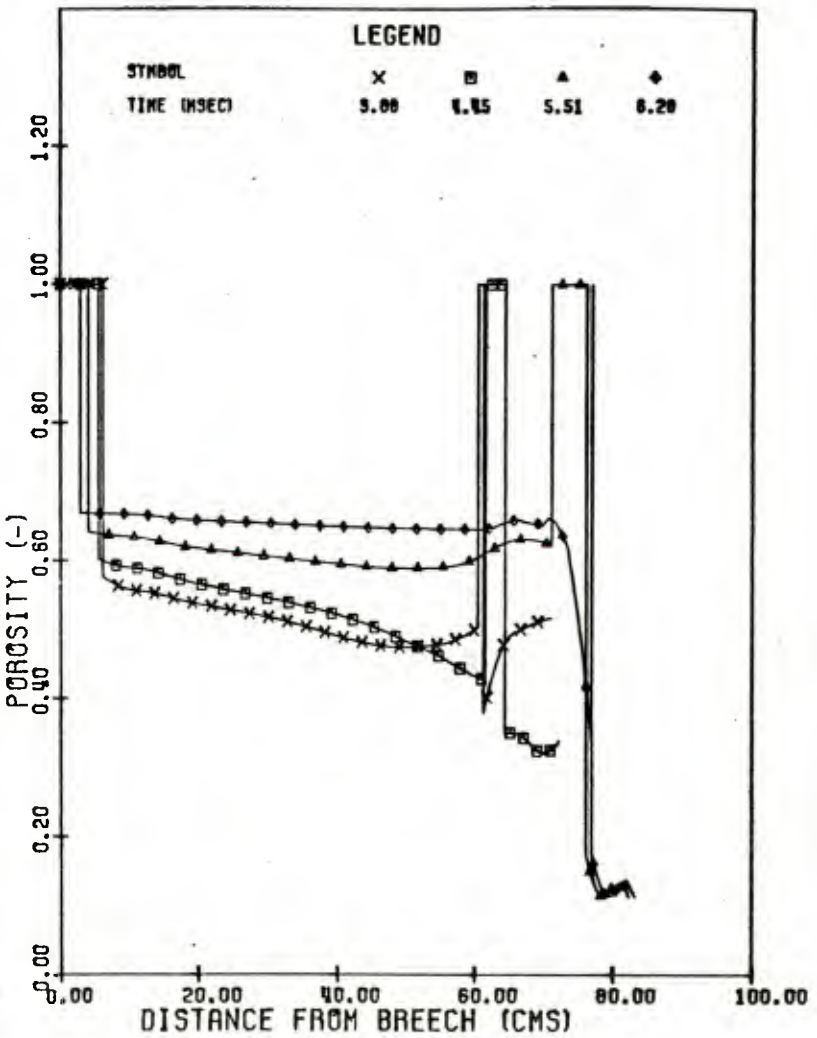

FIG.5.2.2 DISTRIBUTIONS OF POROSITY FOR INSULATED CONFIGURATION PRIOR TO FAILURE OF INSULATING LAYER

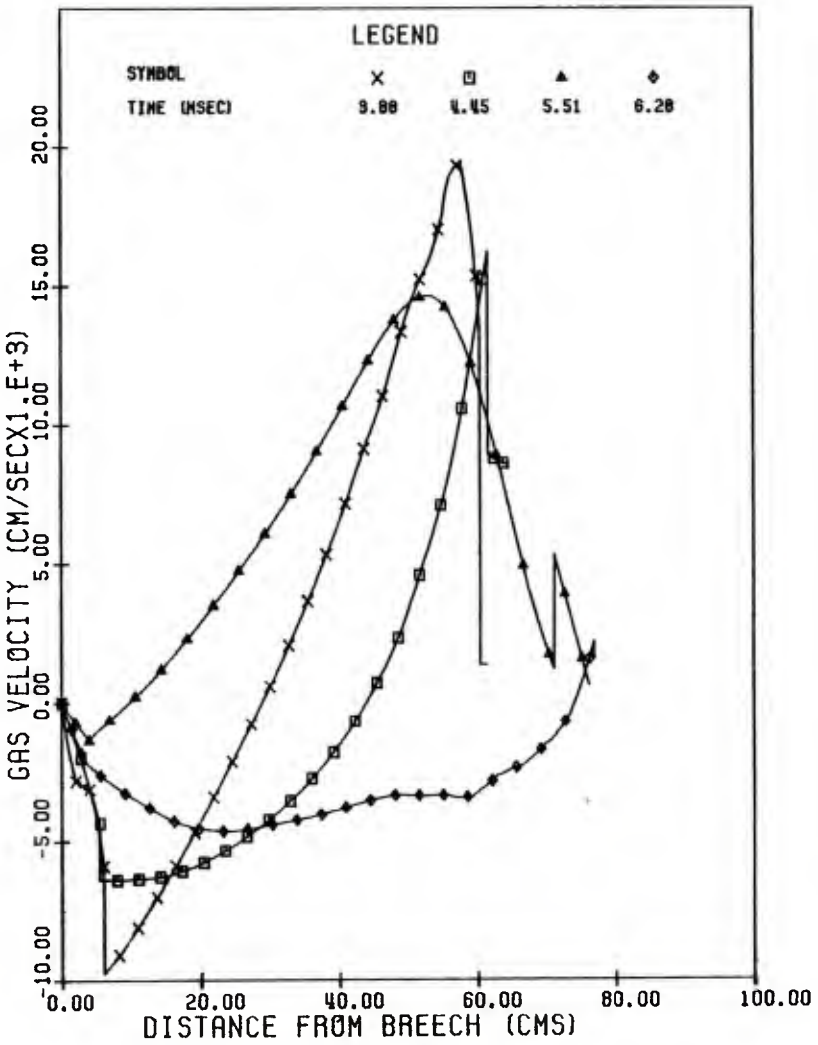

FIG.5.2.3 DISTRIBUTIONS OF GAS VELOCITY FOR INSULATED CONFIGURATION PRIOR TO FAILURE OF INSULATING LAYER

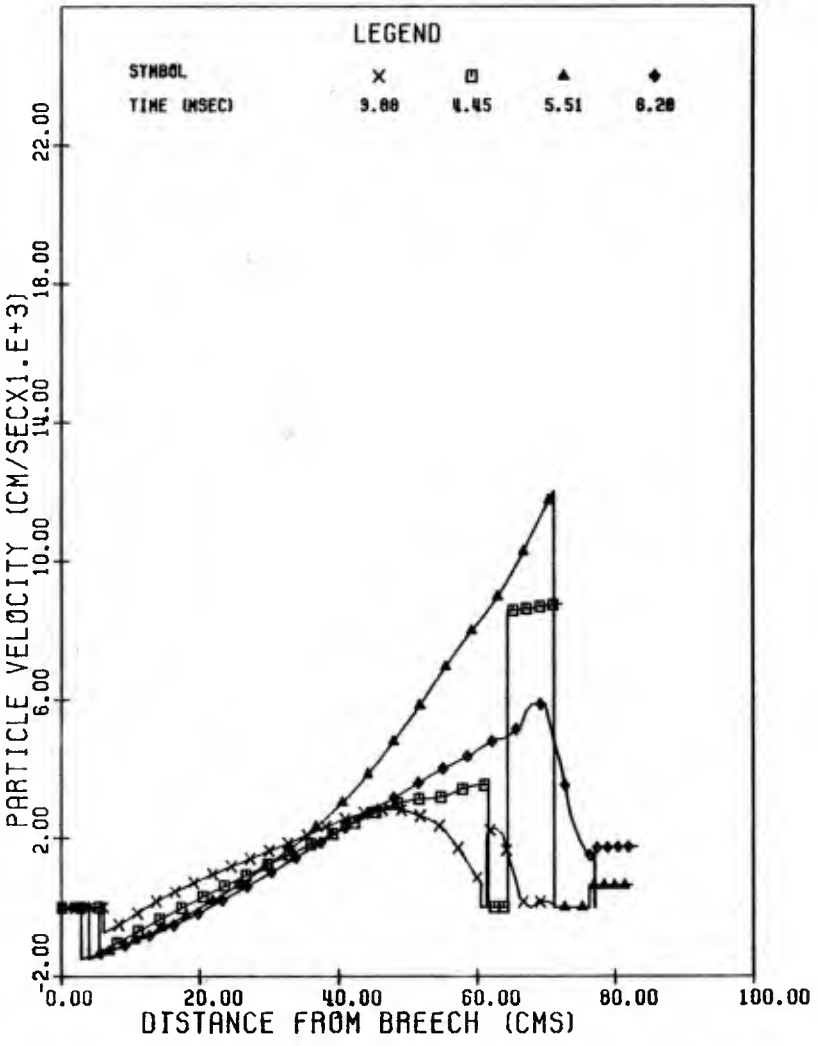

FIG.5.2.4 DISTRIBUTIONS OF PARTICLE VELOCITY FOR INSULATED CONFIGURATION PRIOR TO FAILURE OF INSULATING LAYER

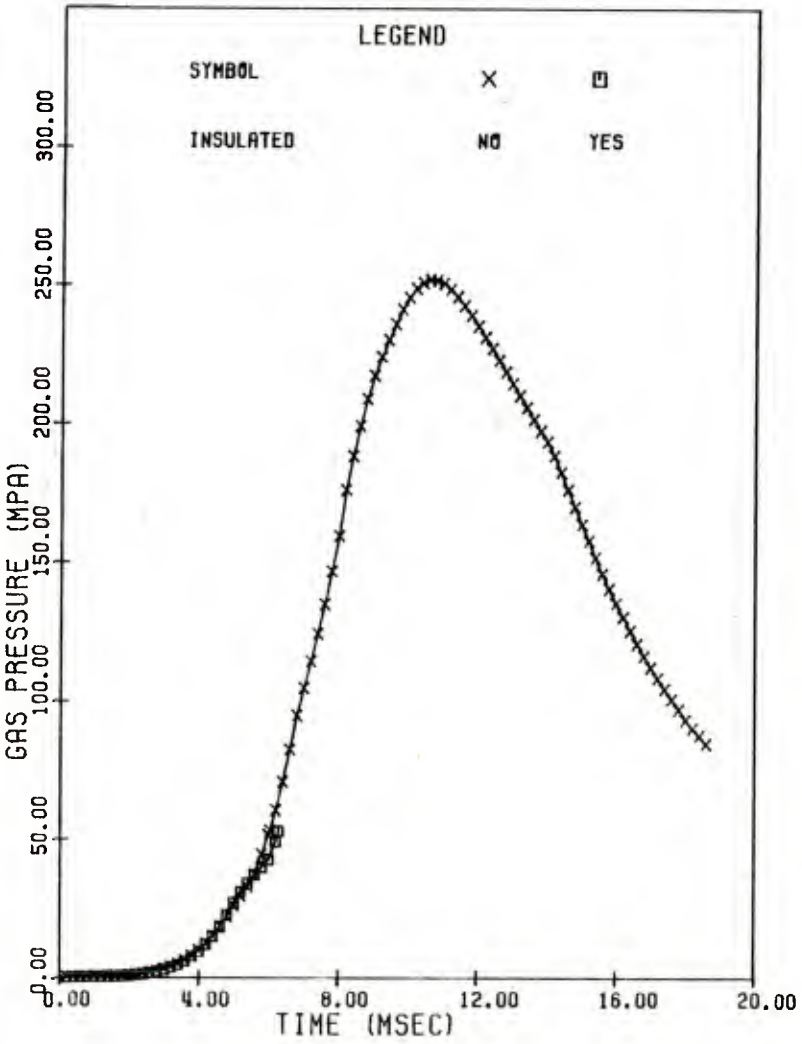

FIG.5.2.5 COMPARISON OF BREECH PRESSURE HISTORY IN INSULATED CONFIGURATION PRIOR TO FAILURE OF INSULATING LAYER WITH THAT OF NOMINAL CONFIGURATION

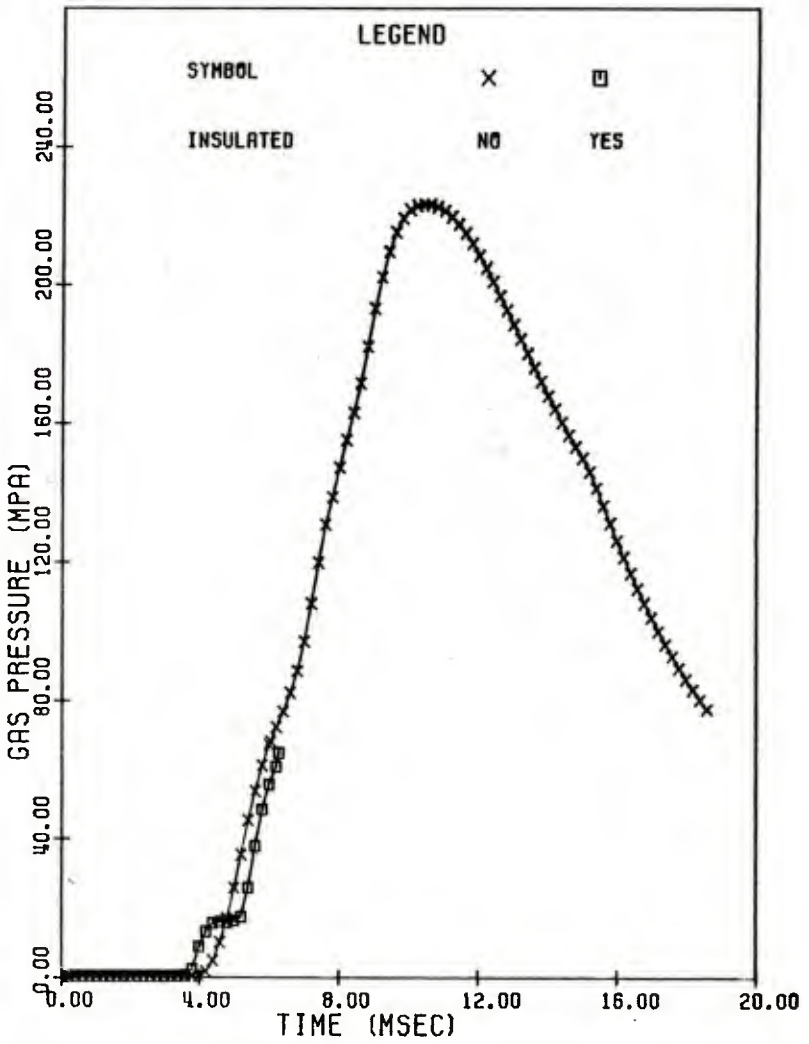

FIG.5.2.6 COMPARISON OF BASE PRESSURE HISTORY IN INSULATED CONFIGURATION PRIOR TO FAILURE OF INSULATING LAYER WITH THAT OF NOMINAL CONFIGURATION

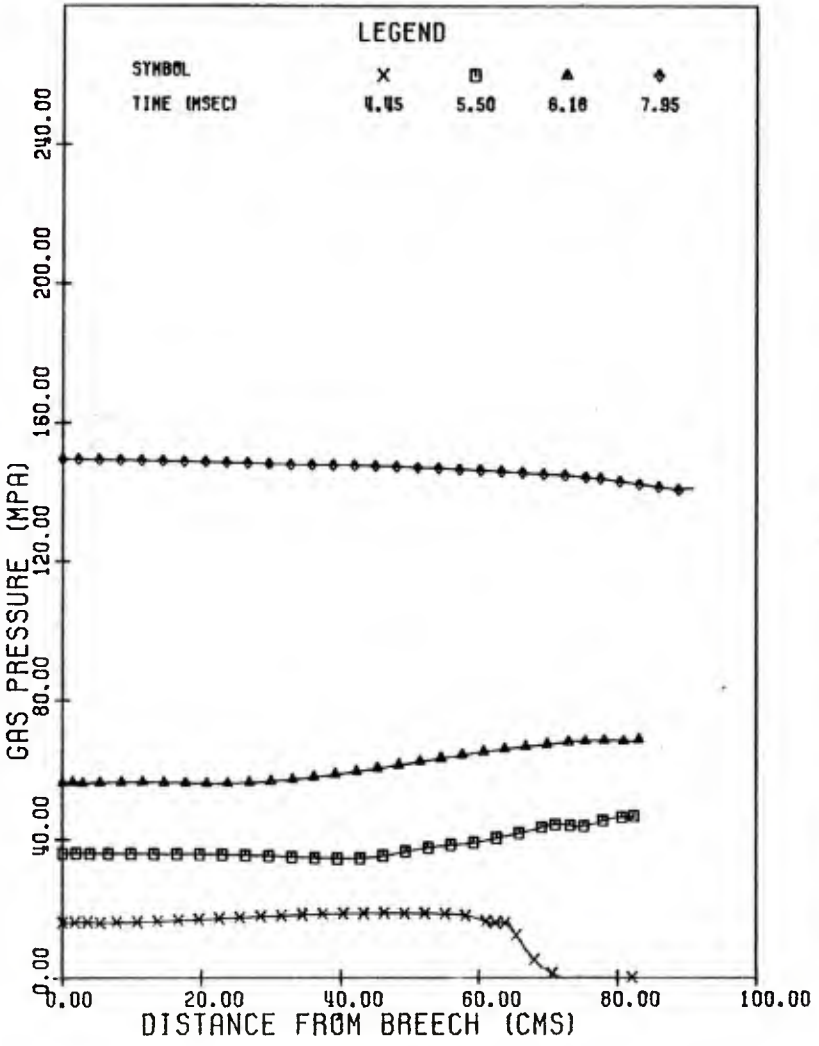

FIG.5.3.1 DISTRIBUTIONS OF PRESSURE FOR INSULATED CONFIGURATION FOLLOWING FLAMESPREADING DELAY OF 0.616 MSEC

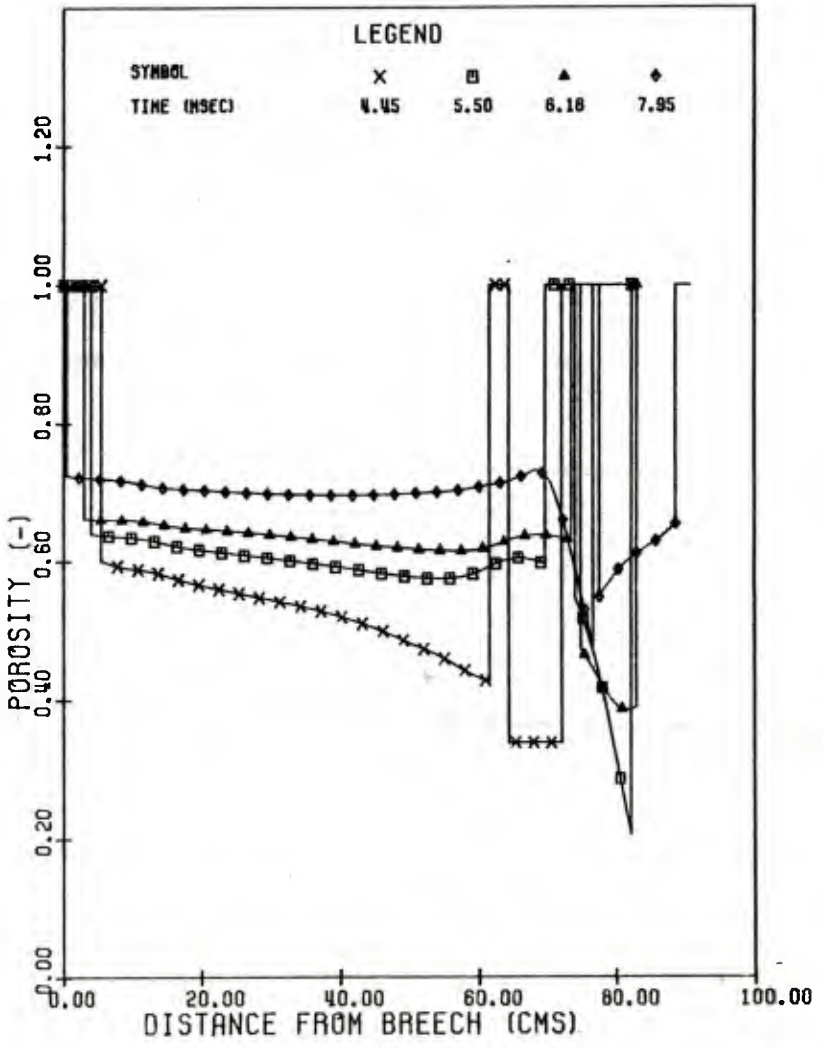

FIG.5.3.2 DISTRIBUTIONS OF POROSITY FOR INSULATED CONFIGURATION FOLLOWING FLAMESPREADING DELAY OF 0.616 MSEC

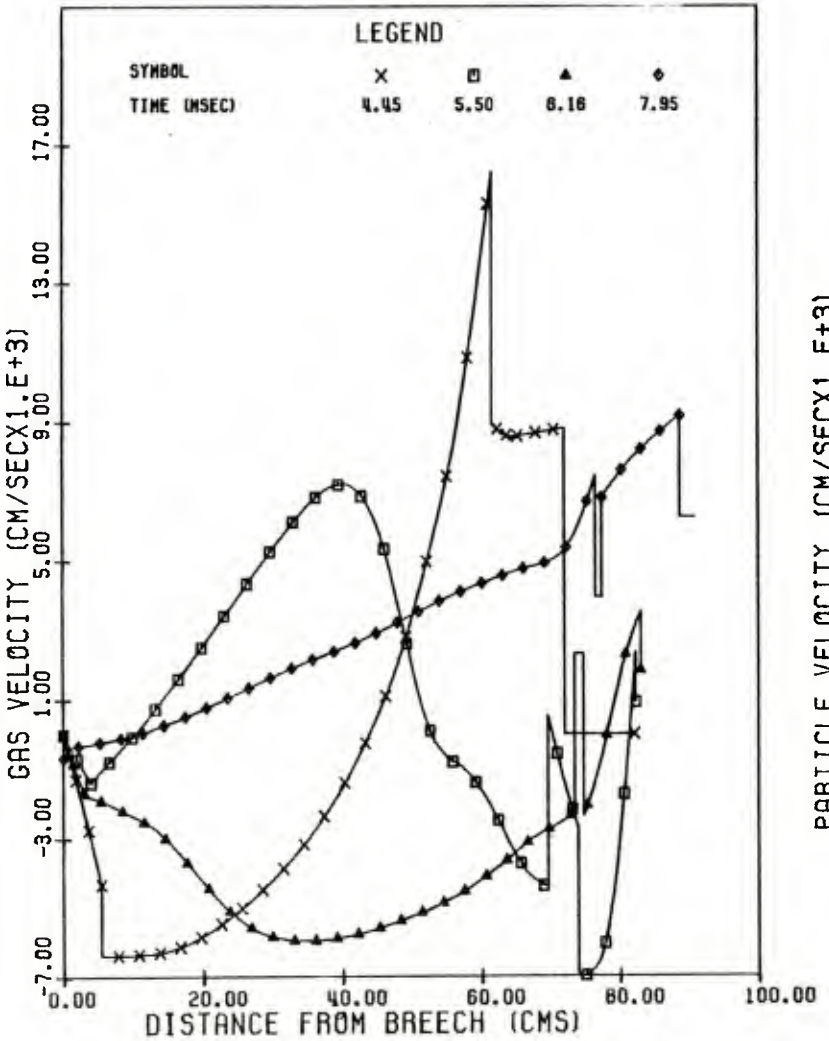

FIG.5.3.3 DISTRIBUTIONS OF GAS VELOCITY FOR INSULATED CONFIGURATION FOLLOWING FLAMESPREADING DELAY OF 0.616 MSEC

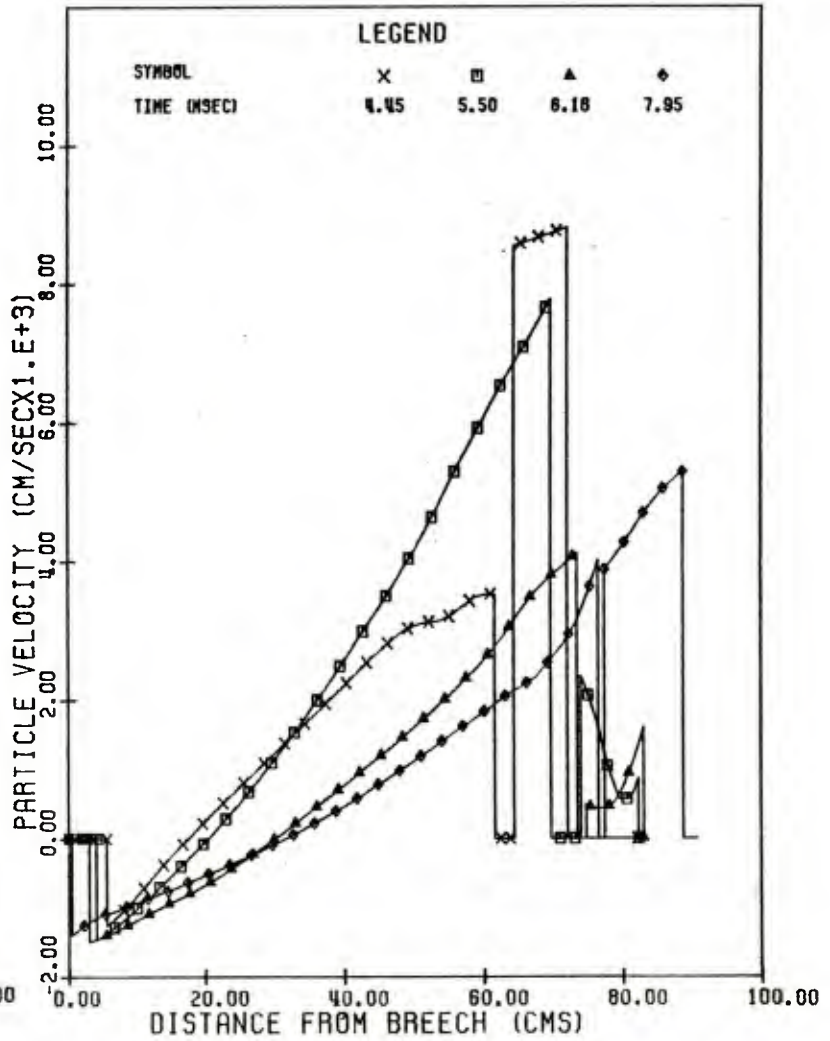

FIG.5.3.4 DISTRIBUTIONS OF PARTICLE VELOCITY FOR INSULATED CONFIGURATION FOLLOWING FLAMESPREADING DELAY OF 0.616 MSEC

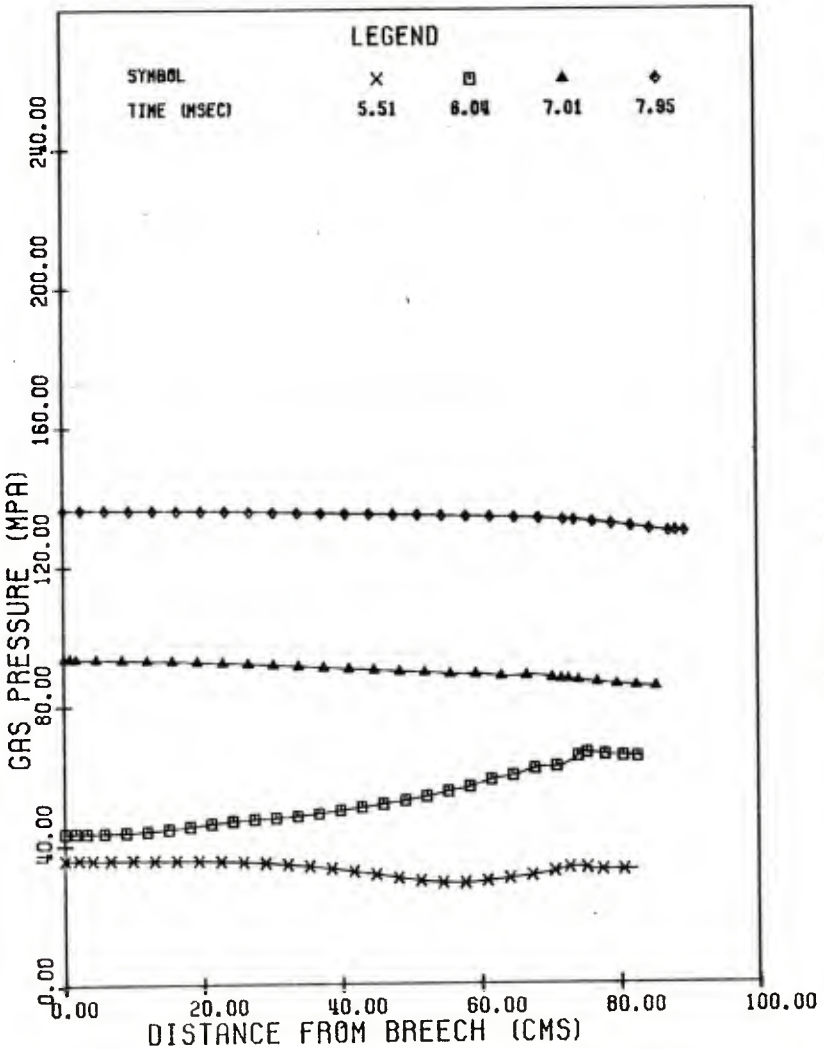

FIG.5.3.5 DISTRIBUTIONS OF PRESSURE FOR INSULATED CONFIGURATION FOLLOWING FLAMESPREADING DELAY OF 1.676 MSEC

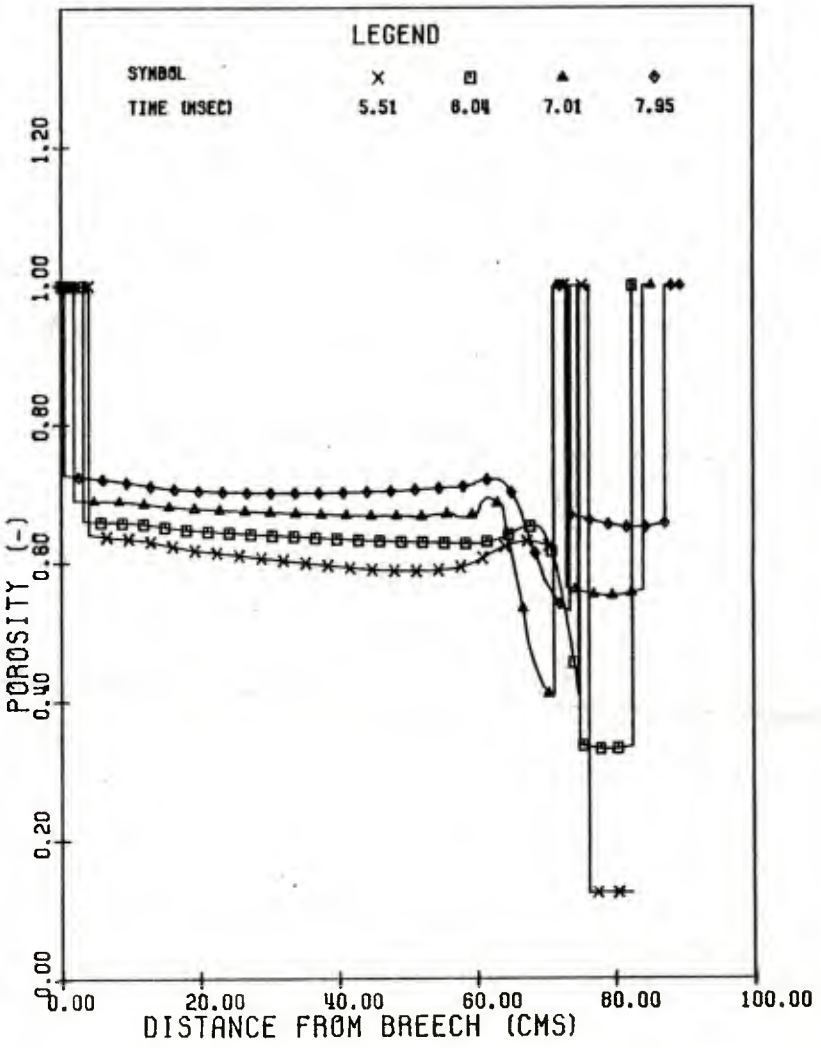

FIG.5.3.6 DISTRIBUTIONS OF POROSITY FOR INSULATED CONFIGURATION FOLLOWING FLAMESPREADING DELAY OF 1.676 MSEC

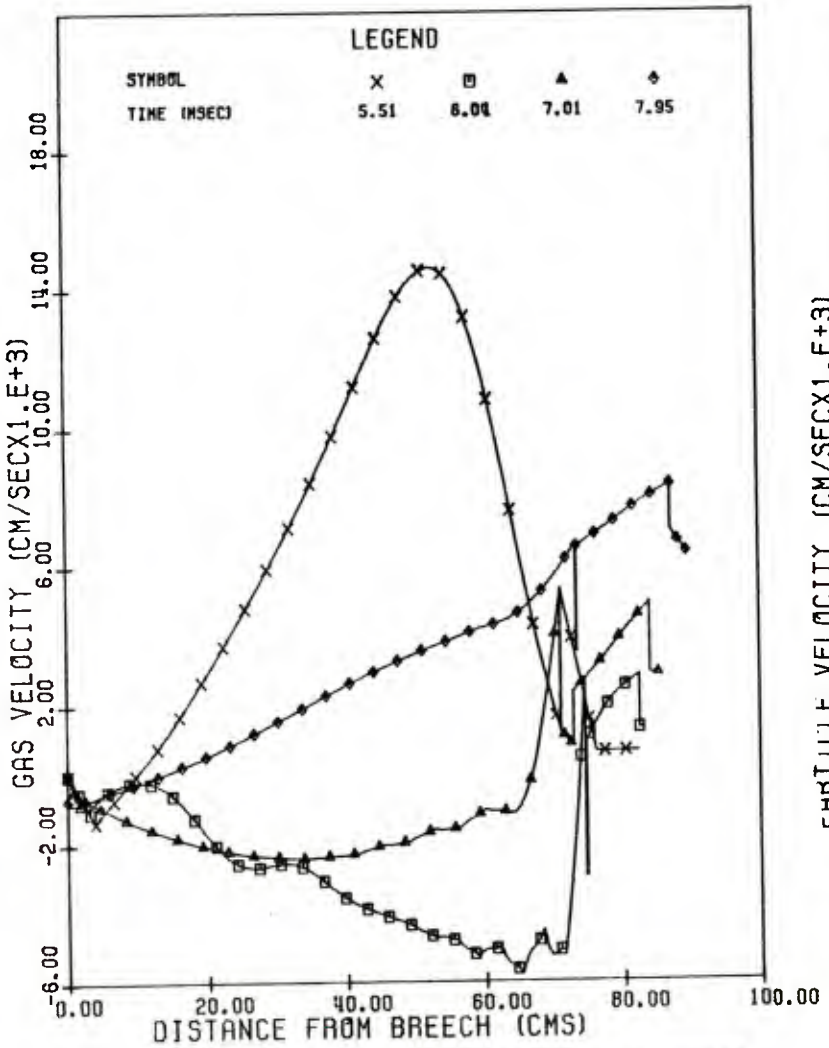

FIG.5.3.7 DISTRIBUTIONS OF GAS VELOCITY FOR INSULATED CONFIGURATION FOLLOWING FLAMESPREADING DELAY OF 1.676 MSEC

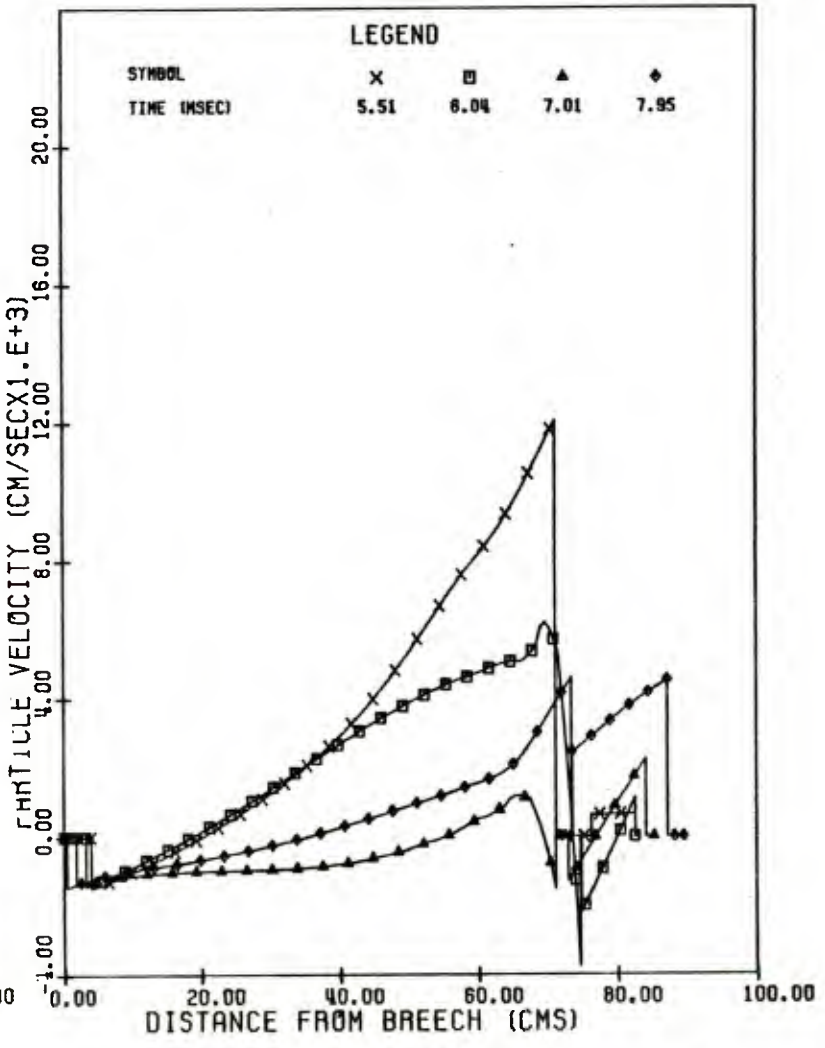

FIG.5.3.8 DISTRIBUTIONS OF PARTICLE VELOCITY FOR INSULATED CONFIGURATION FOLLOWING FLAMESPREADING DELAY OF 1.676 MSEC

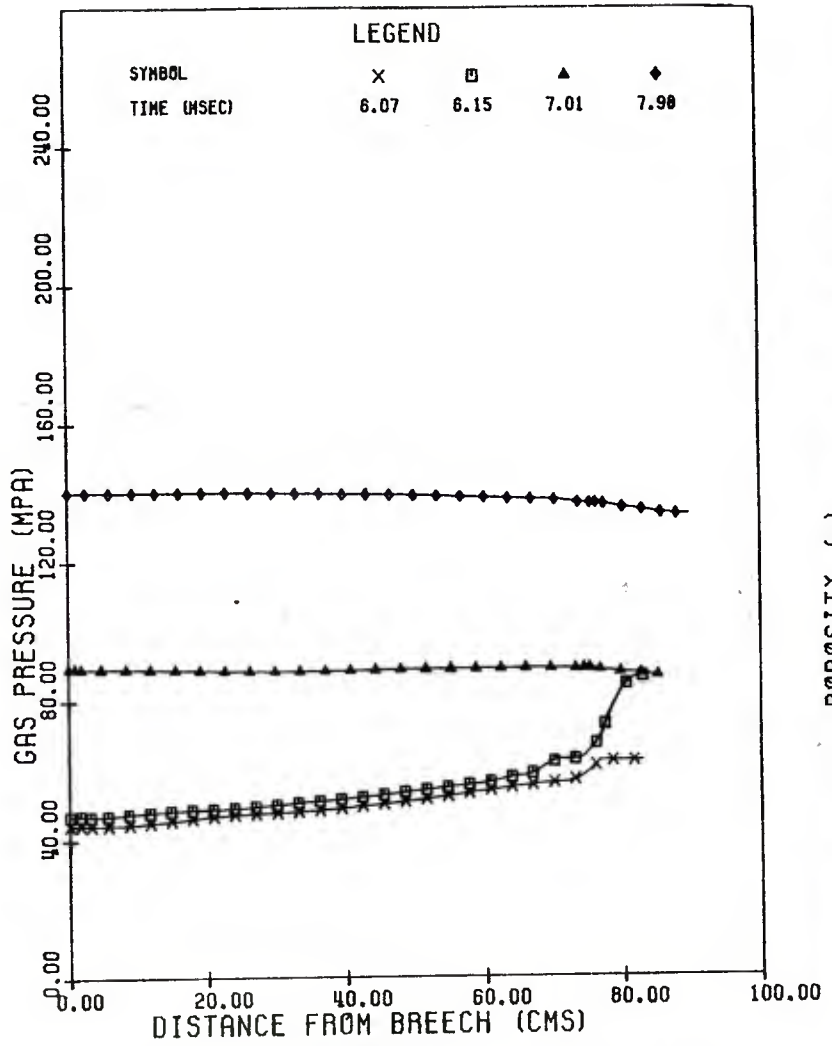

FIG.5.3.9 DISTRIBUTIONS OF PRESSURE FOR INSULATED CONFIGURATION FOLLOWING FLAMESPREADING DELAY OF 2.234 MSEC

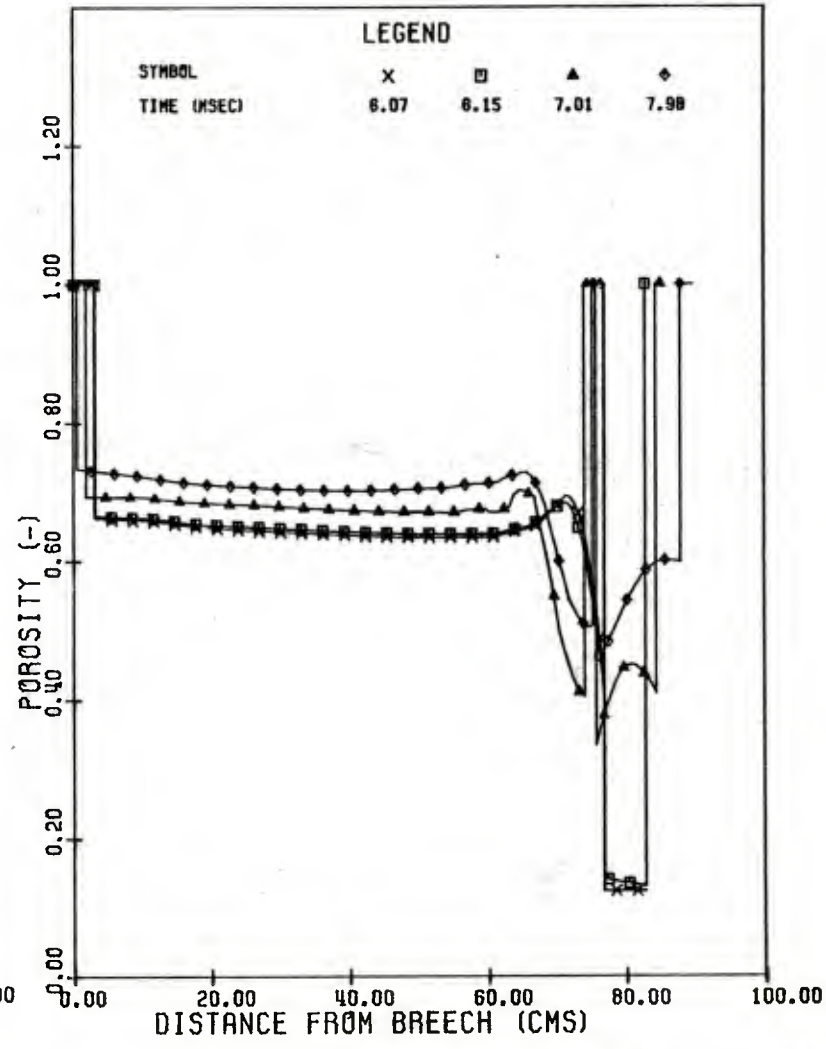

FIG.5.3.10 DISTRIBUTIONS OF POROSITY FOR INSULATED CONFIGURATION FOLLOWING FLAMESPREADING DELAY OF 2.234 MSEC

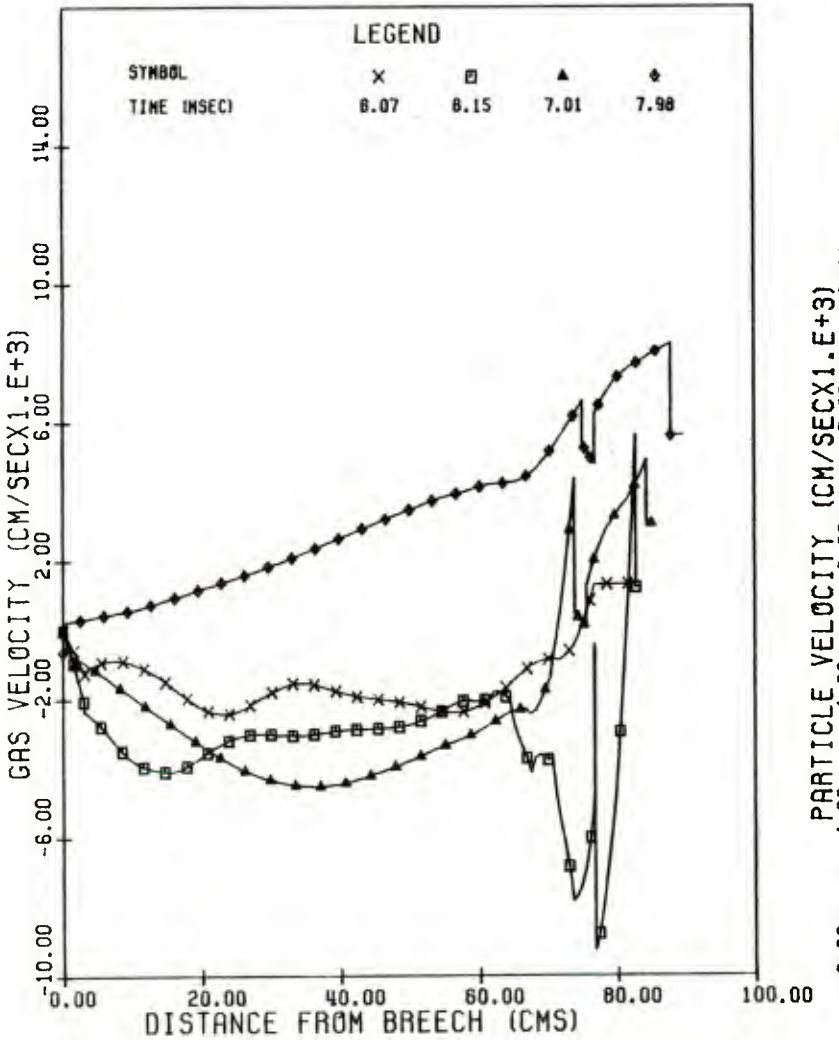

FIG.5.3.11 DISTRIBUTIONS OF GAS VELOCITY FOR INSULATED CONFIGURATION FOLLOWING FLAMESPREADING DELAY OF 2.234 MSEC

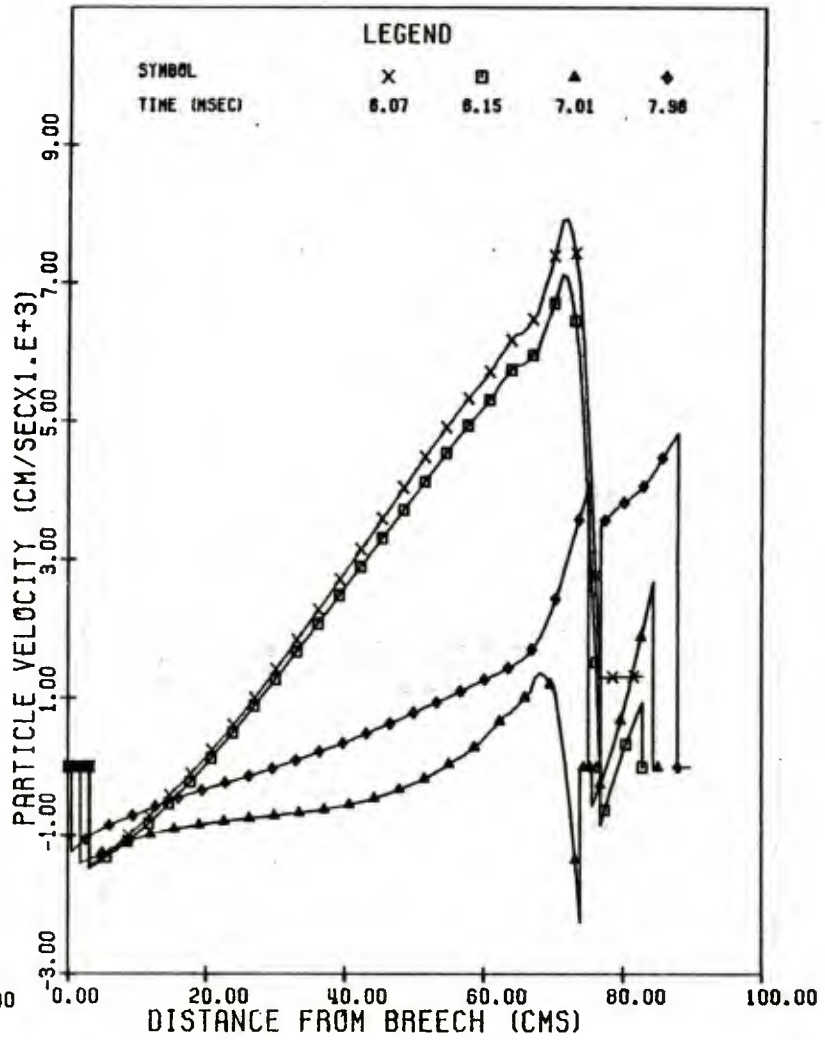

FIG.5.3.12 DISTRIBUTIONS OF PARTICLE VELOCITY FOR INSULATED CONFIGURATION FOLLOWING FLAMESPREADING DELAY OF 2.234 MSEC

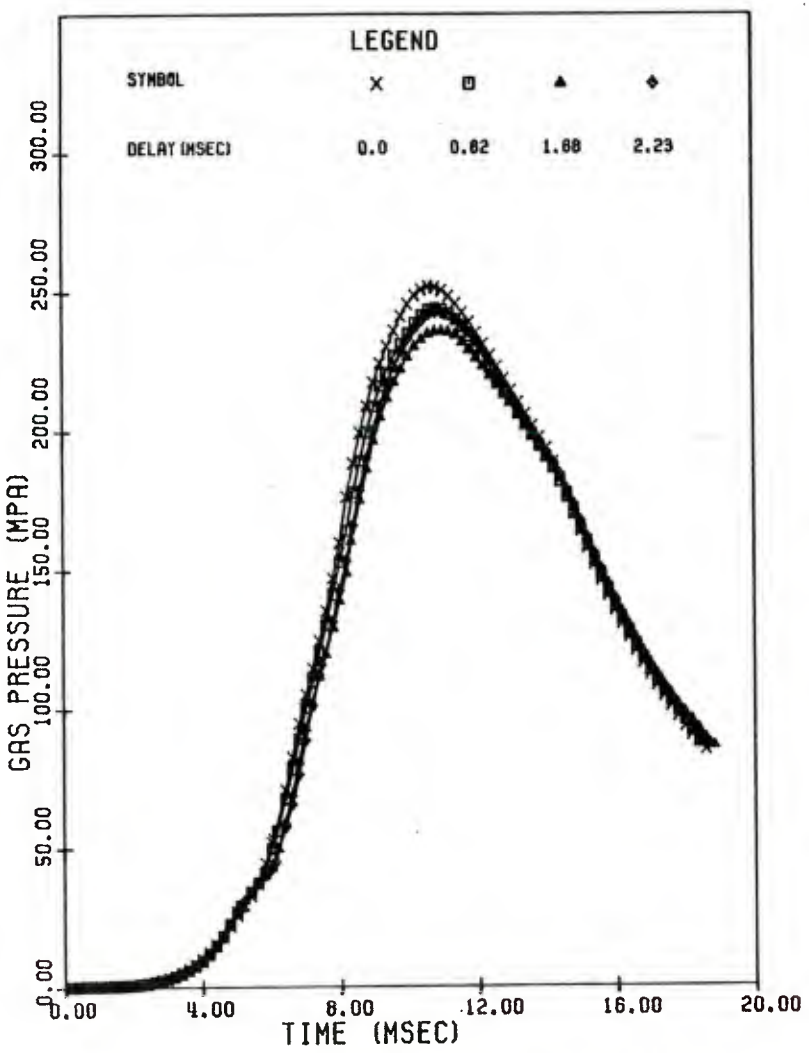

FIG.5.3.13 COMPARISON OF PRESSURE HISTORY IN BREECH OF CHAMBER FOR NOMINAL CONFIGURATION WITH THAT FOR INSULATED CONFIGURATION AND THREE VALUES OF FLAME-SPREADING DELAY

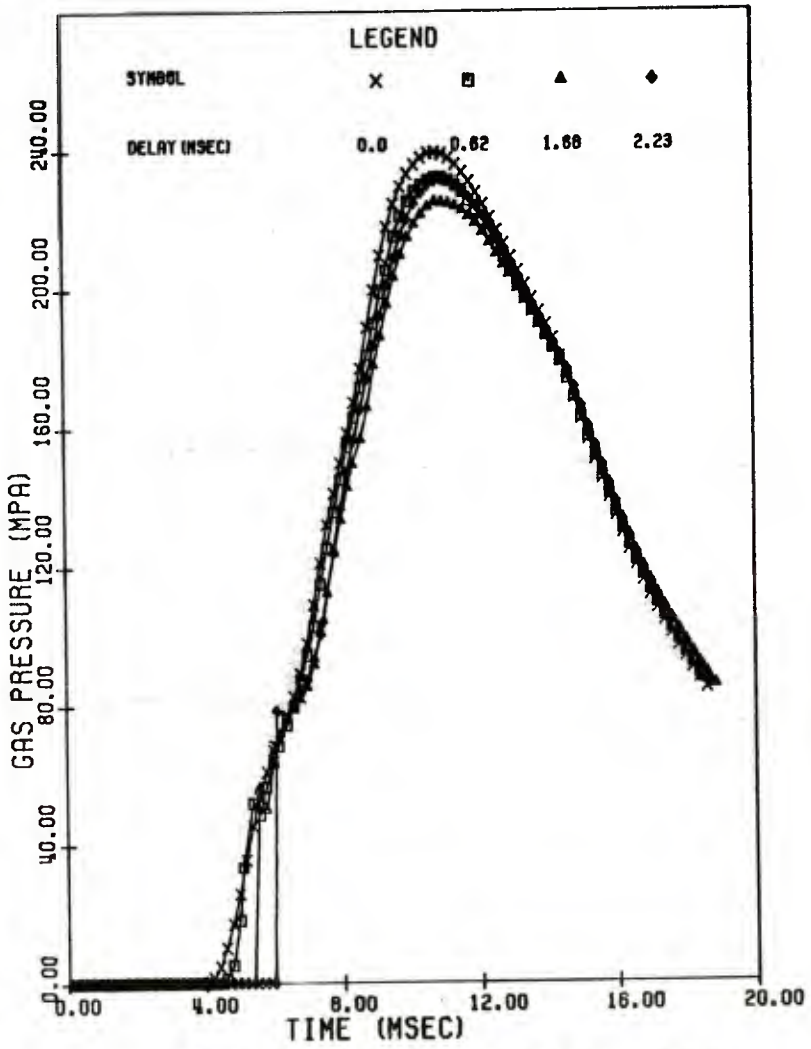

FIG.5.3.14 COMPARISON OF PRESSURE HISTORY IN MOUTH OF CHAMBER FOR NOMINAL CONFIGURATION WITH THAT FOR INSULATED CONFIGURATION AND THREE VALUES OF FLAME-SPREADING DELAY

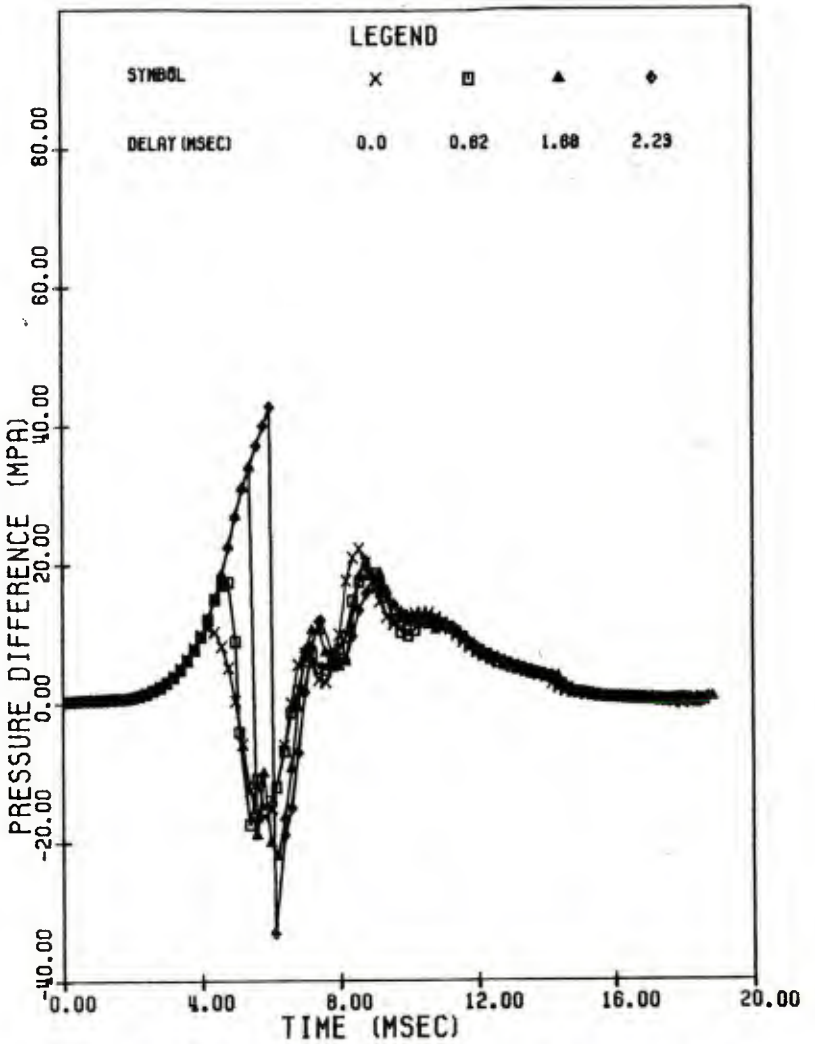

FIG.5.3.15 COMPARISON OF HISTORY OF PRESSURE DIFFERENCE BETWEEN BREECH AND MOUTH OF CHAMBER IN NOMINAL CONFIGURATION WITH THAT IN INSULATED CONFIGURATION FOR THREE VALUES OF FLAMESPREADING DELAY

6.0 DISCUSSION OF RESULTS

Chapters 3.0, 4.0 and 5.0 have provided the results of investigations of certain of those aspects of bag charge phenomenology which are not embedded in the quasi-one-dimensional NOVA code. Here we wish to review the findings of each chapter, separately and in relation to one another. This discussion will lead to the formulation of certain conclusions and recommendations which will subsequently be summarized in chapters 7.0 and 8.0 respectively.

Chapter 3.0 took as its objectives the elucidation of the radial structure of the two-phase flow occurring in a gun propelling charge and the interpretation of these findings in respect to the NOVA code. The scope of enquiry was necessarily limited. We looked at only one type of charge and considered some variations in ullage distribution and primer venting characteristics. Moreover, the study was, itself, conducted on a one-dimensional basis, the flow being regarded as axially uniform and azimuthally symmetric. More complete answers must await the development of multi-dimensional codes and their application to a wide spectrum of problems.

However, several definite conclusions may be drawn from even the present limited study of this topic. We will state these directly and then proceed to a discussion of their implications.

From the comparison of the planar and cylindrical flows, section 3.3, we learned that cylindrical flamespreading is qualitatively similar to planar flamespreading in respect to the structure of the distributions of the state variables. However, cylindrical flamespreading due to a center core igniter is slower than the corresponding planar case. In the particular case under consideration the planar speed was found to be roughly 50% greater than the cylindrical wave speed.

From the study of the influence of external ullage, section 3.4, we found that external ullage has little effect on flamespreading except at the outside of the charge where it favors convection and reduces the ignition delay. The grain velocities at the outside of the bed were found to depend linearly on the magnitude of the external gap, for the cases studied here. However, large grain velocities were not seen, the maximum value being roughly 10 m/sec. Virtually no wave structure was seen in the radial pressure distribution following the conclusion of flamespreading. The gas velocities likewise were strongly damped. However, the porosity distributions were far from uniform even after 2.0 msec, the primer blast creating substantial internal ullage at the expense of the external ullage.

The studies of exterior ignition, section 3.5, showed that considerable compaction of the central portion of the charge can occur if the external rate of pressurization is fairly high. However, bed motion was restricted in this case and the problem of grain impact against the external boundary was avoided. The rate of flamespreading was found to be strongly dependent on the primer strength.

From the point of view of forming a critical evaluation of the validity of the NOVA code the most important findings of chapter 3.0 relate to the radial flow distributions. We have seen that the pressure may justifiably be taken as uniform over each cross section following a brief period of radial flamespreading. Likewise, there is very little velocity associated with either phase at the conclusion of flamespreading. The remaining state variables, other than the porosity, may be treated as uniform. The large variations in temperature and density which occur near the impermeable boundaries due to excessive ignition delays represent model anomalies and are not expected to be present in practice.

However, we found that ullage, or a non-uniform distribution of porosity can be very persistent in the cylindrical flow. It is difficult to generalize this finding to the multi-dimensional case since we can visualize charges in which a center core is not uniformly present. Nonethe-less, it was seen in chapter 4.0 that annular ullage can change substantially the manner of flamespreading and, moreover, serves to reduce the amplitude of axial pressure waves. Therefore, we emphasize the importance of the present finding that one cannot safely assume the charge to be fluidized and uniformly distributed over the cross section of the tube. Moreover, one may question the suitability of an essentially laminar description of the two-phase flow.

By this we mean that we do not consider any of the correlation terms which arise in the two-phase flow equations. We speculate that if, in practice, the ullage is found to disappear rapidly so that the mixture becomes distributed in a uniform manner across each section of the tube, then the flow will lie outside the scope of solutions obtainable with the present governing equations, even in the multi-dimensional case. Conceivably, it may prove to be important to include the effect of turbulent mass diffusion. It is strongly urged that experimental studies be undertaken to investigate the radial structure of the flow with particular reference to the distribution of the solid phase.

From the standpoint of charge design the most important finding of the present study relates to the value of the radial velocity of the solid phase. This is small even in an extreme case of external ullage. Accordingly, the present results indicate that grain fracture due to radial primer blast is unlikely to be a serious problem. It should be noted, however, that the radial velocity will be increased as the primer strength is increased and, as the permeability of the bed is decreased. Therefore, vigorous center core ignition of a finely granulated or strongly consolidated charge might cause difficulties.

In chapter 4.0 we assessed the consequences of treating a typical Army bag propelling charge as though it were one-dimensional. This was done by extending the NOVA code to recognize a region of annular ullage around the bag, the rupture of the bag, mass exchange with the annular ullage and the coupling to the ullage at the ends of the chamber.

We found that, for the particular bag constitutive laws adopted herein, a quasi-one-dimensional model can be seriously in error in so far as flamespreading is concerned, even when heat transfer due to radial

convection is unimportant. It must be emphasized that the assumptions concerning the permeability of the bag are most influential. Indeed, a study of multi-dimensional flow in guns seems pointless unless properly supported by empirical data to define the influence of the bag. We may also speculate that use may be made of the bag permeability as a design parameter in respect to the control of ignition transients just as is bed permeability.

The calculation presented in chapter 4.0 cannot be said to have provided a firm prediction of the actual influence of the annular ullage. The model was too crude and, moreover, we completed the solution using a quasi-one-dimensional model from a point at which the bed was not yet fully expanded in the radial direction. However, the results showed that the chamber pressure history may be remarkably tolerant of a wide variation in the behaviour during flamespreading. Moreover, the influence of neglecting the annular ullage appears to be such as to overestimate the strength of the pressure waves in the gun chamber.

In chapter 5.0 we considered, on a purely theoretical basis, the possible consequences of having an obstruction to the passage of a convective flame through a propelling charge. Physically, we envisage such a condition as arising in a zoned charge for which the bag material itself constitutes the temporary obstruction to the flame. However, under certain anomalous conditions such as those believed to have occurred in a Navy 76mm gun[17], the obstruction might be due to flash suppressant dispersed throughout the bed. It is well known that a mixture of grains of very different sizes may exhibit extremely low porosity due to the intrusion of the smaller particles into the interstices formed by the larger.

The physical consequences of the obstruction are perceived to include compaction of the insulated region, since the gas is unable to penetrate the boundaries, and acceleration in the direction of propagation of the flame.

Two distinct mechanisms can therefore be identified as potential causes of pressure waves in the gun. The acceleration of the insulated region may, if there is sufficient run-up between the charge and the base of the projectile, induce a large velocity in the propelling gas. The subsequent impact of the insulated region against the base of the projectile and concomitant stagnation of the gas may produce a reverse gradient in the same fashion as do the compactible filler materials in Navy cased ammunition. Secondly, the compaction of the insulated region will lead to low voidage so that when the obstruction is finally overcome and ignition occurs, the subsequent combustion will take place in a relatively confined environment. This may result in a significant overpressure.

Apart from these two mechanisms which have been modeled in the study presented in chapter 5.0, we must note the possibility of a third mechanism; due to the strong compaction of the isolated region, fracture may result. This was not modeled.

A major uncertainty in the modeling of the obstruction itself was the formulation of criteria according to which the obstruction is overcome. With increasing pressure accompanied by thermal attack it is expected that penetration of the barrier will eventually occur. Here we used three values of the ignition delay associated with the obstruction. These were based on the only independent data available and are believed to represent a reasonable range of values.

The results have shown quite clearly that at least for the charge configuration considered here, the internal ballistic history is virtually indifferent to a flow obstruction. The consequences of delaying the ignition of 17% of the charge at the forward end are in keeping with an intuitive perception rooted in a lumped parameter picture of the overall process. The cases considered here produced enhanced boundary motion and stagnation as well as considerable compaction of the insulated region. Ignition in the forward region was delayed in such a fashion as to produce rupture at three distinct stages of the flow, namely; with the forward bag in motion, with the bag collapsed against the projectile, and finally with the permeable portion of the charge collapsed against the forward portion.

Only the latter case, in which confinement was greatest, produced a significant change in the first minimum of the pressure difference plot. However, this was quickly damped and the subsequent history differed but little from that of the nominal configuration. The physical explanation for the absence of pronounced pressure wave enhancement is believed to reside in the rapid relaxation of the compacted region to near nominal voidage.

Possibly, a smaller obstructed region would acquire a higher velocity thereby producing a stronger stagnation wave upon impacting the projectile. However, the mass of the compactible filler elements used in Navy cased ammunition and which are associated with the formation of a reverse gradient is much less than that of any probable zone increment. In view of the failure of the present calculations to show any significant stagnation wave associated with the insulated region we conclude that it is unlikely that flow obstruction in conventional medium caliber Army weapons would lead to significant pressure wave structure through this particular mechanism.

Since, moreover, the compacted propellant quickly expands to near nominal porosity following ignition, it is believed that the second mechanism, namely confined burning, is not a probable first cause of strong pressure wave phenomena in medium caliber weapons of the type studied here. We might also mention that the presence of radial ullage, neglected in chapter 5.0, would act to reduce the acceleration of the insulated region since the gas pressure would more completely equilibrate in the axial direction as we saw in chapter 4.0. The probability of fracture of the grains due to impact would be reduced accordingly.

Thus, from the study presented in chapter 5.0, we conclude that flow obstruction, per se, is not a likely cause of pressure waves in medium caliber guns. On the other hand, flow obstruction is reported to have been responsible for a catastrophic malfunction of the 76mm Oto Melara gun. It was conjectured by the investigators of the malfunction[17] that grain fracture, due to the impact of the obstructed region against the base of the projectile, was responsible for the observed overpressure. Accordingly, we conclude that our present findings should be qualified in this respect and that further investigation of the probability of grain fracture is desirable.

Studies of the mechanical response of propellant grains to transient loads of amplitudes of at least 10 Mpa and preferably 100 Mpa are desirable if a theoretical characterization of the occurrence and consequences of grain fracture is to be made.

Moreover, both chapters 4.0 and 5.0 point to a definite need for better characterization of the behaviour of bag materials. Data are required to resolve the permeability of the bag and its response to mechanical and thermal attack. Models of bag charges cannot neglect such data if meaningful predictions are to be made of the path of flamespreading and the formation of pressure waves. Indeed, the bag should be viewed, in our opinion, as an influential element of the ignition train and not simply as a container for the propellant. The present study suggests that by making a suitable choice of bag materials, the designer can exert as much control over the flamespreading path as is customarily achieved using a distributed ignition system. We also conjecture that the bag materials can be selected so as to preserve annular ullage throughout flamespreading, thereby minimizing the amplitude of ignition related pressure waves.

7.0 CONCLUSIONS

(1) Except that flamespreading tends to be slower, the cylindrical two-phase reacting flow demonstrates no essential differences from the planar case.

(2) External ullage has little effect on cylindrical flamespreading. For the nominal 155mm configuration considered only modest radial grain velocities were computed; virtually no wave structure was found in the pressure distributions following the completion of flamespreading.

(3) External ignition of a cylindrical charge having no internal ullage was found to induce quite strong compaction at the center.

(4) Solutions of the cylindrical flow problem showed that following the completion of flamespreading, all the flow variables, except the porosity, become uniform over the cross section of the tube. However, annular ullage was found to be persistent, invalidating the application of a quasi-one-dimensional model of axial two-phase flow to the simulation of bag charges.

(5) A quasi-two-dimensional solution for a bag charge showed that the annular ullage can be extremely influential although the precise consequences of its presence are believed to be strongly dependent on the permeability of the bag material. The annular ullage was found to reduce the amplitude of the history of pressure difference between the breech and mouth of the chamber. For the bag constitutive laws assumed herein, flamespreading was found to proceed in two fronts, one starting at the breech and another starting at the front of the charge as a consequence of convection through the annular gap.

(6) The obstruction of axial flamespreading by bag material was not found to have any significant ballistic consequences. However, it is believed that this conclusion would not hold if the propellant grains were susceptible to fracture.

8.0 RECOMMENDATIONS

(1) It is recommended that experiments be performed to determine the distribution of bagged propelling charges at various stages in the early part of the interior ballistic cycle. From the point of view of modeling it is desirable to know the extent to which a laminar two-phase flow prevails. From the point of view of design it is important to understand the dynamic role played by ullage in respect to flamespreading and the formation of ignition transients.

(2) It is recommended that a determination be made of the permeability and resistance to thermal and mechanical attack of candidate bag materials. Such data are essential for meaningful modeling of bag charges and, moreover, are expected to be useful to the designer who must evaluate the influence of the bag on the path of flamespreading.

(3) Independent data to characterize the mechanical response and the probability of fracture of propellant grains are desired in the transient loading regime for stress amplitudes of at least 10 Mpa and preferably 100 Mpa.

(4) It is recommended that the numerical technology developed herein be linked permanently to the NOVA code to produce an upgraded quasi-two-dimensional version in which a realistic representation may be made of the influence of a center core primer and of annular ullage.

References

1. Gough, P.S. and Zwarts, F.J.
"Theoretical Model for Ignition of Gun Propellant"
Final Report, Part II, Contract N00174-72-C-0223 December 1972

2. Gough, P.S.
"Fundamental Investigation of the Interior Ballistics of Guns"
Final Report, Contract N00174-73-C-0501 1974

3. Gough, P.S.
"The Flow of a Compressible Gas Through an Aggregate Mobile, Reacting Particles"
Ph.D. Thesis McGill University 1974

4. Gough P.S.
"Computer Modelling of Interior Ballistics"
Final Report Contract N00174-75-C-0131 1975

5. Gough, P.S.
"Numerical Analysis of a Two-Phase Flow with Explicit Internal Boundaries"
Final Report Contract N00174-75-C-0259 1977

6. Horst, A., Nelson, C., and May, I.
"Flame Spreading in Granular Propellant Beds: A Diagnostic Comparison of Theory to Experiment"
Proc. AIAA/SAE 13th Joint Propulsion Conference
Orlando, Florida July 1977

7. Summerfield, M.; Caveny, L.H.; Battista, R.A.; Kubota, N.; Gostintsev, Yu, A. and Isoda, H.
"Theory of Dynamic Extinguishment of Solid Propellants with Special Reference to Non Steady Heat Feedback Law"
J. Spacecraft & Rockets v.8, N.3 1971

8. Ergun, S.
"Fluid Flow Through Packed Columns"
Chem. Eng. Progr. vol.48, p89 1952

9 Anderssen, K.E.B.
"Pressure Drop in Ideal Fluidization"
Chem. Eng. Sci. vol.15, pp276-297 1961

10. Batchelor, G.K.
"An Introduction to Fluid Mechanics"
Cambridge University Press 1970

11. Denton, W.H.
"General Discussion on Heat Transfer"
Inst. Mech Eng. and Am. Soc. Mech. Eng. London 1951

12. Gelperin, N.I. and Einstein, V.G.
"Heat Transfer in Fluidized Beds"
Fluidization, edited by J.F.Davidson and D.Harrison
Academic Press 1971

13. Gough, P.S.
"The Influence of an Implicit Representation of Internal Boundaries on the Ballistic Predictions of the NOVA Code"
Proc. 14th Jannaf Combustion Meeting 1977

14. Gough, P.S.
"The Influence of the Representation of Internal Boundaries on the Ballistic Predictions of the NOVA Code"
Final Report Task I Contract N00174-77-C-0103 1977

15. Nelson, C.W., Robbins, F.W. and Gough, P.S.
"Predicted Effects of Transient Burning in Gun Flamespreading"
Proc. 14th Jannaf Combustion Meeting 1977

16. Horst, A.W., May, I.W. and Clarke, E.V.Jr.
"The Missing Link Between Pressure Waves and Breechblows"
Proc. 14th Jannaf Combustion Meeting 1977

17. Olenick, P.J. Jr.
"Investigation of the 76mm/62 Caliber Mark 75 Gun Mount Malfunction"
NSWC/DL TR-3144 October 1975

18. Fisher, E.B. and Graves, K.W.
"Mathematical Model of Double Base Propellant Ignition and Combustion in the 81mm Mortar"
CAL Report DG-3029-D-1 1972

19. Fisher, E.B. and Trippe, A.P.
"Development of a Basis for Acceptance of Continuously Produced Propellant"
CALSPAN Report VQ-5163-D-1 1973

20. East, J.L. and McClure, D.R.
"Projectile Motion Predicted by a Solid/Gas Flow Interior Ballistic Model"
Proc. 10th Jannaf Combustion Meeting 1973

21. Krier,H.; van Tassel, W.F.; Rajan, S. and VerShaw, J.
"Model of Flame Spreading and Combustion Through Packed Beds of Propellant Grains"
Technical Report AAE74-1, University of Illinois at Urbana-Champaign 1974

22. Kuo, K.K.; Koo, J.H.; Davis, T.R. and Coates, G.R.
"Transient Combustion in Mobile Gas-Permeable Propellants"
ACTA ASTRONAUTICA Vol.3 No.7-8 pp574-591 1976

23. Culbertson, D.W. and DeVost, V.F.
"Instrumentation Techniques and the Application of Spectral Analysis and Laboratory Simulation to Gun Shock Problems"
Shock and Vibration Bulletin, 42, part 5, pp47-59 January 1972

24. Eckert, E.R.G. and Drake, R.M.
"Analysis of Heat and Mass Transfer"
McGraw-Hill 1972

25. MacCormack, R.W.
"The Effects of Viscosity in Hypervelocity Impact Cratering"
AIAA 7th Aerospace Sciences Meeting, Paper 69-354 1969

26. Corner, J.
"Theory of the Interior Ballistics of Guns"
New York John Wiley and Sons 1950

27. Rocchio, J.; White, K.; Ruth, C. and May, I.
"Propellant Grain Tailoring to Reduce Pressure Wave Generation in Guns"
Proc. 12th Jannaf Combustion Meeting August 1975

28. Richtmyer, R.D. and Morton, K.W.
"Difference Methods for Initial-Value Problems"
Interscience 1967

29. Nelson, C.W.
"Some Simulations of a 155mm Howitzer with the NOVAE Code"
BRL IMR 451 November 1975

Nomenclature

A	Cross sectional area for two-phase flow
A_g	Cross sectional area of annular ullage. Also, part of control surface occupied by gas phase
A_i	Cross sectional area of tube at center of i^{th} element
A_i'	$dA_i(Z)/dZ$
A_p	Part of control surface occupied by solid phase
B_1, B_2	Burn rate coefficients
b	Covolume
a	Rate of propagation of granular disturbances
a_1	Value of a when bed is in settled condition
D_p	Effective particle diameter, $D_p = 6M_p/\rho_p S_p$
$\dot{d}$	Rate of regression of surface of solid phase
e	Internal energy of gas phase
e_{CHEM}	Chemical energy released by combustion of solid phase
e_{IG}	Chemical energy released by combustion of igniter material
f_s	Steady state velocity dependent interphase drag
g_o	Gravitational acceleration
h	Film coefficient
$\overleftrightarrow{I}$	Unit tensor of rank two
k_p	Thermal conductivity
M_i	Mass of i^{th} lumped parameter element
M_p	Mass of a propellant grain
$\dot{m}$	Rate of mass transfer
Nu_p	Nusselt number based on effective particle diameter
$\vec{n}$	Normal vector
n	Burn rate exponent

Pr	Prandtl number
p	Pressure
q_s	Steady state interphase heat transfer
R	Granular stress due to contacts between particles
R_g	Gas constant
Re_p	Reynolds number based on effective particle diameter
r	Radial coordinate
r_{bag}	Radius of bag
S	Control surface
S_p	Surface area of a grain
T	Temperature
t	Time
$\vec{u}$	Velocity
V	Control volume
V_c	Volume of Lumped Parameter Region
V_g	Part of control volume occupied by gas phase
V_p	Part of control volume occupied by solid phase
$\vec{w}$	Velocity of point on control surface
Z_i, $\dot{Z}_i$	Position, Velocity of Left hand side of i^{th} element
z	Axial position
z_B	Length of Computational Region
z_L, z_R	Position of Left and Right hand sides of computational regions

α_p	Thermal diffusivity of solid phase
α_i, β_i	Coefficients used in back substitution procedure to analyze unloading elements
γ	Ratio of specific heats
ε	Porosity
ε_i	Porosity of i^{th} element
ε_o	Settling porosity of propellant bed
ε_1	Initial porosity of propellant bed
ζ	Non-dimensional spacewise coordinate used in computational scheme
η	Velocity of convected mesh, $\eta = \dot{Z}_L + \zeta\dot{Z}$
κ	Stress attenuation factor
μ	Viscosity
ρ	Density
$\overleftrightarrow{\sigma}$	Stress tensor
$\overleftrightarrow{\sigma}'$	Stress deviator
σ_i	Stress at center of i^{th} element
ψ	Rate of venting of igniter gas
$\vec{\phi}$	Arbitrary vector

The subscript p is used to denote a property of the solid phase. The subscript g denotes a property of the gas in the region of annular ullage. Properties of the gas phase within the bag are unsubscripted. The subscript c is used to denote properties of a region of axial ullage. The subscript IG is used to denote a property of the igniter. We use f to denote a gas phase property at the film temperature.

DISTRIBUTION LIST

No. of Copies	Organization
12	Commander Defense Documentation Center ATTN: DCC-TCA Cameron Station Alexandria, VA 22314
1	Director Defense Advanced Research Projects Agency ATTN: C.R. Lehner 1400 Wilson Boulevard Arlington, VA 22209
2	Director Institute for Defense Analyses ATTN: H. Wolfhard R.T. Oliver 400 Army-Navy Drive Arlington, VA 22202
1	Commander US Army Materiel Development and Readiness Command ATTN: DRCDMD-ST, N. Klein 5001 Eisenhower Avenue Alexandria, VA 22333
1	Commander US Army Aviation Research and Development Command ATTN: DRSAV-E P.O. Box 209 St. Louis, MO 63166
1	Director US Army Air Mobility Research and Development Laboratory Ames Research Center Moffett Field, CA 94035
1	Commander US Army Electronics Research & Development Command Technical Support Activity ATTN: DELSD-L Ft. Monmouth, NJ 07703
1	Commander US Army Communications Rsch and Development Command ATTN: DRDCO-SGS Ft. Monmouth, NJ 07703
1	Commander US Army Missile Research and Development Command ATTN: DRDMI-R Redstone Arsenal, AL 35809
1	Commander US Army Missile Materiel Readiness Command ATTN: DRSMI-AOM Redstone Arsenal, AL 35809
1	Commander US Army Tank Automotive Research and Development Command ATTN: DRDTA-UL Warren, MI 48090
1	Commander US Army Armament Materiel Readiness Command ATTN: DRSAR-LEP-L, Tech Lib Rock Island, IL 61299
2	Commander US Army Armament Research & Development Command ATTN: DRDAR-TSS Dover, New Jersey 07801
6	Commander US Army Armament Research and Development Command ATTN: DRDAR-LCE-CI, J. Lannon DRDAR-LC, J.P. Picard DRDAR-LCE, C. Lenchitz DRDAR-LCE, R.F. Walker SCA-CC, C. Dickey SCA-PP, L. Stiefel Dover, New Jersey 07801

DISTRIBUTION LIST

No. of Copies	Organization
1	Commander US Army White Sands Missile Range ATTN: STEWS-VT WSMR, NM 88002
1	Commander US Army Watervliet Arsenal ATTN: Code SARWV-RD, R. Thierry Watervliet, NY 12189
1	Commander US Army Materials and Mechanics Research Center ATTN: DRXMR-ATL Watertown, MA 02172
1	Commander US Army Natick Research and Development Command ATTN: DRXRE, D. Sieling Natick, MA 01762
1	Director US Army TRADOC Systems Analysis Activity ATTN: ATAA-SL, Tech Lib WSMR, NM 88002
1	Commander US Army Research Office ATTN: Tech Lib P.O. Box 12211 Research Triangle Park, NC 27706
1	Chief of Naval Research ATTN: Code 473 800 N. Quincy Street Arlington, VA 22217
1	Commander US Naval Sea Systems Command ATTN: J.W. Murrin (NAVSEA-0331) National Center, Bldg. 2, Rm 6E08 Washington, DC 20360
2	Commander US Naval Surface Weapons Center ATTN: S.J. Jacobs/Code 240 Code 730 Silver Spring, MD 20910
1	Commander US Naval Surface Weapons Center ATTN: Library Br, DX-21 Dahlgren, VA 22448
1	Commander US Naval Underwater Systems Center Energy Conversion Department ATTN: R.S. Lazar/Code 5B331 Newport, RI 02840
2	Commander US Naval Weapons Center ATTN: R. Derr C. Thelen China Lake, CA 93555
1	Commander US Naval Research Laboratory ATTN: Code 6180 Washington, DC 20375
3	Superintendent US Naval Postgraduate School ATTN: Tech Lib David Netzer Allen Fuhs Monterey, CA 93940
2	Commander US Naval Ordnance Station ATTN: A. Roberts Tech Lib Indian Head, MD 20640
2	AFOSR ATTN: J.F. Masi B.T. Wolfson Bolling AFB, DC 20332

DISTRIBUTION LIST

No. of Copies	Organization
2	AFRPL (DYSC) ATTN: D. George J.N. Levine Edwards AFB, CA 93523
1	Lockheed Palo Alto Rsch Labs ATTN: Tech Info Ctr 3521 Hanover Street Palo Alto, CA 94304
1	Aerojet Solid Propulsion Co. ATTN: P. Micheli Sacramento, CA 95813
1	ARO Incorporated ATTN: N. Dougherty Arnold AFS, TN 37389
1	Atlantic Research Corporation ATTN: M.K. King 5390 Cherokee Avenue Alexandria, VA 22314
1	AVCO Corporation AVCO Everett Research Lab Div ATTN: D. Stickler 2385 Revere Beach Parkway Everett, MA 02149
2	Calspan Corporation ATTN: E. B. Fisher A. P. Trippe P. O. Box 235 Buffalo, NY 14221
1	Energy Incorporated ATTN: Dr. E. D. Hughes Idaho Falls, ID 83401
1	ENKI Corporation ATTN: M. I. Madison 9015 Fulbright Avenue Chatsworth, CA 91311
1	Foster Miller Associates, Inc. ATTN: A. J. Erickson 135 Second Avenue Waltham, MA 02154
1	General Electric Company Armament Department ATTN: M.J. Bulman Lakeside Avenue Burlington, VT 05402
1	General Electric Company Flight Propulsion Division ATTN: Tech Lib Cincinnati, OH 45215
2	Hercules Incorporated Alleghany Ballistic Lab ATTN: R. Miller Tech Lib Cumberland, MD 21501
2	Hercules Incorporated Bacchus Works ATTN: M. Beckstead R. Simmons Magna, UT 84044
1	IITRI ATTN: M.J. Klein 10 West 35th Street Chicago, IL 60615
1	Olin Corporation Badger Army Ammunition Plant ATTN: J. Ramnarace Baraboo, WI 53913
2	Olin Corporation New Haven Plant ATTN: R.L. Cook D.W. Riefler 275 Winchester Avenue New Haven, CT 06504
1	Paul Gough Associates, Inc. ATTN: P.S. Gough P.O. Box 1614 Portsmouth, NH 03801

DISTRIBUTION LIST

No. of Copies	Organization
1	Physics International Company 2700 Merced Street Leandro, CA 94577
1	Pulsepower Systems, Inc. ATTN: L. C. Elmore 815 American Street San Carlos, CA 94070
2	Rockwell International Corp. Rocketdyne Division ATTN: C. Obert J. E. Flanagan 6633 Canoga Avenue Canoga Park, CA 91304
2	Rockwell International Corp. Rocketdyne Division ATTN: W. Haymes Tech Lib McGregor, TX 76657
1	Science Applications, Inc. ATTN: R. B. Edelman 23146 Cumorah Crest Woodland Hills, CA 91364
1	Shock Hydrodynamics, Inc. ATTN: W. H. Anderson 4710-16 Vineland Avenue North Hollywood, CA 91602
1	Thiokol Corporation Elkton Division ATTN: E. Sutton Elkton, MD 21921
3	Thiokol Corporation Huntsville Division ATTN: D. Flanigan R. Glick Tech Lib Huntsville, AL 35807
2	Thiokol Corporation Wasatch Division ATTN: John Peterson Tech Lib P. O. Box 524 Brigham City, UT 84302
1	TRW Systems Group ATTN: H. Korman One Space Park Redondo Beach, CA 90278
2	United Technology Center ATTN: R. Brown Tech Lib P. O. Box 358 Sunnyvale, CA 94088
1	Universal Propulsion Co. ATTN: H. J. McSpadden P. O. Box 546 Riverside, CA 92502
1	Battelle Memorial Institute ATTN: Tech Lib 505 King Avenue Columbus, OH 43201
1	Brigham Young University Dept of Chemical Engineering ATTN: R. Coates Provo, UT 84601
1	California Institute of Tech 204 Karman Lab Mail Stop 301-46 ATTN: F.E.C. Culick 1201 E. California Street Pasadena, CA 91125
1	Case Western Reserve Univ. Division of Aerospace Sciences ATTN: J. Tien Cleveland, OH 44135

DISTRIBUTION LIST

No. of Copies	Organization
3	Georgia Institute of Tech School of Aerospace Eng. ATTN: B. T. Zinn E. Price W. C. Strahle Atlanta, GA 30332
1	Institute of Gas Technology ATTN: D. Gidaspow 3424 S. State Street Chicago, IL 60616
1	Johns Hopkins University Applied Physics Laboratory Chemical Propulsion Information Agency ATTN: T. Christian Johns Hopkins Road Laurel, MD 20810
1	Massachusetts Institute of Technology Dept of Mechanical Engineering ATTN: T. Toong Cambridge, MA 02139
1	Pennsylvania State University Applied Research Lab ATTN: G. M. Faeth P. O. Box 30 State College, PA 16801
1	Pennsylvania State University Dept of Mechanical Engineering ATTN: K. Kuo University Park, PA 16801
3	Forrestal Campus Library Princeton University ATTN: M. Summerfield L. Caveny Tech Lib P. O. Box 710 Princeton, NJ 08540
2	Purdue University School of Mechanical Eng. ATTN: J. Osborn S.N.B. Murthy TSPC Chaffee Hall West Lafayette, IN 47906
1	Rutgers State University Dept of Mechanical and Aerospace Engineering ATTN: S. Temkin University Heights Campus New Brunswick, NJ 08903
1	Rensselaer Polytechnic Inst. Department of Mathematics ATTN: Prof. D. A. Drew Troy, NY 12181
1	Southwest Research Institute Fire Research Section ATTN: W. H. McLain P. O. Drawer 28510 San Antonio, TX 78228
1	Stanford Research Institute Propulsion Sciences Division ATTN: Tech Lib 333 Ravenswood Avenue Menlo Park, CA 94024
1	Stevens Institute of Technology Davidson Laboratory ATTN: R. McAlevy, III Hoboken, NJ 07030
1	University of California, San Diego AMES Department ATTN: F. Williams P. O. Box 109 La Jolla, CA 92037

DISTRIBUTION LIST

No. of Copies	Organization
1	University of Illinois Dept. of Aeronautical Engineering ATTN: H. Krier Transportation Bldg., Rm 105 Urbana, IL 61801
1	University of Minnesota Dept. of Mechanical Engineering ATTN: E. Fletcher Minneapolis, MN 55455
2	University of Utah Dept of Chemical Engineering ATTN: A. Baer G. Flandro Salt Lake City, UT 84112
1	Washington State University Dept of Mechanical Engineering ATTN: Prof. C. T. Crowe Pullman, WA 99163
	Aberdeen Proving Ground
	Dir, USAMSAA Cdr, USATECOM ATTN: DRSTE-SG-H